Numerical Modeling of Microelectrochemical Systems

Adesokan, Bolaji James

Publication date:
2015

Document Version
Publisher's PDF, also known as Version of record

Numerical Modeling of Microelectrochemical Systems

Bolaji James Adesokan

Kongens Lyngby, January, 2015
DTU Compute - PhD-2015-362

Department of Applied Mathematics and Computer Science
Technical University of Denmark
Richard Petersens Plads, Building 324
DK-2800 Kongens Lyngby, Denmark
Phone +45 4525 3031
Fax+45 4588 1399
compute@compute.dtu.dk
www.compute.dtu.dk DTU Compute-PhD-2015-362

Preface

This thesis was prepared at the department of Applied Mathematics and Computer Science, Technical University of Denmark in partial fulfilment of the requirements for acquiring a PhD degree. The project was funded by the Villum Kann Rasmussen centre of Excellence: Nano Mechanical Sensors and Actuators, fundamentals and new directions (NAMEC), and was supervised by Associate Professor Anton Evgrafov (DTU Compute) and co-supervised by Professor Mads Peters Sørensen (DTU Compute).

The following are one article and two manuscripts that result from the PhD research.

1. Bolaji James Adesokan, Anton Evgrafov and Mads Peter Sørensen, Simulating cyclic voltammetry under advection for electrochemical cantilevers. *Journal of Mathematical Methods in Applied Sciences*.DOI: 10.1002/mma.3336 (Published), 2015.
2. Bolaji James Adesokan, Xuelin Quan, Anton Evgrafov, Arto Heiskanen, Anja Boisen and Mads Peter Sørensen, Experimentation and Numerical Modeling of Cyclic Voltammetry for Electrochemical Micro-sized Sensors under the Influence of Electrolyte Flow. *Elecrochimica Acta*. (submitted)
3. Bolaji James Adesokan, Anton Evgrafov and Mads Peter Sørensen, Transient dynamics of electric double layer (EDL) characterized by charge transfer and steric effect. (final stage of preparation)

Furthermore, a conference paper was published during the course of the PhD study

- Bolaji James Adesokan, Xuelin Quan, Anton Evgrafov, Arto Heiskanen, Anja Boisen and Mads Peter Sørensen, Hydrodynamics studies of cyclic voltammetry for electrochemical micro biosensors. *J. Phys. Conf. Ser. 574 012008, 2015.*

I have given the following talks during my three years' research:

- Mathematical Modeling and Optimization of Nano-Mechanical Devices, NAMEC meeting, April 02, 2012.
- Cyclic Voltametry in Biosensors, oral presentation, BIT circus, May 15, 2012.
- Modeling Cyclic Voltammetry for Nanomechanical Biosensors Studies, NAMEC meeting, January 03, 2013.
- Electromechanical Coupling towards Nanomechanical Sensors, NAMEC meeting, June 25, 2013.
- Nanomechanical Cantilever Biosensors - a mathematical view, oral presentation, ITMAN Seminar Series, March 07, 2014.
- Hydrodynamics studies of cyclic voltammetry for electrochemical micro biosensors, 3rd International Conference on Mathematical Modeling in Physical Sciences, August 28-31, 2014.

Lyngby, 31-January-2015

Bolaji James Adesokan

Summary (English)

The PhD dissertation is concerned with mathematical modeling and simulation of electrochemical systems. The first three chapters of the thesis consist of the introductory part, the model development chapter and the chapter on the summary of the main results. The remaining three chapters report three independent papers and manuscripts.

As a preliminary to the study, we describe a general model for electrochemical systems and study their underlying mechanisms through electroanalytical techniques. We then extend the model to a more realistic model for microelectrochemical systems which incorporates the finite size of ionic species in the transport equation. The model presents more appropriate boundary conditions which describe the modified Butler-Volmer reaction kinetics and account for the surface capacitance of the thin electric double layer. We also have found analytical solution for the reactants in the bulk electrolyte that are traveling waves.

The first paper presents the mathematical model which describes an electrochemical system and simulates an electroanalytical technique called cyclic voltammetry. The model is governed by a system of advection–diffusion equations with a nonlinear reaction term at the boundary. We investigate the effect of flow rates, scan rates, and concentration on the cyclic voltammetry. We establish that high flow rates lead to the reduced hysteresis in the cyclic voltammetry curves and increasing scan rates lead to more pronounced current peaks. The final part of the paper shows that the response current in a cyclic voltammetry increases proportionally to the electrolyte concentration.

In the second paper we present an experiment of an electrochemical system in a microfluidc system and compare the result to the numerical solutions. We investigate how the position of the electrodes in the system affects the recorded cyclic voltammetry. The result shows that convection influences the charge transfer dynamics on the electrode surface and hence the cyclic voltammetry recorded. In terms of relative high flow to scan rates, the current response is dominated by the convection due to the fresh supply of reactants towards the electrode surface and quick removal of the products. We also establish that at high scan rates and modest flow rates, peak currents are recorded. Finally, the results show that the position of the electrodes is critical when performing cyclic voltammetry under the flow condition. The numerical results show promising agreement with experimental findings which could be critical in designing highly sensitive electrochemical systems.

The last paper explores the numerical solution which describes the non-linear transient responses to a large applied potential at the electrode in a microelectrochemical system. In our analysis, we account for the finite size properties of ions in the mass and the charge transport of ionic species in an electrochemical system. This term characterizes the saturation of the ionic species close to the electrode surface. We then analyse the responses of the system on the charging of the electric double layer. We consider an arbitrary electrolyte solution that is sandwiched between electrodes and allow for electrochemical reactions at the electrode/electrolyte interface. One of the electrodes is biased with a potential which triggers the reaction and the dynamics of the system. We establish that there is a quick build up of boundary layers in the double layer, but the finite size constraint on the ionic species prevents overcrowding of the ionic species. The result also shows that reactants which undergo charge transfer at the electrode/electrolyte interface crowded the electric double layer and the dynamics of the electric double layer is controlled by the charge transfer.

Summary (Danish)

Emnet for denne PhD afhandling er studiet af elektrokemiske mikrofluid systemer, hvor elektroderne består af mikrobjælker. Fokus er rettet mod indflydelsen af fluid flow på de elektrokemiske processer samt indflydelsen af ultrahøje ion koncentrationer tæt på elektroderne. Den videnskabelige metode er baseret på matematisk modellering samt simulering på computer, men i nært samarbejde med eksperimental fysikere. Afhandlingen er organiseret i 6 kapitler hvoraf de tre første består af en indledning, en udledning af den matematiske model samt et kapitel med simuleringer og resultater. Herefter følger tre kapitler indeholdende en publiceret artikel og to øvrige manuskripter.

Modellen er baseret på Nernst Planck ligningen, som er en partiel differentialligning for ion koncentrationen i en elektrolyt, hvor transport af ioner indgår forårsaget af diffusion, elektriske felt gradienter og fluid flow. Randbetingelserne beskriver de kemiske reaktioner og elektriske ladningsudvekslinger på mikrobjælke elektroderne. Mere specifikt benyttes en modificeret version af Butler-Volmer reaktions kinetic ved elektroderne samt inkorporerer overflade kapacitans forårsaget af det tynde elektriske dobbelt lag. Butler-Volmer randbetingelserne er ulineære så systemet som helhed er ikke-lineært. Det elektriske felt styres af Poison ligningen for det elektriske potentiale. Poison ligningen og Nernst Planck ligningen er koblet. Fluid flowet i den givne geometri beregnes fra Navier-Stokes ligninger.

I afhandlingen simuleres en elektrokemisk analyse metode kaldet cyklisk voltammetri. I denne metode måles strømmen gennem elektrolytten som funktion af en påført tidsperiodisk elektrisk spænding. Den periodiske spænding har "savtak-form, det vil sige den er sammensat af stykkevis lineære funktioner. I den

første artikel undersøges effekten af fluid flow hastigheden, skanfrekvenser, og koncentrations variationer på cyklisk voltammetri. Cyklisk voltammetri udviser hysterese og det er vist at hysteresløjfen reduceres ved høje fluid hastigheder. Høje scanfrekvenser fører til mere udprægede strøm toppe. Simuleringer viser at strøm responsen i cyclisk voltammetri er proportional med ion concentrationen.

De simulerede cycklisk voltammetri kurver for en mikrofluid elektrokemisk celle med mikro bjælker som elektroder er blevet direkte sammenholdt med eksperimentelle resultater. Med passende estimation af parametre og modelopbygning er der opnået rigtig fornuft overensstemmelse mellem computer simuleringer og målinger. Resultaterne viser at konvektion har indflydelse på ladningsudveksling ved elektroderne i den strømmende fluid og dermed på strøm-spændingskurverne i cyklisk voltammetri. Ved relative høje flow hastigheder i forhold til scanfrekvenser er strøm responsen domineret af konvektion på grund af tilførsel af nye reaktanter på elektrode overfladen samt hurtig fjernelse af reaktions produkterne. Placeringen af mikrobjælke elektroderne i fluid strømmen spiller ligeledes en væsentlig rolle for cyklisk voltammetri.

I sidste kapitel i afhandlingen studeres effekten af ionernes endelig størrelse for opbygning af ion koncentrationen ved mikrobjælke elektroderne. Såfremt man ikke tager hensyn til ion størrelsen divergerer ion koncentrationen ved elektroderne under påvirkning af store spændinger. For at undgå denne singularitet indføres en concentrations afhængig diffusionskonstant i Nernst Planck ligningenerne. Denne ikke-lineære diffusionkonstant er faktisk singulær ved mætnings concentrationen, som opstår når ionenerne er pakket helt sammen og er i kontakt med hinanden. Denne situation svarer til uendelig ionstrøms hastighed. Dette lyder som et paradoks, men det ikke-lineære diffusionsled i Nernst Planck ligningenen regulariserer koncentrationen ved elektroderne således at den ikke overskrider koncentrationen for tættest pakkede ioner. Simuleringer viser at det ikke-lineære diffusionsled føre til dannelse af kink formede randlag i ionkoncentrationen. Det er også vist analytisk at for simple tilfælde med ladningsneutralitet eksistere ikke-lineære løbende bølgerløsninger af ion koncentrationen, analogt til shockbølger og solitoner.

Acknowledgements

First, I would like to thank my supervisors Associate Professor Anton Evgrafov and Professor Mads Peter Sørensen for their support and immense commitment to the project and for their patient in sharing their knowledge for the completion of my studies. I am very grateful for their effort and guidance that was put into this project. Thank you very much.

This work was supported by the Villum Kann Rasmussen centre of Excellence: Nano Mechanical Sensors and Actuators, fundamentals and new directions (NAMEC). I am indeed grateful for their financial support that I have received.

I am indebted to all the people who have made this work a success, especially my colleague Xuelin Quan from DTU Nanotech for her support in carrying out the experiments. I am also very grateful to Associate Professor Arto Heiskanen of DTU Nanotech for your patience and your guidance in electrochemistry which I was a novice at the start of the thesis. I would also like to say a big thank you to Professor Yuri Gaididei for your interesting and inspiring conversation whenever you visit DTU Compute.

This work would not have been a success if not for the moral support of some wonderful people that I met in Copenhagen. This list is long, but I would like to specially mention Øistein Wind-Willassen who made me settled in at the department, the IFS at DTU, Yemi and Chichi, Adebowale and Bimpe, Solomon and Lucy, Sunday and Miriam. Thank you for your great help. I would also like to thank my friends Kayode and Moyosore Imole from the Netherlands and of course Austin and Adaora Ezejiofor from Germany. My sincere gratitude

also my colleagues from Copenhagen Christian Centre; John, Allan and Greg. Thank you for your prayers.

I would like to specially thank my wonderful wife Mary Oluwafunke and our special children Ayomide and Oluwaseyi for their care and endless support. To my parents Eyinade and Alice Adesokan, and my brother Adewale and sisters Mojirayo and Odunayo, I say a big thank you. I am also indebted to my second parents, Samuel and Grace Matesun, thank you for always been there. Lastly, I am eternally grateful to God for giving me the opportunity to pursue this PhD degree.

Contents

Chapter 1

Introduction

Electrochemical systems are all around us. They have become indispensable and found widespread applications in industrial processes such as oil drilling and oil refining, corrosion industry, waste water treatment, toxic gas monitoring, medical applications - implantable electrochemical systems for monitoring diabetic patients. Electrochemical systems are also present in biochemical environments as well as in systems such as automobile emission control, microchips, lab on chips, electro analytical devices, and airplanes. They are also found in electronic devices that have become part of our everyday life; for example the batteries that power our gadgets like mobile phones, laptops and tablets, are electrochemical systems. Another electrochemical system that is gaining pace in popularity is the fuel cell for generating alternative energy. The list is inexhaustible.

A quick search of electrochemical systems on Google Scholar takes about 0.08secs and results in over a million articles on the subject. So why are we interested in a vastly studied subject? The study of electrochemical systems is still very relevant and keeps expanding due to its vast area of applications, especially since the effort for miniaturisation of electrochemical devices started about forty years ago [1]. In this thesis, we shall study the mathematical modeling and analysis of microelectrochemical systems and its reactions.

An electrochemical system is a system that comprises of electrodes and an electrolyte solution by which one form of energy is converted to another, typically, a

chemical energy is converted to electrical energy and vice versa. The electrodes can be of any type and shape but mostly they are conductors or semi conductors either in solid or liquid form, for example, carbon rod - graphite, copper wire, nickel rod, silicon rod, zinc rod, mercury, amalgams etc. The electrolyte can come in form of a liquid solution in which soluble ions are present e.g. Na^+, Cl^-, H^+. They can also occur in form of fused salts, solid electrolytes and conductive polymers, e.g. molten NaCl-KCl eutectic, sodium β-alumina, Nafion [2].


Alessandro Volta
(1745-1827)

Alessandro Volta's famous invention of Voltaic pile in the 1800s which results in electricity was the first electrochemical system reported. However, the foundation of the modern understanding of the electrochemical systems started with Michael Faraday's famous experiment on electrolysis in the 1830s. He famously developed quantitative laws which relate the amount of electricity produced in an electrochemical system to the amount of the transformed chemical substances. Around 1880, Nernst and Planck [3, 4] developed the mathematical model of a working electrochemical system where they describe the system as a stream of the ionic species controlled by diffusion, migration and convection. Their model results in the systems of differential equations of elliptic and parabolic type. This model is termed Poisson-Nernst-Planck equation (PNP).

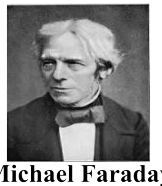
Michael Faraday
(1791 - 1867)

The rapid progress in electrochemical technologies in the early twentieth century triggered the development of experimental designs and the theory governing the electrochemical system. Over the years, there have been many reviews reporting the advancement of the studies of electrochemical systems. The analysis of electrochemical systems has been examined in textbooks [5, 6, 7, 2, 8, 9, 10], reviews and several journal publications. Bard *et al* and Newmann *et al* [2, 8] gave a comprehensive and thorough analysis of the subject. Leddy *et al* [11] provides a review of historical perspectives on the topic while Bard *et al* and Volgin *et al* [12, 13] present recent reviews on the subject where they briefly introduce the history of the topic and present a review of earlier publications on the subject while focusing primarily on the applications of electrochemical systems in different fields. Prentice *et al* [14] surveyed early publications on the numerical aspects of the subject in which they detailed comprehensive collections of methods and examined critical analysis of both the numerical and the electrochemical aspects of the subject. In addition, Schlesinger *et al* [15] has also provided a recent review that focuses mainly on the numerical techniques.

By the mid 20th century, the theory describing the mass transfer process of streams of ions in an electrochemical system was well developed. Typically, the

migration term in the commonly used Nernst-Planck model allows one to determine the distribution of the electrical potential which requires solving Poisson's equation that relates the electric field to the space charge density. Generally, the charge density is set to zero, which is referred to as the electroneutrality condition. This condition significantly simplifies solving the Nernst-Planck equations and the corresponding distribution of the electrical potential. However, such approximation is only applicable to systems characterized by the dimension of an electrochemical system far greater than that of the space charge density. Such a system is termed a macro electrochemical system.

Around 1980s, miniaturized electrochemical systems became available and started a billion dollar industry of micro electroanalytical devices [16, 17, 18] especially in the biosensor industry. Micro/nano electrochemical systems come with great advantages and have led to new technologies and methodologies. One of the advantages of such systems is the decrease in ohmic potential drop across the electrolyte. Another advantage is the formation of fast steady state signals as well as the increase in the measured current as a result of enhanced mass transport at the electrode surface. In addition, there is an increase in the signal to noise ratio in a micro electrochemical system. This is essential in the design of highly sensitive electrochemical sensors. Furthermore, micro electrochemical systems have the advantage of recording high current densities and abilities to measure currents and charges in micro/nano amperes. Nevertheless, the mathematical treatment of analysis of such systems differs from that of a macro system.

For microelectrochemical systems the electrode-electrolyte interface plays a crucial role and consequently limits to what extent the simplified models for macro systems can be applied. For example, if a potential of more than 50mV is applied to an electrode in a microelectrochemical system, the ionic concentration is usually overestimated by the theory [19, 20]. One of the reasons for this feature is the fact that ionic species are treated as point charges and the finite size of ions is discarded as in macro systems. This assumption becomes invalid because close to the electrode surface the ion concentration can get very high due to the crowding effect and electroneutrality breaks down in this region. As a consequence, the ion transport model should account for the finite size of ions and the model must be coupled to appropriate boundary conditions which incorporate the region where electroneutrality breaks down. Furthermore, in modeling microelectrochemical systems the surface charge density cannot be set to zero which means that Poisson's equation couples directly to the Nernst-Planck equation through the concentration field. In addition, the presence of a very small coefficient in the highest derivative of the Poisson's equation in a microelectrochemical system introduces boundary layers, which makes the problem mathematically challenging both numerically and analytically.

The model for a microelectrochemical system divides the ionic streams in the electrolyte solution into two regions, namely the electroneutral bulk region (as in the macro model) far away from the electrode and the electric double layer (EDL), a region adjacent to the electrode. The electric double layer is a set of nested layers, which consists of the inner compact layer referred to as the Stern layer, and the outer diffuse layer also known as the Debye layer. The typical width of an EDL is about 1-10Å depending on the electrolyte solution. Within the electric double layer there is usually no net charge separation which means that one or more ionic species can occur in excess and hence electroneutrality condition does not hold in this region. Typically, the Stern layer of the double layer is considered to be the compact layer where ions adhere to the surface of the electrodes and a capacitive effect of the ions within the compact layer is included while formulating the appropriate boundary conditions. The most important work on the Stern layer was performed both theoretically and experimentally by Stern and Grahame, respectively [21, 22]. On the other hand, the Debye layer is the region where the diffuse-charge effect of the ionic species is normally accounted for. In addition, the dynamical charging of the layer is considered to have essential effect on the charge transfer kinetics at the electrode-electrolyte interface.

Numerous authors have attempted to incorporate models for the electric double layer in modeling of ion and charge transport in a microelectrochemical system. Bazant *et al* and Chu *et al* [23, 24] have considered steady state transport model and studied the diffuse charge effect in the electric double layer. They adopted the classical Poisson-Nernst-Planck equations for a binary and symmetric electrolyte but neglect the steric effect due to the finite size of ions. Their model is suitable for the dilute electrolyte solution. Time dependent transport models have also been studied in [25, 26, 27] for a binary and symmetric electrolyte albeit without taking the steric effect into account. These models have been extended by Bazant *et al*, Kilic *et al* and Olsen *et al* [28, 29, 30] to investigate concentrated electrolyte under large applied potential while accounting for the finite size effect of the ions. In their studies, they solved the modified Poisson-Nernst-Planck equations that is valid for binary and symmetric electrolytes which is characterized by large potentials. The authors included an extra term in the chemical potential and mass flux to account for the finite size of ionic species. Furthermore, in their model they have prescribed blocked electrode boundary conditions which means there are no electrochemical reactions at the electrodes.

In many practical applications, ionic charges of higher valence are present in an electrochemical system. For example, the human blood plasma contains high concentration of Na^+, Ca^{2+}, Mg^{2+}, Cl^-, HCO_3^-, HPO_3^{2-}, SO_4^{2-}. It is therefore essential to model electrochemical systems in a general sense of arbitrary valence charges. In addition, in most realistic electrochemical systems,

reactions on electrode surfaces allow for passage of a current, which means that the conservation laws at the electrode-electrolyte interface must be augmented by the introduction of Faradaic current at the surface of the electrode and its corresponding electrolyte flux density.

1.1 Thesis Structure

The thesis is structured as follows:

In the first chapter we give a historical overview of an electrochemical system from macro to micro systems. This is followed in chapter two where we consider the concept of an electrochemical system by explaining the components and the makeup of its system. We then proceed to systematic modeling of an electrochemical system and clearly differentiate between the macro and micro electrochemical systems. We state some important results in chapter three and finally we present three independent articles and manuscripts that emerge from this project. We conclude in the last chapter and describe consideration for the future work.

Chapter 2

Mathematical Modeling of Electrochemical Systems

In this section, we introduce the general concept of an electrochemical system. We define each component that makes up an electrochemical system and systematically develop the mathematical model of a working system. We distinguish between a macro and a micro electrochemical system. Special attention is given to how boundary conditions are defined for both macro and micro electrochemical systems. Part of the formulation was adapted from references [8, 20]. We also introduce the concept of electroanalytical techniques that characterize the working of an electrochemical system.

2.1 Electrochemical Systems: concepts and components

An electrochemical system is a network of interrelated components where chemical changes spontaneously induce electric current due to the application of an external potential, see Figure 2.1. The system can be complicated by several factors. Ions can interact with each other and/or the solvent, they can also interact with the boundary of the electrodes and other boundaries present in

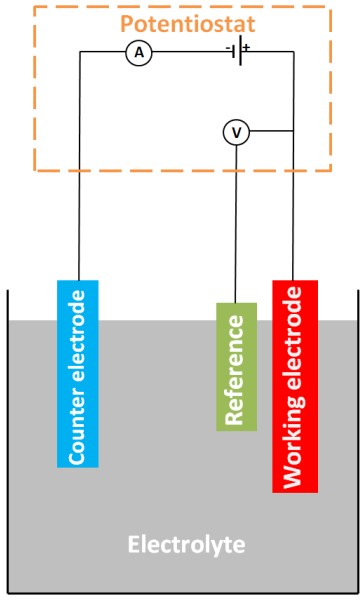

Figure 2.1: An electrochemical system

the system. In what follows, we present the components of an electrochemical system.

2.1.1 Electrodes

Electrodes are media through which free or delocalized electrons move due to conduction. Typically, there are no chemical changes during conduction. However, electrons move only within the electrodes and the wires that connect the external circuit to the electrodes. At the electrodes surface, reduction and oxidation occur. Often, reduction occurs at the negatively charged cathode electrode. Here, one equivalent of ions reduced requires one equivalent of the electron to be absorbed by the electrode. In addition, any reduction must be accompanied simultaneously by oxidation occurring at the anode, the positively charged electrode. As a consequence, there must be at least two electrodes to have a functional electrochemical system. Typically, there are three types of electrodes in a working electrochemical system. They are described below.

Working electrode

The working electrode is the electrode of interest in which the electrochemical reaction is monitored. Its potential is sensitive to the electrolyte's concentration. A typical working electrode is made from a chemically inert conductor. The most common types include platinum, gold, glassy carbon, graphite and mercury. These electrodes usually have a good positive potential range.

Counter electrode

The counter electrode is an auxiliary electrode which acts as a source or sink of electrons in an electrochemical system. The presence of a counter electrode in an electrochemical system allows the current to pass through the electrolyte solution so that it does not pass through the reference electrode. This allows for removal of varying voltage at the reference electrode due to voltage drop or polarization at the reference electrode. In an ideal system, the potential of the counter electrode must remain constant in order to ensure that any change in potential of an electrochemical system is assigned to the working electrode.

In principle, the nature of the counter electrode should have little or no effect on an electroanalytical measurement. However, if the surface area of the counter electrode is small relative to the working electrode area inaccuracies may arise due to the additional resistance imposed by the counter electrode. For this reason, it is wise to keep the surface area of the counter electrode relatively large. Also, the counter electrode should be made of an electrochemically inert material such as platinum or graphite.

Reference electrode

The reference electrode is used to stabilize against voltage drops and polarization effects that would be unavoidable in a two-electrode system. The main purpose of the reference electrode is to provide a stable, well-known half-reaction on which to reference the redox process occurring at the working electrode. Reference electrode ensures that any change in an electrochemical system goes through the electrolyte thereby affecting the potential of the working electrode. By convention, the reference electrode is the anode.

2.1.2 Electrolyte

The electrolyte is a medium that supports free moving ions and conducts an electric current. An electrolyte consists of moving charged particles that constitute the electric current. Usually, electrolytes are found in the form of acids, alkalis or salts and most often they contain at least two ions flowing in the opposite directions; positively charged cations and negatively charged anions which are attracted to negative and positive electrodes, respectively. One exception to this is the lithium ion which migrates from one electrode to another in the lithium battery. Their electrical conduction is usually accompanied by chemical changes. Usually, there is no electron flow in the solution, but through the electrode and the external connected wires. Apart from the main electrolyte that partakes in an electrochemical reaction within an electrochemical system, a supporting electrolyte is often added to the system to increase the ionic conductivity of the medium. With the electrolyte one minimizes solution resistance to charge flow through the electrochemical system. It also minimizes migration as a means of mass transport to the electrode. However, the supporting electrolyte does not partake in the electrochemical reaction.

2.1.3 External wires

The final component of an electrochemical system is the external wire that connects the electrodes to the load so that electrons can flow between the electrodes. The current that flows through the external wire in an electrochemical system is the measure of the flux of electrons which corresponds to the flux of reactants or products transformed during the electrochemical reactions.

Having introduced the components of an electrochemical system, we proceed by explaining the mechanism of the processes that are involved in an electrochemical system and develop the mathematical model of a working electrochemical system. We start with the mathematical model of a macro electrochemical system.

2.2 Electrode reaction and kinetics of electron transfer

When the potential at the electrodes is disturbed, the ions in the electrolyte solution may decompose and results in net chemical changes in the region close

to the electrode surface. The electrochemical conversion results in a net flux of ionic species at the surface of the electrode and by such a net flux of electrons results in electrical current flowing through the external circuit. The overall process is called the electrode reaction.

An electrode reaction usually involves interchange of charges between electrons from the electrode and ionic species in the electrolyte. There are three major steps involved in the process: (1)reactants migrate towards and/or outward the electrode surface through the mechanism of mass transfer; (2)ionic species close to the surface of the electrode, through charge transfer, absorb or release electron to form product depending on the sign of the potential of the electrode; and finally (3)the products move away from the electrode and fresh reactants move towards the electrode surface. The differences between the conductivity of the electrode and the electrolyte solution allows for continuous flow of electricity at the electrode/electrolyte interface.

Consider the following electrode reaction,

$$O + ne^- \underset{k_a}{\overset{k_c}{\rightleftharpoons}} R, \tag{2.1}$$

where O and R are the reactants and product respectively, and n is the number of electrons participating in the reaction, k_a, k_c are oxidation and reduction rate constants respectively. By Faraday's law, the rate of an electrode reaction and the current density is given as

$$\frac{dN}{dt} = \frac{j}{nF} \tag{2.2}$$

where N is the number of moles of the reactants, j is the current density and F is the Faraday's constant. Assuming the constant current density through the electrode surface, the total current I flowing through the electrode surface can be obtained by multiplying the surface area A of the electrode with the current density, thus, $I = jA$.

Furthermore, the net electrical current flowing through the external circuit during the electrochemical reactions at the electrode/electrolyte interface is given as $I = I_a - I_c$ where $I_a,\ I_c$ are the anodic and cathodic currents due to oxidation and reduction, respectively. This implies that the current density satisfies the following relation

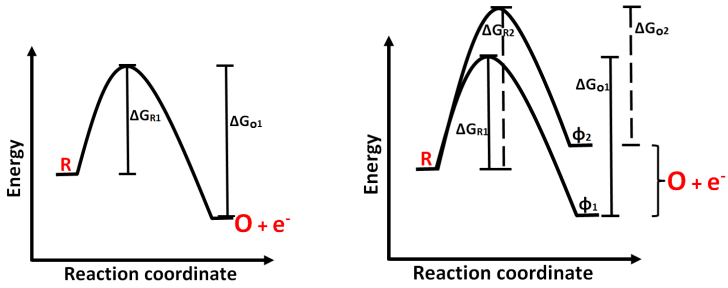

Figure 2.2: Reaction coordinate showing the effect of change in electrode potential on the free energy curves.

$$\begin{aligned} j = \frac{I}{A} &= j_a - j_c \\ &\underbrace{=}_{eqn(2.2)} nF\left(\frac{dN_a}{dt} - \frac{dN_c}{dt}\right), \end{aligned} \tag{2.3}$$

and by the law of mass action for the reaction (2.1) the current density from (2.3) can finally be written as

$$j = nF(k_a C_R - k_c C_O) \tag{2.4}$$

where C_O and C_R are the surface concentration of reactants and product respectively.

For a fixed voltage ϕ_1, Figure (2.2a) shows the thermodynamic response of an electrochemical reaction. Denote the activation free energy for both oxidation and reduction by $\triangle G_{O1}$ and $\triangle G_{R1}$, respectively.

If the electrode potential is reduced to a potential ϕ_2, as shown in Figure (2.2b), then the activation energy for the oxidized reaction is lowered to $\triangle G_{O2}$ and hence the energy is increased by an amount $nF(\phi_2 - \phi_1)$. This implies that for the oxidized reaction the activation barrier is effectively lowered by a fraction $\beta nF(\phi_2 - \phi_1)$. Let us denote the fraction by β, the symmetric factor. On the other hand, for the reduced reaction, the activation energy is raised to $\triangle G_{R2}$ and increased by an amount $(1-\beta)nF(\phi_2 - \phi_1)$.

In summary, the activation energies by both oxidation and reduction have been shifted as follows

$$\begin{aligned} \triangle G_{O2} &= \triangle G_{O1} + \beta nF(\phi_2 - \phi_1), && (2.5)\\ \triangle G_{R2} &= \triangle G_{R1} - (1-\beta)nF(\phi_2 - \phi_1). && (2.6) \end{aligned}$$

We replace the difference in potential by a reference potential ϕ and define transfer coefficients $\alpha_a = (1-\beta)n$ and $\alpha_c = \beta n$ for the oxidized and reduced reactions respectively, to obtain the following

$$\begin{aligned} \triangle G_{O2} &= \triangle G_{O1} + \alpha_c F\phi, && (2.7)\\ \triangle G_{R2} &= \triangle G_{R1} - \alpha_a F\phi. && (2.8) \end{aligned}$$

As in other chemical reactions, the electrochemical reaction rates are obtained through the Arrhenius equation

$$k_a = k\exp\left(\frac{-\triangle G_R}{RT}\right), \quad k_c = k\exp\left(\frac{-\triangle G_O}{RT}\right), \tag{2.9}$$

where k is a constant, R and T are the gas constant and the absolute temperature respectively. We substitute equations (2.7) and (2.8) into equation (2.9) and obtain

$$k_a = k\exp\left(\frac{-\triangle G_{R1}}{RT}\right)\cdot\exp\left(\frac{\alpha_a F\phi}{RT}\right), \quad k_c = k\exp\left(\frac{-\triangle G_{O1}}{RT}\right)\cdot\exp\left(\frac{-\alpha_c F\phi}{RT}\right). \tag{2.10}$$

Since $\triangle G_{O1}$ and $\triangle G_{R1}$ are the activation energies at the reference potential the following holds

$$k_a = \tilde{k}_a\exp\left(\frac{\alpha_a F\phi}{RT}\right), \quad k_c = \tilde{k}_c\exp\left(\frac{-\alpha_c F\phi}{RT}\right), \tag{2.11}$$

with

$$\tilde{k}_a = k\exp\left(\frac{-\triangle G_{R1}}{RT}\right), \quad \tilde{k}_c = k\exp\left(\frac{-\triangle G_{O1}}{RT}\right). \tag{2.12}$$

From equations (2.4), (2.11) we derive the current density observed in an electrochemical reaction to be

$$j = nF\left[\tilde{k}_a C_R\exp\left(\frac{\alpha_a F\phi}{RT}\right) - \tilde{k}_c C_O\exp\left(\frac{-\alpha_c F\phi}{RT}\right)\right]. \tag{2.13}$$

At equilibrium, the rate of the electrochemical reaction is zero. This implies that equation (2.13) is set to zero. Let ϕ_0 be the equilibrium potential at which

this happens so that we have

$$\tilde{k}_a C_R \exp\left(\frac{\alpha_a F \phi_0}{RT}\right) = \tilde{k}_c C_O \exp\left(\frac{-\alpha_c F \phi_0}{RT}\right), \tag{2.14}$$

and when we take the logarithm of both sides and re-arrange we obtain the expression for the equilibrium potential as

$$\phi_0 = \frac{RT}{nF}\left[\ln\left(\frac{\tilde{k}_c}{\tilde{k}_a}\right) - \ln\left(\frac{C_R}{C_O}\right)\right]. \tag{2.15}$$

Expression given in (2.15) is the Nernst equation, see for example [2, 20, 8].

When there is an electrochemical reaction across the electrode/electrolyte such that there is a departure from the equilibrium potential, overpotential η is recorded. Overpotential is modeled as the difference between the electrode potential and the corresponding equilibrium potential,

$$\eta = \phi - \phi_0. \tag{2.16}$$

If we substitute equations (2.15) and (2.16) into equation (2.13) we obtain

$$\begin{aligned} j \;=\; & nF\tilde{k}_a C_R \exp\left(\frac{\alpha_a F}{RT}\left[\eta + \frac{RT}{nF}\ln\left(\frac{\tilde{k}_a}{\tilde{k}_c}\right) - \frac{RT}{nF}\ln\left(\frac{C_R}{C_O}\right)\right]\right) \\ & -nF\tilde{k}_c C_O \exp\left(\frac{-\alpha_c F}{RT}\left[\eta + \frac{RT}{nF}\ln\left(\frac{\tilde{k}_a}{\tilde{k}_c}\right) - \frac{RT}{nF}\ln\left(\frac{C_R}{C_O}\right)\right]\right) \end{aligned} \tag{2.17}$$

When we perform a few manipulations with equation (2.17) we obtain

$$j = j_0\left[\exp\left(\frac{\alpha_a F}{RT}\eta\right) - \exp\left(\frac{-\alpha_c F}{RT}\eta\right)\right], \tag{2.18}$$

where j_0 is the exchange current density defined by

$$j_o = nF\tilde{k}_a^{-\beta}\tilde{k}_c^{1-\beta}C_R^{-\beta}C_O^{1-\beta}.$$

It is the measure of the rate of exchange of the reactant and the product at the electrode/electrolyte interface at the equilibrium. It also expresses the height at which both the reactant and the product are at the same activation energy level. The expression in equation (2.18) is the famous Butler-Volmer equation

developed by Butler, Volmer and Erdey Gruz [31, 32] in the 1930s. It characterizes the rate of electrode reactions as a result of overpotential across the electrode/electrolyte interface and two kinetic parameters of the reactions. The Butler-Volmer equation suggests that the potential drop from the electrode to the bulk electrolyte triggers the electrochemical reaction kinetics.

Finally, the Butler-Volmer equation (2.18) is the standard electrochemical approach to model reaction kinetics across the electrode/electrolyte interface. However, it fails to account for the structure of the electrode/electrolyte interface which is crucial in order to model a microelectrochemical system. Instead of considering the potential drop between the electrode and the bulk electrolyte, we postulate that there is a local potential drop across a thin dielectric layer coating, the Stern layer, which is the closest layer to the electrode from the electrolyte. In addition, we also assume that electron transfer happens at this layer which means that the potential within the Stern layer also affects the reaction kinetics. In the section on electric double layer, we suggest the boundary condition such that the Stern layer satisfies a Robin type boundary condition where the normal electric field equates the Stern layer potential. We shall combine this boundary condition with the Butler-Volmer equation for the charge transfer reactions, thereby providing a more realistic boundary conditions for a microelectrochemical system. An interesting review on the historical review of such an approach can be found in [27].

In what follows, we will introduce another process that affects the reaction kinetics and phenomena on which the whole electrochemical system is based.

2.3 Mass transfer

From the previous section, we have established that the current recorded in an electrochemical system can be influenced by the applied potential and the reaction kinetic constants. On the other hand, before we record any current electrode reactions across the electrode/electrolyte interface must occur. For any net reaction to take place at an appropriate rate, reactants and the products must be transported to and from the surface of the electrode in order to balance the net flux and influence the electrical current recorded across the electrode/electrolyte interface. In this section, we discuss three mechanisms of mass transport of reactants in the electrolyte solution towards the electrode surface and the means, by which the ionic products are transferred back into the electrolyte solution.

Convection

Convection stems from a force on the electrolyte solution. In convection, the whole electrolyte solution travels. The ionic species in the electrolyte solution move towards and leave the electrode surface by being driven in a moving electrolyte solution. Motivated by the experiment reported in our Paper II, we introduced convection into the electrochemical system through a controlled pump so that only laminar flow profile is considered. The details can be found in Paper I and Paper II.

In the microfluidic system studied in the papers, the solution is introduced from the left hand side and pumped through the pipe with outlet on the right hand side. The convective flux of the ionic species C_j traveling at an average velocity, v is given as

$$N_{conv} = vC_j. \tag{2.19}$$

Diffusion

Diffusion occurs in all solutions due to concentration gradients. Typically, diffusion does not occur due to any physical force, but due to uneven electrolyte solution seeking to maximize its entropy. The Brownian motion of all ionic species tries to enhance regions of low concentration from the region of higher concentration. Diffusion is very significant in an electrochemical system because electrochemical reactions occur at the surface of the electrode. As a consequence, the concentration of the reactants will always be lower at the electrode surface than in the bulk electrolyte solution. However, the concentration of the products near the electrode will be higher compared to the ones further into the electrolyte solution.

The diffusive flux is proportional to the concentration gradient with the diffusion coefficient as its proportionality. Since a positive concentration gradient will induce a flux towards a negative direction, we model the diffusive flux for ionic species C_j as follows

$$N_{diff} = -D_j \nabla C_j, \tag{2.20}$$

where D_j is the diffusivity of ionic species j. This is called the first Fick's law.

Migration

Mass transfer due to migration is a consequence of the electrostatic effect which results from the application of potential difference between the electrodes and the presence of charged ionic substances in the electrolyte solution. The application of potential difference between the electrode surfaces creates a charged surface, thereby attracting or repelling any charged species near the electrode due to the presence of the electrostatic forces. Let ϕ be the local potential in any region of the electrolyte bulk solution. Then, the flux due to migration can be written as

$$N_{mig} = -z_j u_j F C_j \nabla\phi, \tag{2.21}$$

where z_j, u_j are the charge and the mobility of the ionic species j.

In what follows, we formally establish the mathematical model which describes a working electrochemical system.

Total ionic flux in the bulk electrolyte

In an electrolyte solution the total flux is given as the contribution of fluxes due to diffusion, migration and convection which is

$$N_j = -\underbrace{D_j \nabla C_j}_{diffusion} \quad -\underbrace{u_j z_j F C_j \nabla\phi}_{migration} \quad + \underbrace{C_j v}_{convection}. \tag{2.22}$$

If we use the Nernst-Einstein equation, we can re-write expression (2.22) as follows

$$N_j = -D_j \left(\nabla C_j + \frac{z_j F}{RT} C_j \nabla\phi \right) + C_j v, \tag{2.23}$$

which equivalently can be re-written as

$$N_j = -\frac{D_j}{RT} C_j \nabla \left(RT \ln(C_j) + z_j F \phi \right) + C_j v. \tag{2.24}$$

From thermodynamics, the electrochemical potential of ionic species j of uniform concentration C_j and potential ϕ in an electrolyte solution can be defined by

$$\mu_j = \mu_j^o + RT \ln(\gamma_j C_j) + z_j F \phi, \tag{2.25}$$

where μ_j^o and γ_j are the standard electrochemical potential and the activity coefficient, respectively. We can therefore re-formulate the total ionic flux within the electrolyte solution as follows

$$N_j = -\frac{D_j}{RT} C_j \nabla \mu_j + C_j v. \tag{2.26}$$

This implies that the gradient of the electrochemical potential seems to be the driving force for migration and diffusion, although the flux is still complicated by the presence of the convection in the system. As will be seen later, the activity coefficient γ_j shall be modeled to account for the finite size of ionic species in the bulk electrolyte.

2.3.1 Mass and charge conservation

In this section, we start by considering the charge conservation where we define the total current in an electrolyte solution and then state the mass conservation for the concentration of the ionic species.

In an electrolyte solution, the movement of ionic species contributes to the total net current. If we assign the charge Fz_j to the flux of the ionic species and sum them over all species, then the total net current in the electrolyte solution is given by

$$i = F \sum_j z_j N_j. \tag{2.27}$$

We substitute the flux expression (2.24) into equation (2.27) and expand the resulting expression to obtain

$$i = -F^2 (\sum_j z_j^2 u_j C_j) \nabla \phi - F \sum_j z_j D_j \nabla C_j + F (\sum_j z_j C_j) v. \tag{2.28}$$

Equation (2.28) suggests that the net current in the electrolyte solution due to ionic species is determined by both the concentration and the potential gradient as well as the velocity of the electrolyte solution. Since in an electrolyte bulk solution the concentration of the charged ionic species must be electrically

neutral, then the electroneutrality condition is defined as

$$\sum_j z_j C_j = 0. \tag{2.29}$$

The last term in the electrical current equation (2.28) is the electroneutrality condition and hence the equation for the current becomes

$$i = -\kappa \nabla \phi - F \sum_j z_j D_j \nabla C_j, \tag{2.30}$$

where κ is the electrolyte conductivity defined by

$$\kappa = -F^2 \sum_j z_j^2 u_j C_j. \tag{2.31}$$

Now recall the ionic flux equation (2.24). For each ionic species j the equation describing the mass balance is given by

$$\frac{\partial C_j}{\partial t} = -\nabla \cdot (-u_j z_j F C_j \nabla \phi - D_j \nabla C_j + C_j v) + S_j. \tag{2.32}$$

Equations (2.32) are commonly referred to as the Nernst-Planck equations. Here, S_j is the source or sink term which could be used to describe any bulk reaction to produce or consume ions in the electrolyte solution. Throughout this work, we set $S_j = 0$ since no species are allowed to be created in the bulk electrolyte.

When we multiply the Nernst-Planck equations (2.32) by Fz_j and sum over j we obtain

$$\frac{\partial}{\partial t} \sum_j (F z_j C_j) = -\nabla \cdot \sum_j F z_j (-z_j u_j F C_j \nabla \phi - D_j \nabla C_j + C_j v), \tag{2.33}$$

and by electroneutrality condition (2.29) the left hand side equals zero. The convective term on the right hand side also vanishes due to the electroneutrality condition. And when we substitute the expression for current (2.28) into the mass balance equation equation (2.33), we obtain the following equation for the conservation of charges:

$$\nabla \cdot i = 0, \tag{2.34}$$

Equations (2.32) and (2.34) couple the ionic concentration and the electric potential in the bulk electrolyte. However, in order to close the system we need to

determine the velocity field v due to the convective term. This can be done by solving the Navier-Stokes equations for an incompressible flow,

$$\nabla \cdot v = 0 \,, \tag{2.35}$$

$$\rho\left(\frac{\partial v}{\partial t} + v \cdot \nabla v\right) = -\nabla p + \mu_D \nabla^2 v + s_f \,. \tag{2.36}$$

The fluid density is denoted by ρ, p is the pressure, μ_D is the dynamic viscosity and finally s_f denotes an external force per unit volume [33, 34]. Finally, equations (2.32), (2.34), (2.35) and (2.36) must be solved with the appropriate boundary conditions.

2.3.2 Boundary conditions

As we have established in the electrode kinetics section, the measured current in an electrochemical system depends both on the potential at the surface of the electrode - at least within the thin layer above it and the electrochemical reactions. It is necessary to prescribe the right boundary conditions to properly complete the model. At the inlet, we specify constant concentrations of the ionic species and a no flux boundary condition $-n \cdot N_j = 0$ on the fluidic cell walls, where n is the unit normal pointing towards the electrolyte. At the outlet of the cell we specify $D\dfrac{\partial C_j}{\partial n} = 0$. At the insulating surfaces $\partial\Omega_{ins}$ there is no current flow, which means that the normal current density i_n across such a boundary is zero, that is

$$i_n = 0 \qquad \text{on} \qquad \partial\Omega_{\text{ins}}. \tag{2.37}$$

In other words, from the conservation of the electric current (2.34) we can prescribe Neumann type boundary conditions

$$\kappa\frac{\partial \phi}{\partial n} = -\sum_j z_j D_j \frac{\partial C_j}{\partial n} \qquad \text{on} \qquad \partial\Omega_{\text{ins}} \,. \tag{2.38}$$

However, at the electrode surface the ionic flux for each species j can be modeled

by the normal current density determined from electrode kinetics,viz

$$\kappa \frac{\partial \phi}{\partial n} + \sum_j z_j D_j \frac{\partial C_j}{\partial n} = i_n(C_j, \phi, v; \phi_{app}) \qquad \text{on} \qquad \partial\Omega \, . \tag{2.39}$$

Here ϕ_{app} is the applied potential on the electrode surface. The electrode kinetics is given by the Bulter-Volmer Equation established in equation (2.18).

Finally, the boundary conditions for the Navier-Stokes equations (2.35) and (2.36) can be prescribed depending on the geometry of the computational domain. Normally, one prescribes no-slip and no penetration conditions for the velocity field at the both the insulated boundary and at the surface of the electrode. An inlet and outlet flow conditions must also be prescribed for the pressure variable. We considered specific cases in Paper I and Paper II.

2.4 Electroanalytical techniques

Electroanalytical methods are techniques that can be used to detect and characterize chemical and physical properties of materials in an electrochemically charged fluidic environment. These techniques can be used to illustrate mass transport (diffusion, convection, migration), thermodynamics, reaction kinetics, surface chemistry of an electrochemical system. In this thesis, we consider the cyclic voltammetry (CV) technique. The full model for the cyclic voltammetry can be found in Paper I and Paper II.

In a CV measurement, a series of electric potentials is applied at the working electrode. These potentials vary piecewise linearly and periodically with time as seen in Figure 2.3. The electrical current response is then recorded and plotted against the applied potentials. The applied potentials control the surface concentration of the redox couple that participate in an electrochemical reaction.

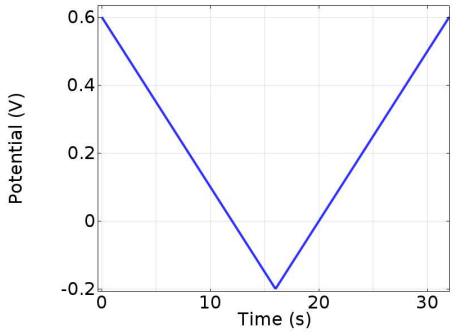

Figure 2.3: Plot of forward and backward scan for applied potential over a period of time.

The slope of the line in Figure 2.3 is the scan rate of the cyclic voltammetry. It measures how fast the applied potential is swept forward and backward during the voltammetry measurement. The scan rate in Figure 2.3 is 50mV/s and corresponds to the experimental duration of about a quarter of an hour. In Figure 2.4, we record the current response and the corresponding evolving concentration profile of the reactants and the products at the surface of the electrode.

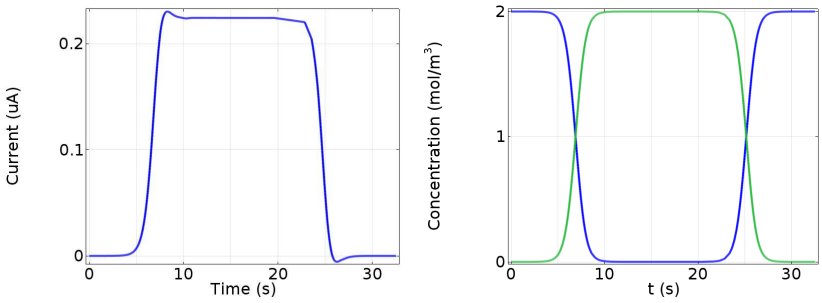

Figure 2.4: Plot of a) current recorded over time, b) evolution of concentration of ionic species over time, blue (reactants), green (products).

When the potential scan is initiated for the first sweep, current increases and the start out concentration (the blue colour line in Figure 2.4b) of the reactants is driven towards zero. At the period when the concentration at the electrode surface is zero, the gradient of the concentration relaxes due to mass transport such that the corresponding current also relaxes. Finally, the concentration of

the reactants return to its initial value at the surface of the electrode when the potential scan is reversed for the second sweep. The same is true for the corresponding current recorded.

2.5 Finite size ion and electric double layer (EDL)

The central feature in this thesis is the modeling of microelectrochemical systems. Up until now, the models we have presented are suited for describing macroelectrochemical systems and the one in which the electrolyte solution can be considered dilute. Although the models have been used as an approximation to a microelectrochemical system in several studies, they are not entirely accurate. One of the drawbacks of the model is that the model treats the ionic species as point charges despite the fact that ions naturally have finite sizes; the diameter of an ion with its hydration shell is usually 3-6Å. Therefore, the detailed molecular structure of the ion is significant in the model formulation for the micro-size systems.

When the potential is applied to the electrodes they get polarized and charges move to their surfaces. Since the electrolyte solution also contains charged ions electric field is generated close to the surface of the electrode and hence, attracts counter ions. However, if ions are treated as point charges, then the ionic concentration gets very large which leads to crowding of ions in the region of the electric double layer. In order to overcome this problem, we introduce the finite size effect of the ionic species into the model.

Recall, the electrochemical potential of ionic species j

$$\mu_j = \mu_j^o + RT\ln(\gamma_j C_j) + z_j F\phi \tag{2.40}$$

from the ionic flux equation (2.26).

The activity coefficient γ_j can be directly related to the ion diameter a and can be used to account for the finite size of the ionic species. Let the maximum concentration of the ions be given by $c_{max} = a^{-3}$ [35], then by [36]

$$\gamma_j = \frac{1}{1 - \sum_j a^3 C_j}. \tag{2.41}$$

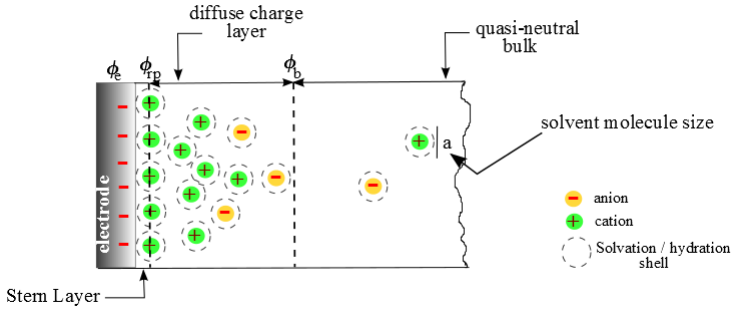

Figure 2.5: schematic of double layer

When we insert equation (2.41) into equation (2.26) we obtain

$$N_j = -D_j \left(\nabla C_j + \frac{z_j F}{RT} C_j \nabla \phi + \frac{a^3 C_j}{1 - \sum_j C_j a^3} (\sum_j \nabla C_j) \right) + C_j v. \qquad (2.42)$$

Notice that the third term in equation (2.42) is a singular diffusion term that leads to the saturation of the ionic species close to the electrode surface. It represents the finite size of the ionic species in the formulation.

In the model development for the conservation of mass, we have assumed electroneutrality which is a zero constraint on the sum of ionic concentration present in an electrolyte. However, this is only true in the bulk electrolyte solution. There is a layer where there is an imbalance of charges and where the electroneutrality conditions breaks down, this layer is the electric double layer. The structure of double layer combines the Stern layer and the diffuse layer, see Figure (2.5).

The Stern layer is considered the charge free layer that is sandwiched between the electrode and the layer immediately before the diffuse layer. It is a region, which accounts for the intrinsic capacitance of the compact part of the electrode-electrolyte interface. The compact-layer charge may contain solvated ions at the points that are closest to the electrode. The capacitance also accounts for the dielectric polarization of the solvation layer. Hence, Stern layer thickness is an adjustable parameter that can be used to study the composition of the double layer.

The diffuse layer is the region containing the non-zero space charge density. Consequently, there are large electrical field strengths. In this layer, the gra-

dient of the ionic species concentration counters the electric field forces acting on the ionic species. Therefore, the gradients of the ionic concentration and the electrical potentials in the diffuse layer are very large compared to steady changes in the electroneutral bulk electrolyte. The combination of the composition of Stern and the diffuse layers makes the double layer to have great influence on the rate of charge transfer at the electrodes.

The classical Butler-Volmer equation reported in equation (2.18) indicates that electrochemical reactions are triggered by the over-potential, that is, the drop in potential between the electrode and the bulk electrolyte solution. However, when including the double layer into the picture of the electrochemical reaction, the proper boundary condition for the potential drop should come from the potential drop across the Stern layer as this is where the reactions actually takes place. The potential drop across the Stern layer results from the strength of the electrical field at the reaction plane according to the following,

$$\triangle\phi_s = \lambda_S \nabla\phi \cdot \mathbf{n} \tag{2.43}$$

where λ_S is the effective width of the Stern layer of the electric double layer, and $\mathbf{n}$ is the normal pointing towards the electrolyte solution. The left hand side of equation (2.43) is the difference between the applied potential ϕ_{appl} and the electric potential $\phi\Big|_{rp}$ at the reaction plane shown in Figure 2.5.

We replace the overpotential in the Butler-Volmer equation in (2.18) by the potential drop across the Stern layer and we finally obtain

$$j = \left[k_a C_O \exp\left(\frac{\alpha_a F}{RT}\triangle\phi_s\right) - k_c C_R \exp\left(\frac{-\alpha_c F}{RT}\triangle\phi_s\right)\right]. \tag{2.44}$$

In conclusion, for a microelectrochemical system we substitute the fluxes in the equation of mass balance (2.32) by (2.42). In addition, we solve for the local potential appearing in the mass balance equations via the Poisson's equation with its source as the charge density, that is

$$-\nabla\cdot(\varepsilon_b\nabla\phi) = F\sum_j z_j C_j, \tag{2.45}$$

where ε_b is the dielectric permitivity. Notice that the right hand side is not zero for a microelectrochemical system. The boundary conditions to solve the system of equations are given by (2.43) and (2.44), respectively.

In the next section, we present the main results based on the implementation of the finite element method of the derived models.

Chapter 3

Summary of main results

This section is divided into two parts. The first part describes the results and contribution of Papers I and II. We present the solution to equations (2.32), (2.34), (2.35), (2.36) coupled with the boundary conditions defined in chapter 2. The experimental set-up for the model is described in Paper II. The second part highlights the contribution of Paper III where we present the results of the model for microelectrochemical systems. The model accounts for the structure of the electrode/electrolyte interface and also incorporates finite size properties of the ionic species. We conclude this section by summarizing the major contributions of this thesis.

Part I

In Paper II, we introduce the experimental set-up of an electrochemical system in which the electrolyte solution is transported by all the mechanisms of mass transfer. Full details of the experiment can be found therein. Here, we are interested in setting up the numerical solution using the Finite Element method (FEM) program COMSOL [37]. We do not give details of the theory of FEM. However, there are unlimited resources where the theory and numerics of FEM have been reported, for more details readers are referred to [38, 39, 40, 41], among others.

Figure 3.1 shows the fluidic cell which approximates the experimental setup. Only the working electrode is shown. As reported in Paper II, the fluidic cell can be approximated by a 2-dimensional computational domain because of the laminar nature of the flow. The full details can be found in Paper II.

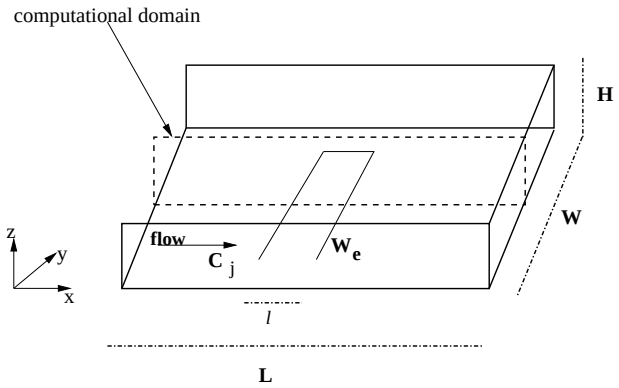

Figure 3.1: schematic of the fluidic cell.

We validate the results of simulation of the model and assess the accuracy of the solution method by systematic mesh refinement until there are no changes in the estimated response current curves. A typical mesh refinement for computation is shown in Figure 3.3.

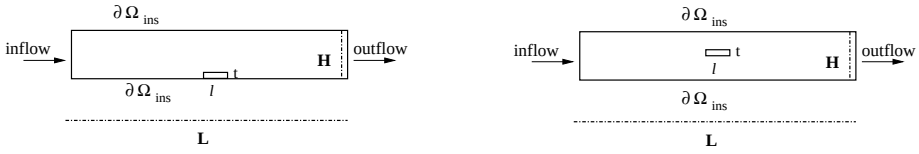

Figure 3.2: Plot of a) computational domain of an electrode placed at the bottom of the fluidic cell, b) computational domain of an electrode place in the middle of the fluidic cell.

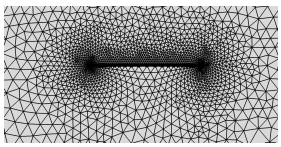

Figure 3.3: Plot of a zoomed-in mesh grid showing dense elements around a mid placed electrode.

The high density of the mesh is due to local systematic mesh refinement around the electrode where there are large solution gradients. In order to ensure compromise between computational time and the accuracy of the results we have used about 35000 elements in our computations. For the time integration, we have employed the implicit Euler method that is stable for the numerical computations.

We used a two step approach for solving the coupled fluid and ion-transport problems. First, we solve for the steady state solution to the incompressible Navier-Stokes equations and then substituted the steady state solution of the velocity field into the ion transport problem. The fluid flow problem was solved by discretizing the computational domain using the linear Lagrange finite elements for the pressure field and quadratic elements for the velocity field. In addition, we employed quadratic elements for the ion transport problem while the linear Lagrange element was chosen for the potential field.

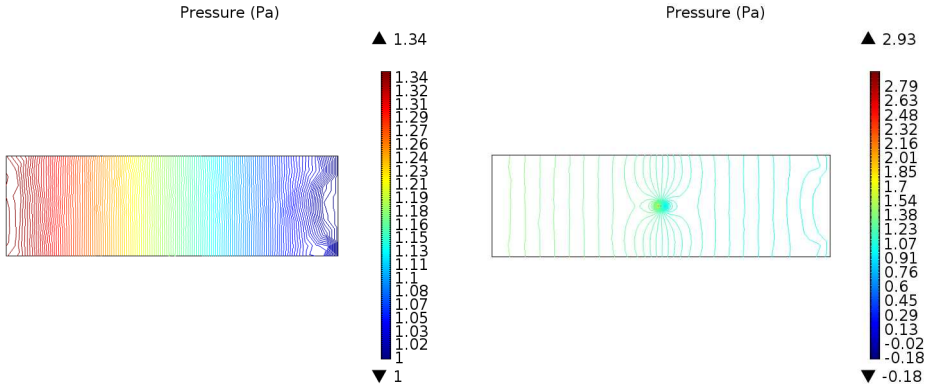

Figure 3.4: Plot of a) contour field with electrode on the floor, b) contour field with electrode in the middle.

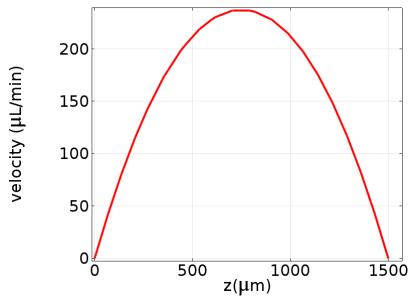

Figure 3.5: Flow profile across z-axis of the channel.

Figure 3.4a and Figure 3.4b are the contour plots of the pressure across the z-axis of the fluidic cell for both the electrodes placed at the bottom and the middle of the the fluidic cell, respectively. Figure 3.5 also shows the velocity profile across the z-axis. It is clear from the figures that fresh reactants are always in constant supply at the working electrode placed in the middle of the cell. This is because the maximum velocity is at the tip of the parabolic profile of the velocity. Therefore, at a high scan rate, there is either the high concentration of the products or the reactants that are close to the surface of the electrode. Consequently, we expect higher currents to be recorded in the system with the electrode in the middle. More detailed analysis is considered both in Paper I and Paper II.

In what follows, we present a series of cyclic voltammetries for various scenarios from the simulated electrochemical system from the previous section. We have chosen laminar volumetric flow rates ranging from 0 - $250\mu L/min$. Figures 3.6a,b show cyclic voltammetry curves for systems with both electrodes in the middle as well as on the bottom of the fluidic system. They depict the effect of flow rates on the CV.

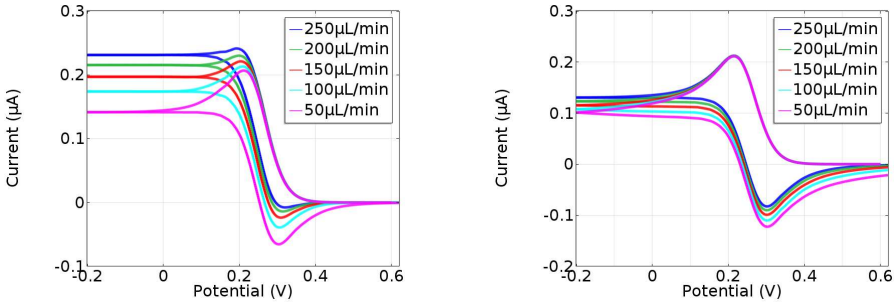

Figure 3.6: Plot of a) cyclic voltammetry recorded at the electrode placed in the middle of the fluidic cell, b) cyclic voltammetry recorded at the electrode placed at the bottom of the fluidic cell.

Taking a closer look at Figure 3.6a, at flow rates of about 50 - $150\mu L/min$ peak currents are observed. The reason is that during the forward scan there is an accelerated electrode/electrolyte reaction and fast enough to allow charge exchange and results in an increase in current recorded. However, due to the reaction at the surface of the electrode, the concentration of the reactants is depleted and the current soon is controlled by the diffusion of the reactants towards the electrode. On the other hand, as the flow rate increases to about $250\mu L/min$, the CV curve becomes thinner and the peak current disappears as saturation is quickly reached. This is due to the rapid inflow of the reactants and quick removal of the products induced by the convection. There is a reduction

in diffusion layer thickness for electro active species and hence mass transport is controlled by the convection.

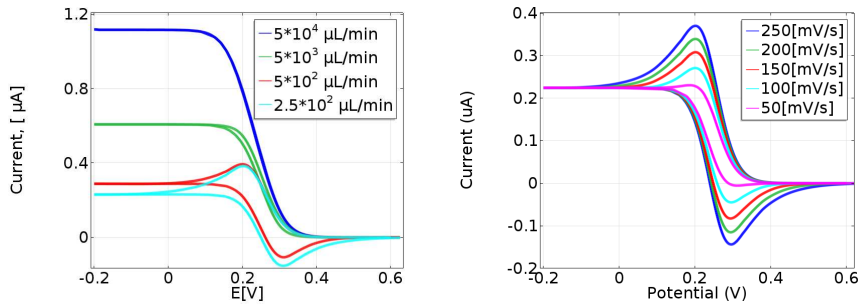

Figure 3.7: Plot of a) cyclic voltammetry showing very high flow rate recorded at the electrode placed in the middle of the fluidic cell, b) cyclic voltammetry recorded at the electrode placed in the middle of the fluidic cell showing the effect of scan rate.

For the case of Figure 3.6b, peak currents are always recorded for any choice of moderate flow rates. This could be explained by our earlier argument that for a bottom placed electrode, the rate of furnishing the electrode surface with fresh reactants is slow. Hence, the reactants close to the surface of the electrode will always undergo reduction or oxidation, thereby recording peak current at all time. However, in an extreme case of high volumetric flow rate (usually beyond the laminar flow regime) as in Figure 3.7a the hysteresis in the CV curve completely disappear. The system is completely dominated by convection. We also present CV curves and the effect of the scan rates in Figure 3.7b. There is clearly a corresponding increase in scan rate and the currents recorded with highest scan rate showing the highest peak current. The faster the scan rate, the faster the diffusion layer is established over a shorter distance.

In conclusion, we have shown the simulation of cyclic voltammetry using the flexible and the powerful finite element solver COMSOL. This allows to solve problems with complex geometry and provides the framework that leads to complex design of an electrochemical system. However, the main result here is that we can now assess the influence of the convection and the scan rate to the dynamics of the electrochemical system. The result also shows that placement of the electrodes is very essential.

Part II

In this section, we solve the model for an electrochemical system that incorporates the finite size properties of the ionic species and account for the electrode/electrolyte structure of the interface. The aim of this section is to summarize the topic covered in Paper III. The extensive mathematical derivations can be found in Paper III and the extended non-dimensionalization of the model equations are found in Appendix A. Here, we explain interesting numerical results and highlight an analytical result that provide insight into the dynamics of the electric double layer to the bulk layer. We strongly emphasize here that a system of one dimension is considered because higher dimensions still pose challenges. This study serves as a motivation to overcome limitations found in higher dimensions.

We start by lifting some of the formulations from Paper III. Consider the dimensionless mass transport and Poisson's equations involving an anion C_1 and a cation C_2 and the local potential in a microelectrochemical system,

$$\frac{\partial C_1}{\partial t} = k_1 \frac{\partial}{\partial x}\left(\frac{\partial C_1}{\partial x} - z_1 C_1 \frac{\partial \phi}{\partial x} + \frac{\nu C_1}{1-\nu(C_1+C_2)}\frac{\partial (C_1+C_2)}{\partial x}\right), \tag{3.1}$$

$$\frac{\partial C_2}{\partial t} = k_2 \frac{\partial}{\partial x}\left(\frac{\partial C_2}{\partial x} + z_2 C_2 \frac{\partial \phi}{\partial x} + \frac{\nu C_2}{1-\nu(C_1+C_2)}\frac{\partial (C_1+C_2)}{\partial x}\right), \tag{3.2}$$

$$-\epsilon^2 \frac{\partial^2 \phi}{\partial x^2} = z_2 C_2 - z_1 C_1, \tag{3.3}$$

with the following boundary conditions

$$k_1\left(\frac{\partial C_1}{\partial x} - z_1 C_1 \frac{\partial \phi}{\partial x} + \frac{\nu C_1}{1-\nu(C_1+C_2)}\frac{\partial (C_1+C_2)}{\partial x}\right) = j_F, \tag{3.4}$$

$$k_2\left(\frac{\partial C_2}{\partial x} + z_2 C_2 \frac{\partial \phi}{\partial x} + \frac{\nu C_2}{1-\nu(C_1+C_2)}\frac{\partial (C_1+C_2)}{\partial x}\right) = j_F, \tag{3.5}$$

$$\phi\Big|_{rp} = \phi|_e \mp \delta\epsilon \frac{\partial \phi}{\partial x}\Big|_{rp}. \tag{3.6}$$

Here, $j_F = k_R C_{1,S}\exp(-\alpha z_1 \triangle\phi_s) - k_O C_{2,S}\exp((1-\alpha) z_2 \triangle\phi_s)$. We comment here that equations (3.1 - 3.6) are derivations from the equations presented in

section 2.5. See the derivation in Paper III. All the parameters are also defined therein.

We numerically solve the model with two case scenarios. The case with a blocked electrode where there is no charge transfer $j_F = 0$ and the case with $j_F \neq 0$ where only the cation reacts at the electrode. The domain of computation is $0 \leq x \leq 1$ and dimensionless potentials of 0 and 10 are applied at the left and right boundary respectively. Throughout the computation, we have chosen $\delta = 0.1$ which means the diffuse layer is ten times the Stern layer.

Model validation

We validate our numerical computations by considering an interesting case proposed by [23]. They solved a steady state problem where one of the ionic species reacts and is absorbed by the electrode. The model does not contain the finite size properties but incorporated Stern's boundary conditions. We set up the same problem with the finite size constraint and solve the equivalent transient problem.

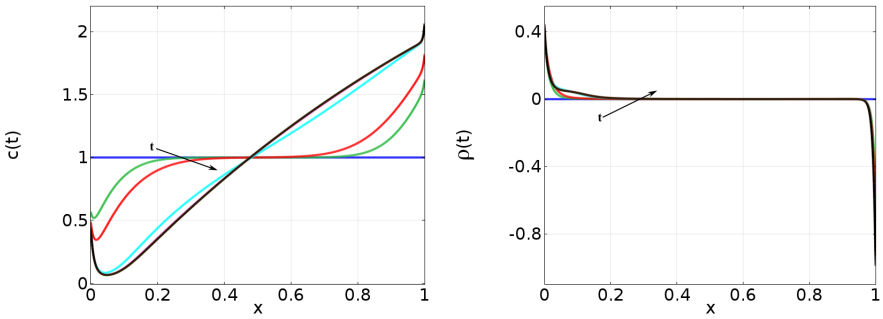

Figure 3.8: Plot of a) evolution of concentration , b) evolution of charge density.

It is interesting to see that the results approach the steady state solutions for the concentration, potential and the charge density, see Figures 3.8-3.9 as reported in [23], page 1471. In what follows we now present the summary of the results below.

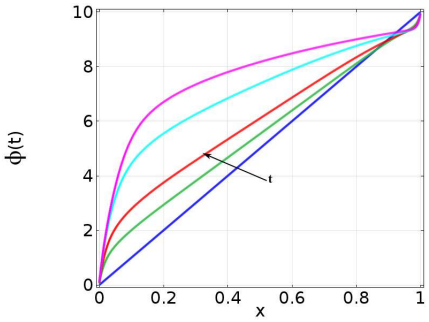

Figure 3.9: Plot of evolution of potential.

Case: $z_2 = -z_1 = 1, \epsilon = 0.1, \nu = 0.25$

For this particular case, we define the total concentration $c(t) = (C_1 + C_2)/2$, and the total charge density $\rho(t) = (C_2 - C_1)/2$. We solve for both the blocked electrodes ($j_F = 0$) case and the case with ion exchange ($j_F \neq 0$) in order to show the importance the Faradaic reactions at the electrode/electrolyte interface. Here, only the cation undergoes ion exchange. We consider the time $t = 0, 0.5, 2, 3, 4, 5$.

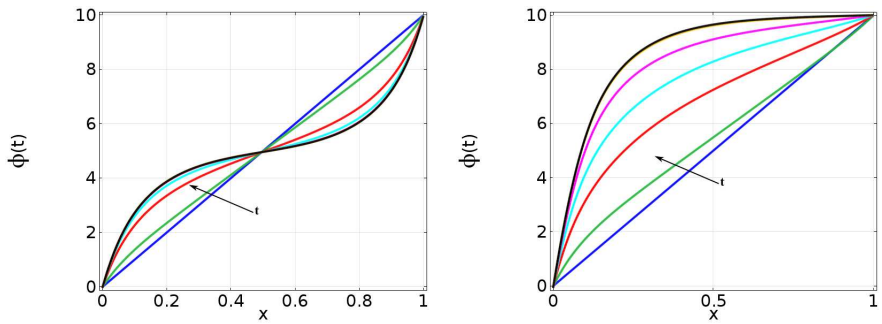

Figure 3.10: Plot of a) evolution of potentials for the case with blocked electrodes, b) evolution of potentials for the case with charge transfer.

Figure 3.10 shows a comparison between the system potentials for the case with blocked electrodes (left) and the case with charge transfer (right). Observe that for the case of blocked electrodes, the evolution of potentials in the region $0 \leq x \leq 0.5$ increases with time while the other half show decrease in potentials. It is

interesting to see that the increase and the decrease are of the same proportion. The slope taken at both ends in the vicinity very close to the electrode are equal, that is, equal magnitude of electric field in the electric double layer.

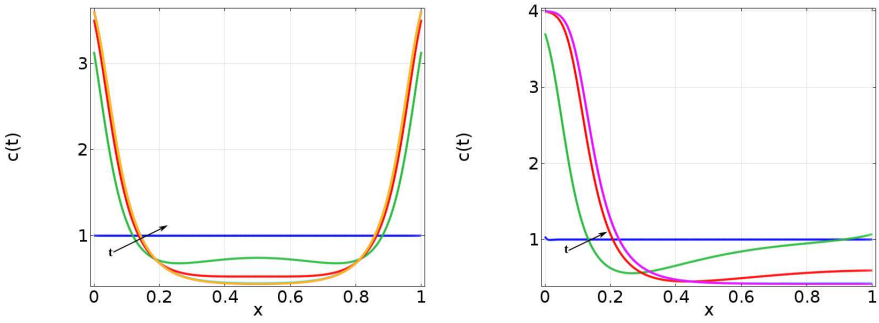

Figure 3.11: Plot of a) evolution of concentration for the case with blocked electrodes, b) evolution of concentration for the case with charge transfer.

For a microelectrochemical system the close proximity of the electrodes means migration plays a prominent role in the ion transport. But the steep slope of the potential field around the double layer means the huge electric field will repel and/or attract each ionic species depending on its charge. This is observed in Figure 3.11a which shows the evolution of ionic concentration in time for the case of blocked electrodes. The boundary layer formed by quick accumulation of charges is evident. Notice the symmetry in Figure 3.11a. Equal amount of the species move in the opposite direction towards the boundary where it is crowded. Another observation is that the concentration in the bulk approaches zero ionic concentration.

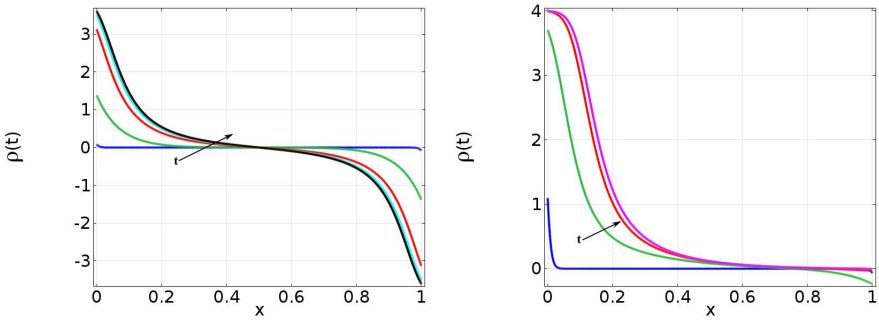

Figure 3.12: Plot of a) evolution of charge density for the case with blocked electrodes, b) evolution of charge density for the case with charge transfer.

On the other hand, in the case with the ion exchange in Figure 3.10b, we observe a very steep gradient, electric field, of the potential close to the left electrode than the right electrode. This is the consequence of large amount of reacting ions, in this case the cation, accumulating faster in the boundary layer. Note that the total amount of the anion must be fixed and under the influence of the electric field its distribution becomes unbalanced and since electroneutrality must hold in the bulk electrolyte, equal amount of the anion and cation concentration must be present. This is clearly observed in the charge density displayed in Figure 3.12. An interesting observation is that in the bulk electrolyte the charge density is close to zero. This means that equal amount of ionic species is present in the bulk region. Hence, the approximation of the electroneutrality holds in the bulk electrolyte. However, notice the boundary layers in this case extends towards the bulk electrolyte. Finally, at time $t = 5$, we observe that both the anion and the cation concentration are zero close to the right electrode in Figure 3.12b.

Case: $z_1 = -1, z_2 = 2, \epsilon = 0.01, \nu = 0.25$

The results for the case with different valencies are presented in this section. We show the time evolution of the anion and the cation separately in Figure 3.13. The results are plotted for time $t = 0.001, 0.01, 2.5, 5$. We observe that at earlier time $t = 0.001$, both the anion and the cation are driven towards zero values close to the electrodes on the left and the right, respectively. Furthermore, they migrate towards the electrodes on the right and the left, respectively.

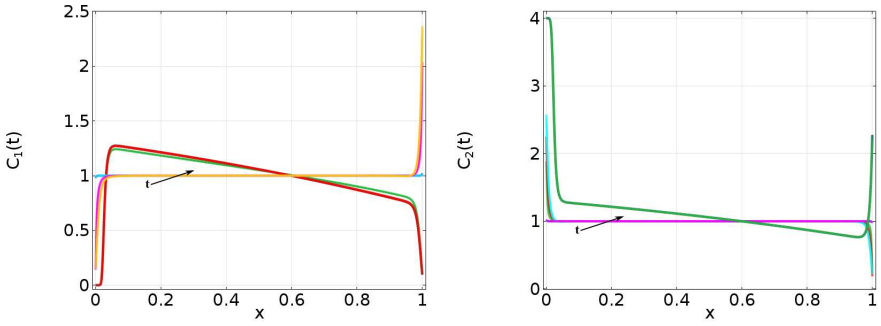

Figure 3.13: Evolution of concentrations of a) anion and b) cation, for the case $z_1 = -1,\ z_2 = 2,\ \epsilon = 0.01$.

After some time, the anion tends towards zero in the vicinity of both electrodes. This is because it diffuses towards the bulk electrolyte in order to satisfy the

electroneutrality condition. However, an interesting observation for the cation shows that the excess concentration accumulate on the right which is a complete deviation from the case treated in the previous section. Notice the charge density shown in Figure 3.14 where electroneutrality holds in the bulk region except in the double layer.

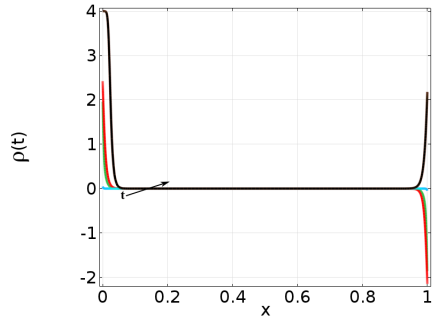

Figure 3.14: Evolution of charge density for the case $z_1 = -1,\ z_2 = 2, \epsilon = 0.01$.

Parameters ν, ϵ

Figure 3.15 shows the effects of the finite ion size properties and the parameter that characterizes the double layer. We have used the previous example for both cases.

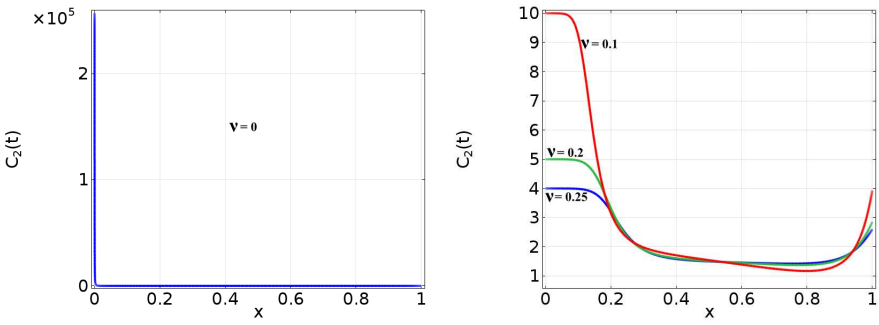

Figure 3.15: Plot of cation field for the cases a) $\nu = 0$, b) $\nu = 0.1, 0.2, 0.25$.

The absence of the steric effect shows that ion concentration goes to infinity while when it is present, the ion concentration is bounded by the inverse of the

value of ν. We also consider the effect of the parameter ϵ. For a large value, the double layer extends towards the bulk electrolyte.

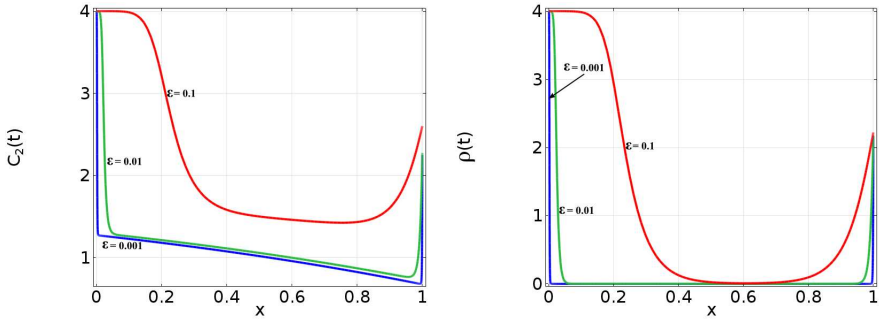

Figure 3.16: Plot of cation field a) $C_2(t)$ b) charge density $\rho(t)$, for the cases $\epsilon = 0.001, 0.01, 0.1$.

In summary, we have been able to extend the blocked electrodes type system to the case which involves reactions at the electrodes. We have also solved for the case with different valencies of the ionic species in an electrolyte solution. The transport equations we solved account for the finite size effect and incorporates the compact boundary conditions.

The analytical solution to the concentration of the bulk electrolyte

This section is motivated by the numerical results from the previous section. The solutions depict traveling wave behaviour close to the electrode, therefore we investigate the behaviour in what follows. In the bulk electrolyte electroneutrality condition, $z_1C_1 = z_2C_2$ holds. Consider again the mass transport equations

$$\frac{\partial C_1}{\partial t} = k_1 \left(\frac{\partial C_1}{\partial x} - z_1 C_1 \frac{\partial \phi_0}{\partial x} + \frac{\nu C_1}{1 - \nu(C_1 + C_2)} \frac{\partial (C_1 + C_2)}{\partial x} \right), \tag{3.7}$$

$$\frac{\partial C_2}{\partial t} = k_2 \left(\frac{\partial C_2}{\partial x} + z_2 C_2 \frac{\partial \phi}{\partial x} + \frac{\nu C_2}{1 - \nu(C_1 + C_2)} \frac{\partial (C_1 + C_2)}{\partial x} \right). \tag{3.8}$$

We then multiply equations (3.7) and (3.8) by k_2 and k_1 respectively, and after a few re-arrangements we invoke the electroneutrality condition and obtain

$$\frac{\partial C_1}{\partial t} = \frac{\partial}{\partial x}\left(D_{[\nu,C_1]}\frac{\partial C_1}{\partial x}\right), \tag{3.9}$$

which is a non-linear diffusion equation for C_1 with effective diffusivity

$$D_{[\nu,C_1]} = \frac{k_1 k_2\left(\frac{z_1+z_2}{z_1k_1+z_2k_2}\right)}{1-\nu\left(\frac{z_1+z_2}{z_2}\right)C_1}, \tag{3.10}$$

that depends on both the variable C_1 and the steric effect parameter ν.

To solve equation (3.9), we introduce the following constants

$$L_1 = k_1k_2\left(\frac{z_1+z_2}{z_1k_1+z_2k_2}\right) \text{ and } \mathrm{L_2} = \nu\left(\frac{\mathrm{z_1}+\mathrm{z_2}}{\mathrm{z_2}}\right),$$

therefore equation (3.9) becomes

$$\frac{\partial C_1}{\partial t} = -\frac{L_1}{L_2}\frac{\partial}{\partial x}\left(\frac{\partial}{\partial x}\left[\ln(1-L_2C_1)\right]\right). \tag{3.11}$$

Now, we propose a function

$$\sigma(t,x) = -\ln(1-L_2C_1), \tag{3.12}$$

and with a few manipulations, equation (3.9) becomes

$$e^{-\sigma}\frac{\partial \sigma}{\partial t} = L_1\frac{\partial}{\partial x}\left(\frac{\partial \sigma}{\partial x}\right). \tag{3.13}$$

We therefore, seek a travelling wave solution $\sigma(x,t) \equiv c(\xi)$ with $\xi = x - vt$ that satisfies the following ODE

$$v\frac{\partial e^{-c}}{\partial \xi} = L_1\frac{\partial}{\partial \xi}\left(\frac{\partial c}{\partial \xi}\right). \tag{3.14}$$

Integrating equation (3.14) gives

$$L_1\frac{\partial c}{\partial \xi} = ve^{-c} + L_3, \tag{3.15}$$

where L_3 is the constant of integration. Since due to relation (3.12) $C \to 0$ as $x \to +\infty$ would imply that $c \to 0$ as $\xi \to +\infty$ and $\frac{\partial c}{\partial \xi} \to 0$, L_3 from equation (3.15) can easily be obtained to be $L_3 = -v$. We integrate equation (3.15) and obtain

$$e^{-c} = \frac{1}{1 + e^{-\frac{v}{L_1}\xi}}. \tag{3.16}$$

When we insert equation (3.16) into the relation (3.12) we finally obtain a wave solution for C_1 ,

$$C_1 = \frac{z_2}{\nu(z_1 + z_2)} \left(\frac{1}{1 + e^{v(x-vt)\left(\frac{z_1 k_1 + z_2 k_2}{z_1 + z_2}\right)}} \right). \tag{3.17}$$

Using electroneutrality condition $z_1 C_1 = z_2 C_2$ we obtain the concentration for the cation

$$C_2 = \frac{z_1}{\nu(z_1 + z_2)} \left(\frac{1}{1 + e^{v(x-vt)\left(\frac{z_1 k_1 + z_2 k_2}{z_1 + z_2}\right)}} \right). \tag{3.18}$$

We plot the solution of the bulk concentrations given by equations (3.17) and (3.18).

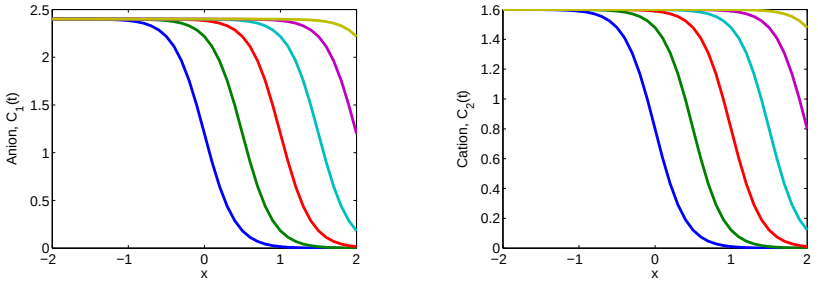

Figure 3.17: Travelling wave solutions,$z_1 = 2,\ z_2 = 3,\ v = 10,\ 0 \le t \le 5$.

Figure 3.11 shows the travelling waves in equations (3.17) and (3.18) for $x \in [-2, 2]$ with travelling wave speed v. The solutions are localized kink like solutions with a finite concentration far to the edge of the center of the wave and the concentration ahead of the wave. The concentration C_1 rises from zero and converges to the finite value $\frac{z_2}{\nu(z_1+z_2)}$. From equation (3.9), this limit corresponds to having a vanishing denominator in the effective diffusivity (3.10), and hence is an upper limit for this concentration. The same is true for C_2. A characteristic

feature of the travelling wave solution is the uniform electroneutrality. For an electrolyte in a tube, the travelling wave solution corresponds to an inflow from the left of ions at a concentration equal to the upper limit arising from the steric effect and that this ion density is pushed into the tube. We imagine that the tube initially is filled with solvent through which the ions are transported.

3.1 Contributions of the thesis

The study of microelectrochemical systems is still an emerging field with lots of potentials to be explored as well as grounds to be covered. Here, we list some of the contributions of the present study, which we hope will improve and impact the application of microelectrochemical systems.

The first part of the thesis deals with mathematical modelling and numerical approximation of a microelectrochemical system using the well known Nernst-Planck equation coupled with the Poisson equation. The motivation for the first part of the thesis comes from the need to improve the experimental design of the microelectrochemical system. We validate the numerical model of a cyclic voltammetry experiment for a flowing electrolyte solution in a microfluidic channel against a corresponding physical experiment. We find that the placement of the electrodes in a channel plays a very important role in this model. This is one of the distinctions of this study compared to numerous studies that have been reported in the articles, for example, [42, 43, 44, 45, 46, 47, 48]. We have also shown the effects of the moderate and extreme flow rates on the cyclic voltammetry experiment.

The electrochemical reactions considered in the first part of the thesis are believed to be triggered by the potential drop between the electrode and the bulk electrolyte solution. There is also an approximation of the electroneutrality condition, which means that the right hand side of the electric potential equation is zero. However, for microelectrochemical systems the electrode/electrolyte interface plays a crucial role in the electrochemical reactions. Furthermore, the electroneutrality does not hold near the electrode/electrolyte interface. The second part of the study attempts to solve a general microelectrochemical model by incorporating these conditions into the model equations. In the second part of the thesis, we provide a general framework which allows for electrolytes of any valence as opposed to a binary electrolyte solution that have been considered in previous studies, [23, 29, 30, 49, 50].

As noted by Olsen *et al* [30], for most electrochemical reactions, it is not enough to assume binary electrolyte solutions. This has been a daunting task even for

the steady state case [51]. Here, we numerically solved the problem in the framework of general/arbitrary electrolytes even for the transient case. We have also extended previous studies to the case with Faradaic reactions at the electrode/electrolyte interface. We observe that charge transfer complicates the dynamics of the electric double layer. The presence of non-zero right hand side and a small conductivity occurring at the left hand side of the Poisson equation ensure the build up of boundary layers near the electrode/electrolyte interface. We were able to establish this from the numerical results. Finally, we establish that the ionic concentrations in the bulk electrolyte move with the solvent as a traveling wave. This could serve as a starting point for an interesting discussion on the theoretical analysis of equations (3.1) and (3.2).

Chapter 4

Numerical modeling of Electroanalytical techniques

Paper I

Special Issue Paper

Mathematical Methods in the Applied Sciences

Received 17 September 2014

Published online in Wiley Online Library

(wileyonlinelibrary.com) DOI: 10.1002/mma.3336
MOS subject classification: 35G50 - Nonlinear higher-order systems (PDEs)

Simulating cyclic voltammetry under advection for electrochemical cantilevers

B. J. Adesokan, A. Evgrafov and M. P. Sørensen*†

Communicated by M. Otani

We present a mathematical model describing an electrochemical system involving electrode–electrolyte interaction. The model is governed by a system of advection–diffusion equations with a nonlinear reaction term at the boundary. Our calculations based on such model demonstrate the dynamics of ionic currents in the electrolyte. The model allows us to predict the effect of varying flow rates, scan rates, and electrolyte concentration of the electrochemical system. Copyright © 2014 John Wiley & Sons, Ltd.

Keywords: cyclic voltammetry; Butler–Volmer; advection; cantilever sensors

1. Introduction

The invention of biochemical sensing cantilevers, also known as electrochemical sensors, has brought new trends to the technological advancements in medical diagnostics, pharmacy, agriculture, and food, among others [1–5]. It has also opened a new exciting direction in biochemical research [6–11]. These devices usually undergo changes in their electrical, chemical, and mechanical properties when present in an electrochemically charged fluidic environment. This forms the basis for using cantilever-based electrochemical sensors in detecting electroactive substances in fluids.

It is essential that these devices translate biochemical recognition into electrical signals [12, 13]. This means that the device must be coupled with fast electroanalytical techniques in order to characterize the signals on real-time basis. In recent years, cyclic voltammetry (CV) has become one of the most important electroanalytical techniques in sensing applications. The choice is due to its inherent advantages for ultra small environments and its rich information content [14]. In CV measurements, a periodic time varying voltage is applied to the working electrode. Typical choices are piecewise linear and periodic voltages. The electric current response is then recorded, from which the total accumulated charge at the electrode surface can be found [15–17].

Conventionally, CV measurements are carried out with electrodes in a container with a still electrolyte solution. However, recent developments in electrochemical-based sensing has led to hydrodynamic voltammetric techniques [18] where electrodes are placed in a fluidic cell with the electrolyte solution being pumped through the cell. Hence, mass-transport by convection must be accounted for in the system. For sensor design and optimization, the current response of the system can then be exploited in order to perform quantitative analysis. Over the years, several authors [19–22] have analysed CV in which mass-transport is only due to diffusion. On the other hand, combined convection and diffusion driven mass-transport for the electro-active species have been investigated by numerical modelling and simulations in References [18, 23–25].

Furthermore, several authors have also analysed CV within the framework of mathematical theory, while few others have suggested various numerical approaches that analysed CV. Ayabe and Nicholson [26, 27] gave the first extensive theoretical and numerical analysis on CV. Their approach was based on solving integral equations for planar electrodes. Feldberg [28, 29] later suggested to use explicit finite difference method, which he termed digital simulation. However, Szabo and Shoup [30] argued that the Feldberg's method becomes unstable for CV at low scan rates. While most of their approaches have considered special types of electrodes, they have studied electrochemical systems in which the electrolyte solution is at rest without flow. In our study, we use the finite element method for solving an electrochemical model taking into account transport of ions in the electrolyte due to diffusion, electrical forces, and convection. We investigate the effect of flow rates, scan rates, and concentration on CV curent–voltage curves.

Department of Applied Mathematics and Computer Science, Technical University of Denmark, Richard Petersens Plads, Building 324, 2800 Kgs. Lyngby, Denmark
** Correspondence to: M. P. Sørensen, Department of Applied Mathematics and Computer Science, Technical University of Denmark, Richard Petersens Plads, Building 324, 2800 Kgs. Lyngby, Denmark.*
† E-mail: mpso@dtu.dk

2. Mathematical model

In this section, we shall derive a mathematical model for the dynamics of ionic currents in an electrolyte. The transport of ions is induced by diffusion, mobility due to electric fields and convection by fluid flow of the electrolyte. The conservation of ions then leads to the Nernst–Planck equation. In electrochemistry, charge transfer at the electrodes is taken care of by suitable boundary conditions and will be treated in the subsequent section. The electric field arising from the electrodes and modified by charges in the electrolyte is determined from a Poisson equation. Finally, the flow is assumed to be Newtonian governed by the Navier–Stokes equations. Our aim is to simulate CV, that is, determine the electrode current as function of the applied voltage, where the voltage varies periodically as a triangle wave and piecewise linear. The response of the current is non-instantaneous to the applied voltage, and hence, CV curves show hysteresis.

We start our derivation of the mathematical model by considering the electrochemical reaction on the working electrode

$$O + e^- \rightleftharpoons R, \tag{1}$$

where O and R represent the reactants and products, respectively. When the potential is applied to the electrode, the solution looses its equilibrium state, and reactions occur at the electrode surface. However, the system attempts to relax the electrolyte solution back to its original equilibrium state. Hence, the electrode reaction continues in a loop. The electrode kinetics is triggered by the overpotential, which is the potential difference between the electrode and the adjacent electrolyte solution. In our mathematical model derived in the succeeding text, the overpotential enters only through the boundary condition. In addition, electrode kinetics also causes electrode surface concentration to change because of exchange of ions at the electrode. The ionic flux of species $j, j = 1, 2, \ldots, N$, in an electrolyte is described by Bard and Faulkner and Newmann *et al*. [15, 16]

$$N_j = -z_j u_j F C_j \nabla\phi - D_j \nabla C_j + C_j \underline{v}\,. \tag{2}$$

N is the number of ions, C_j is the concentration of ion j, D_j is its diffusion constant, z_j is the charge, and u_j is the mobility caused by the electric field given by the gradient of the electric potential ϕ. Faraday's constant is denoted by F, and $\underline{v}$ denotes the flow velocity of the electrolyte. Current is generated due to the motion of all charged species in the bulk electrolyte solution. The total current $\underline{i}$ then becomes

$$\underline{i} = F \sum_j z_j N_j\,. \tag{3}$$

The conservation of mass for species j in the bulk solution is given by the Nernst–Planck equation

$$\frac{\partial C_j}{\partial t} = -\nabla \cdot N_j + R_j\,. \tag{4}$$

Here, R_j is the heterogenous chemical reaction that may occur in the solution. For our analysis, we shall assume that there is only electron transfer reaction at the electrodes, that is, $R_j = 0$. The electrolyte is electrically neutral except within a very thin layer close to the electrode. This layer is called the electric double layer. We do not explicitly take this layer into account in this study. For an electrically neutral solution, the following holds:

$$\sum_j z_j C_j = 0. \tag{5}$$

If we multiply equation (4) by Fz_j and sum over j, we obtain

$$F \frac{\partial}{\partial t} \sum_j z_j C_j = -\nabla \cdot F \sum_j z_j N_j\,, \tag{6}$$

and by combining the electroneutrality condition (5) with (6), we obtain the conservation law

$$\nabla \cdot \underline{i} = 0\,, \tag{7}$$

for electric charges within the solution. We have used the expression given in (3). Furthermore, we expand equation (7) by inserting the ionic flux given by (2) and obtain

$$\nabla \cdot \left(\sum_j z_j^2 u_j C_j F^2 \nabla\phi + F \sum_j z_j D_j \nabla C_j - F \sum_j z_j C_j \underline{v} \right) = 0, \tag{8}$$

and due to equation (5), the following holds:

$$\nabla \cdot (-\kappa \nabla\phi) = F \sum_j z_j \nabla \cdot (D_j \nabla C_j)\,, \tag{9}$$

where $\kappa = F^2 \sum_j z_j^2 u_j C_j$ is the electrolyte conductivity. For computational purposes, κ is assumed to be constant under the assumption of the presence of a supporting electrolyte, which increases electrolyte solution conductivity and reduces the solution resistance.

Finally, in order to close the system, we need to determine the velocity field $\underline{v}$ of the electrolyte. This can be performed by solving the Navier–Stokes equations for a viscous incompressible flow,

$$\nabla \cdot \underline{v} = 0 \,, \tag{10}$$

$$\rho \left(\frac{\partial \underline{v}}{\partial t} + \underline{v} \cdot \nabla \underline{v} \right) = -\nabla p + \mu \nabla^2 \underline{v} + \underline{s}_f \,. \tag{11}$$

The fluid density is denoted ρ, p is the pressure, μ is the dynamic viscosity, and finally, s_f denotes an external force per unit volume [31, 32]. The total coupled system of partial differential equations to be solved consists of (4), (9), (10), and (11). As no time derivatives enter in (9) and (10), the model is a differential algebraic system. Furthermore, it is autonomous for $\underline{s}_f = 0$ in (11). However, the system is forced through the boundary conditions as will be clear from the next section.

In the ion transport term (2), we assume constant diffusion D_j for species j. However, at the electrodes, the ion concentration can easily be so high that we need to include steric effects, that is, the concentration becomes high enough that the ions touch each other [33]. In this case, the diffusion transport can be modelled by

$$N_j^{diffusion} = a_j^3 D_j \frac{C_j \nabla \left(\sum_{i=1}^{N} C_i \right)}{1 - \sum_{i=1}^{N} a_i C_i} \,, \tag{12}$$

where a_j is the diameter of ion j. This nonlinear diffusion term leads to the saturation of ion concentrations at the surface of the working electrode. Similar nonlinear and singular diffusion terms play an important role in models of biofilm growth [34, 35]. In biofilm growth, a singular diffusion term leads to rapid proliferation of the biofilm. For pure mathematical results on reaction diffusion equations or porous media equations with nonlinear diffusion terms, a survey can be found in [36]. However, our system extends the models studied in [34, 36] by considering the electric field equation and the Navier–Stokes equations.

3. Boundary conditions

In the following, we shall specify the boundary conditions for the microfluidic cell depicted in Figure 1. This cell has been chosen to be as simple as possible in order to ease building a mathematical model, yet sufficiently comprehensive to provide insight into the influence of the convective flow, scan rates, and concentration of reactants on CV. Figure 1 only shows the part of the cell containing the working electrode of width w_e and length ℓ placed at the bottom of the cell. The counter electrode is placed far to the left of the working electrode and not shown in the figure. Both electrodes may represent cantilevers in an electrochemical sensor device, however, neglecting the possibility of bending [9, 37]. The counter electrode ensures that the current that flows into the electrolyte solution through the working electrode leaves the solution. In addition, we may insert a reference electrode in order to maintain a stable and constant potential at the working electrode. There is normally no current flow through the reference electrode. Furthermore, we consider a cell where $H \ll W < L$, and accordingly, we assume that transport of ions and fluidic motion can be considered two-dimensional. This means that we restrict our model to the cross-sectional xz-plane at $y = 0$ in Figure 1. The cell containing the electrolyte has walls at which no ionic current can pass, there are inflow and outflow boundary conditions and finally chemical reactions on the surface of the electrodes.

At the insulating surfaces $\partial\Omega_{ins}$ of the cell, the current density is prescribed by

$$i_n = 0 \; on \; \partial\Omega_{ins} \,. \tag{13}$$

Using this condition together with the conservation of electric charge (9), we obtain the Neumann type boundary condition

$$\kappa \frac{\partial \phi}{\partial n} = -z_j D_j \frac{\partial C_j}{\partial n} \; on \; \partial\Omega_{ins} \,. \tag{14}$$

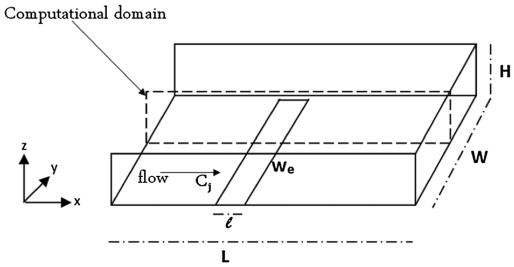

Figure 1. Computational domain of the microfluidic cell with one electrode of dimension $w_e \times \ell$ placed at the bottom of the cell.

However, at the electrode–electrolyte interface, the ionic flux for each species can be described by specifying the normal current density according to

$$\kappa \frac{\partial \phi}{\partial n} + z_j D_j \frac{\partial C_j}{\partial n} = i_n(C_j, \phi, v; \phi_{app}) \text{ on } \partial\Omega \,. \tag{15}$$

We shall specify the current density i_n from the electrode kinetics using the Butler–Volmer relation [15, 16]

$$i_n = i_o \left[exp\left(\frac{\alpha_a F}{RT}\eta\right) - exp\left(\frac{-\alpha_c F}{RT}\eta\right)\right] , \tag{16}$$

on the electrode surface. Here, i_o is the exchange current density, which depends on the concentration of the reactants, F is the Faraday's constant, R is the gas constant, α_a and α_c are the anodic and cathodic transfer coefficients, respectively, and η is the overpotential. The overpotential is defined by

$$\eta = \phi_{app} - \phi_l - E_f \,, \tag{17}$$

where ϕ_{app} is the applied potential at the electrode surface during CV measurements. E_f is the thermodynamic equilibrium potential at which no current flows, and ϕ_l is the electrostatic potential within the electrode–electrolyte interface. This potential is measured at the outer edge of the boundary layer. The applied potential as a function of scanning time is modelled by

$$\phi_{app}(t) = \begin{cases} \phi_{min} + \nu t & \text{if } 0 \le t \le \mathcal{T}, \\ \phi_{max} - \nu t & \text{if } \mathcal{T} \le t \le 2\mathcal{T}. \end{cases}$$

where ν is the scan rate and $\mathcal{T} = \frac{\phi_{max} - \phi_{min}}{\nu}$ is the half cycle period. For a CV curve, one calculates the total current measured against the applied voltage on the surface of the electrode by integrating the current density expressed by (16) at the electrode surface

$$i_{cv} = \int_{\partial\Omega} i_n dS \,. \tag{18}$$

Finally, the boundary conditions for the Navier–Stokes equations (10) and (11) are no-slip and penetration conditions on the microfluidic cell wall and on the surface of the electrode. For the inlet flow, we considered a pressure driven flow with a fully developed parabolic flow profile given by

$$v_x = v_{max}\left[1 - \frac{(z - (H/2))^2}{(H/2)^2}\right], \tag{19}$$

$$v_z = 0 \,, \tag{20}$$

and characterized by its maximum velocity v_{max} [38]. The v_x, v_z are the components of the velocity along the x and z axes, respectively. The parameter H is the channel height (Figure 1). This approximation is valid because the flow regime is characterized by low Reynolds number and as a result of the assumption $H \ll W < L$. Hence, the flow velocity is assumed uniform across the y-direction. Finally, we prescribe a constant pressure at the outlet.

Table I. Table of parameters used in the simulation.

Parameters	Values	Definition
C_b	1 mM	Bulk concentration
ρ	997 kg/m^3	Fluid density
z_j	$-1/1$	Ionic valencies
P	1 Pa	Outlet pressure
μ	0.36 mPa	Dynamic viscosity
T	298 K	Room temperature
D	1×10^{-10}m^2/s	Diffusion constant
F	96485 C/mol	Faraday's constant
R	8.314J/(mol K)	Gas constant
α_a, α_c	0.5	Anodic and cathodic transfer coefficient
u_j	2.529×10^{-8}m^2/Vs	Ionic mobility
l	400 μm	Electrode length
w_e	100 μm	Electrode width
t	550 nm	Electrode thickness
L	12 mm	Channel length
H	2 mm	Channel height

4. Numerical results

We have implemented the model (4), (9), (10), (11), and the boundary conditions in the finite element multiphysics software package COMSOL [39, 40]. Table I shows the parameter values used in the simulations. In the current simulations of CV, electrode surface potential is varied according to a piecewise linear and periodic curve. Figure 2 shows a typical potential-time graph over one period. The slope ν of the first half of the curve is termed the scan rate.

Figure 3(a) shows the concentration profile of the reactant O without flow at time $t = 16.25$ in a simulation of CV. The reactant migrates towards the electrode, transfers charges to the electrode leading to the product R leaving the electrode. The mobility of the ions is due to the diffusion and electric forces, which are proportional to the gradient of the electric potential ϕ. Figure 3(a) shows how the concentration of the reactant O is depleted close to the electrode.

The case where convection is present is shown in Figure 3(b). We observe how the products are flushed away from the electrode due to the flow, and fresh reactants are supplied from the left-hand side to the electrode. Here, the mass transport is dominated by convection.

4.1. *Effect of the flow rate on cyclic voltammetry*

Figure 4 shows a series of voltammograms at different flow rates. It is clear that the flow rate affects the recorded current. At low-flow rates, the diffusion and electric-field-induced mobility dominates the mass transport, which allows the ionic species to react with the surface of the electrode. As a consequence, we observe a peak of the current in the cyclic voltammogram. Furthermore, the usual hysteresis is present due to delayed response of the current to the applied voltage, a delay resulting from non-instantaneous response to the applied voltage of the ion concentration. Diffusion and electric mobility of the ions in out of equilibrium situations results in transient dynamics.

Increasing the flow rates reduces the hysteresis in the CV curve. We believe this is due to more rapid inflow of reactants O and fast convection induced removal of the products R. In addition, the current drops at the electrode surface and the products of the reactants are depleted faster away from the electrode. The effect could be seen as the current recorded flattens out without a peak current. This implies that convection dominates the mass transport in this case.

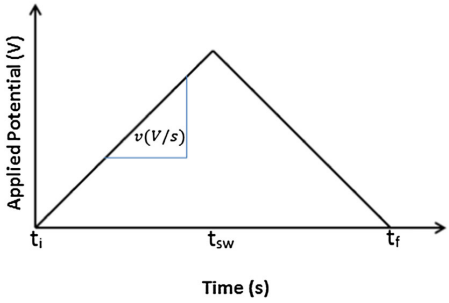

Figure 2. A piecewise linear curve for the applied electric potential versus time shown over one period. The scan rate ν is defined as the slope of the first half part of the curve.

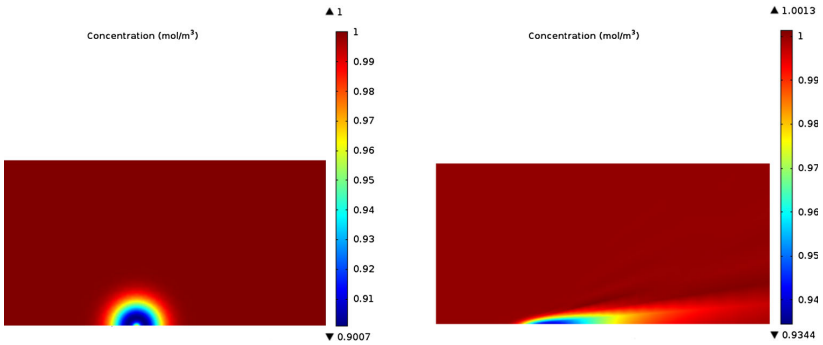

(a) Concentration of reactant O without flow. (b) Concentration of reactant O with flow.

Figure 3. Concentration of the species reactant O as function of position (x, z) at time $t = 16.25$.

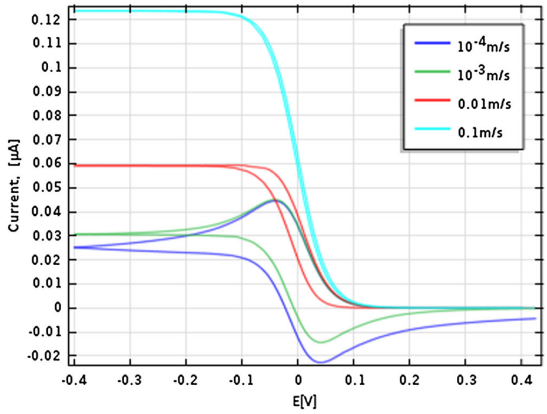

Figure 4. Cyclic voltammetry curves as a function of flow rates. The scan rate is 50 mV/s.

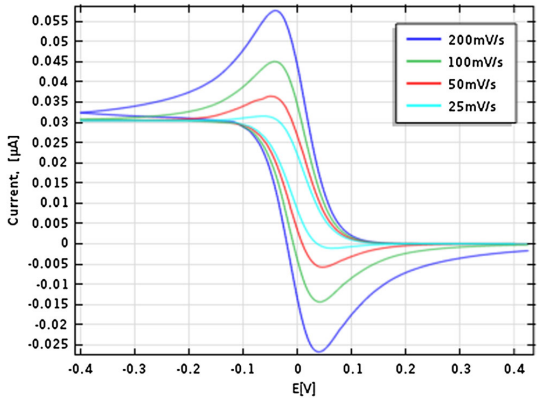

Figure 5. Cyclic voltammetry curves as a function of scan rates. The fluid velocity is $\underline{v} = 0$.

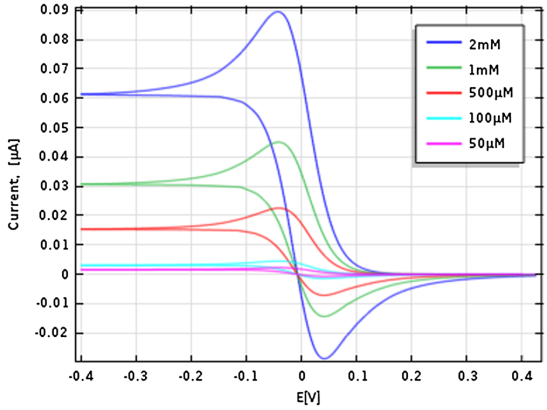

Figure 6. Cyclic voltammetry curves as a function of electrolyte bulk concentration. The fluid flow velocity is $\underline{v} = \underline{0}$.

4.2. *Effect of the scan rate on cyclic voltammetry*

In Figure 5, we show simulations of CV current voltage curves at different scan rates but without convective flow. At higher scan rates, the hysteresis becomes more pronounced, caused by the non-instantaneous response of the current to the applied voltage due to diffusion and electric-field-induced mobility of ions.

4.3. *Effect of reactant concentration on cyclic voltammetry*

Intuitively, we expect that for higher concentration of ions in the electrolyte, higher current values will be recorded. The results in Figure 6 show that the peak current varies linearly with the reactant concentration. The figure also shows that the hysteresis effect is not influenced by the reactant concentration.

5. Conclusions

We have set up a simple model that describes an electrochemical system from which CV was simulated. The model allows us to investigate the effect of flow rates, scan rates, and concentration on the CV curves. The main results are that higher flow rates lead to the reduced hysteresis in the current voltage curves and increasing scan rates lead to more pronounced current peaks. In the CV current voltage characteristics, the current increases proportionally to the electrolyte concentration.

Acknowledgements

We acknowledge financial support from the Villum Kann Rasmussen centre of Excellence: Nano Mechanical Sensors and Actuators, fundamentals and new directions (NAMEC). We thank Messoud Efendiev for very fruitful discussions on the fundamental mathematical properties of reaction–diffusion–advection equations and his ever inspiring lectures and visits to our department.

References

1. Jimenez-Jorquera C, Orozco J, Baldii A. ISFET based microsensors for environmental monitoring. *Sensors* 2009; **10**:61–83.
2. Tsoukalas D, Chatzandroulis S, Goustouridis D. *Capacitive Microsensors for Biomedical Applications Encyclopedia of Medical Devices and Instrumentation*. John Wiley & Sons, Inc.: Hoboken, New Jersey, 2006.
3. Fritz J. Cantilever biosensors. *The Analyst,* Milton Road, Cambridge, UK, 2008; **133**(7):855–863.
4. Jianhong P, Fang T, Thomas T. Glucose biosensor based on the microcantileverm. *Analytical Chemistry* 2004; **76**(2):292–297.
5. Si S-H, Huang K-L, Lu C-Y, Yao S-Z. Electrodeless piezoelectric quartz crystal sensor for determination of total urinary reducing sugar. *Microchemical Journal* 1999; **62**(3):328–335.
6. Moulin AM, O'Shea SJ, Welland ME. Microcantilever-based biosensors. *Ultramicroscopy* 2000; **82**:23–31.
7. Gruber K, Horlacher T, Castelli R, Mader A, Seeberger PH, Hermann BA. Cantilever array sensors detect specific carbohydrate-protein interactions with picomolar sensitivity. *ACS Nano* 2011; **5**:3670–3678.
8. Hansen KM, Ji H-F, Wu G, Datar R, Cote R, Majumdar A, Thundat T. Cantilever-based optical deflection assay for discrimination of DNA single-nucleotide mismatches. *Analytical Chemistry* 2001; **73**(7):1567–1571.
9. Nugaeva N, Gfeller KY, Backmann N, Lang HP, Düggelin M, Hegner M. Micromechanical cantilever array sensors for selective fungal immobilization and fast growth detection. *Biosensors and Bioelectronics* 2005; **21**(6):849–856.
10. Hwang KS, Lee S-M, Kim SK, Lee JH, Kim TS. Micro- and nanocantilever devices and systems for biomolecule detection. *Annual Review of Analytical Chemistry* 2009; **2**:77–98.
11. Waggoner PS, Craighead HG. Micro- and nanomechanical sensors for environmental, chemical, and biological detection. *Lab on A Chip* 2007; **7**(10):1238–55.
12. Grieshabe D, MacKenzie R, Voros J, Reimhult E. Electrochemical biosensors - sensor principles and architectures. *Sensors* 2008; **8**(3):1400–1458.
13. Cruys-Bagger N, Badino SF, Tokin R, Gontsarik M, Fathalinejad S, Jensen K, Toscano MD, Sørensen TH, Borch K, Tatsumi H, Väljamäe P, Westh P. A pyranose dehydrogenase-based biosensor for kinetic analysis of enzymatic hydrolysis of cellulose by cellulases. *Enzyme and Microbial Technology* 2014; **58**:68–74.
14. Wang J, Polsky R, Tian B, Chatrathi MP. Voltammetry on microfluidic chip platforms. *Analytical Chemistry* 2000; **72**(21):5285–5289.
15. Bard AJ, Faulkner RF. *Electrochemical Methods: Fundamentals and Applications* 2nd ed. John Wiley & Sons.
16. Newmann J, Thomas A, Karen E. *Electrochemical Systems* 3rd ed. Wiley-Interscience: Hoboken, New Jersey, 2004.
17. Compton RG, Banks CE. *Understanding Voltammetry* 2nd ed. Imperial College Press: Covent Garden, London, 2011.
18. Compton RG, Fisher AC, Wellington R, Dobson PJ, Leigh PA. Hydrodynamic voltammetry with microelectrodes: channel microband electrodes; theory and experiment. *The Journal of Physical Chemistry* 1993; **97**(40):10410–10415.
19. Orlik M. Digital simulation of cyclic voltammetry in a two-electrode system and its application to the kinetics of bis(biphenyl)chromium(i) in n, n-dimethylformamide. *Journal of Electroanalytical Chemistry* 1997; **434**:139–152.
20. Orlik M. An improved algorithm for the numerical simulation of cyclic voltammetric curves affected by the ohmic potential drops and its application to the kinetics of bis(biphenyl)chromium(i) electroreduction. *Journal of Electroanalytical Chemistry* 2005; **575**(2):281–286.
21. Yang S, Yang W, Sun G, Knickle H. Secondary current density distribution analysis of an aluminum-air cell. *Journal of Power Sources* 2006; **161**(2): 1412–1419.
22. Deng Z-X, Lin X-Q. Digital simulation of fast cyclic voltammogram by integration of the double layer charging current. *Journal of Electroanalytical Chemistry* 1999; **464**:215–221.

23. Wain AJ, Compton RG, Le Roux R, Matthews S, Fisher AC. Microfluidic channel flow cell for simultaneous cryoelectrochemical electron spin resonance. *Analytical Chemistry* 2007; **79**(5):1865–1873.
24. Chung M-H. A numerical method for analysis of tertiary current distribution in unsteady natural convection multi-ion electrodeposition. *Electrochimica Acta* 2000; **45**(24):3959–3972.
25. Ferrigno R, Brevet PF, Girault HH. Finite element simulation of the amperometric response of recessed and protruding microband electrodes in flow channels. *Journal of Electroanalytical Chemistry* 1997; **430**(1–2):235–242.
26. Matsuda H, Ayabe Y. On the theory of the randles-sevcik cathode-ray polarography. *Z. Electrochemistry* 1955; **59**:494–503.
27. Nicholson RS, Shain I. Theory of Stationary Electrode Polarography. Single Scan and Cyclic Methods Applied to Reversible, Irreversible, and Kinetic Systems. *Anal. Chem.* 1964; **36**(4):70–723.
28. Feldberg SW, Bard AJ. *Electroanalytical Chemistry*. Marcel Dekker: New York, 1969.
29. Feldberg SW, Mattson JS, Mark HB, MacDonald HC,Jr. *Computers in Chemistry and Instrumentation*. Marcel Dekker: New York, 1972.
30. Szabo A, Shoup D. Chronoamperometric current at finite disk electrodes. *Journal of Electroanalytical Chemistry* 1982; **140**:237–245.
31. Batchelor GK. *An Introduction to Fluids Dynamics*. Cambridge University Press: Cambridge, 1967.
32. Fuhrmann J, Linke A, Langmach H. A numerical method for mass conservative coupling between fluid flow and solute transport. *Applied Numerical Mathematics* 2011; **61**:530–553.
33. Kilic MS, Bazant MZ. Steric effects in the dynamics of electrolytes at large applied voltages. ii. Modified Poisson-Nernst-Planck equations. *Physical Review E* 2007; **75**:1–11.
34. Efendiev MA. *Evolution Equations Arising in the Modelling of Life Sciences*. Birkhäser: Basel, 2013.
35. Sonner S, Efendiev MA, Eberl HJ. On the well-posedness of a mathematical model of quorum-sensing in patchy biofilm communities. *Mathematical Methods in the Applied Sciences* 2011; **34**:1667–1684.
36. Efendiev MA. *Attractors for Degenerate Parabolic Type Equations*, Vol. 192. Mathematical Surveys and Monographs, American Mathematical Society, 2013.
37. Quan X, Fischer Lee M, Boisen A, Tenje M. Development of nanoporous gold electrodes for electrochemical applications. *Microelectronic Engineering* 2011; **88**:2379–2382.
38. Bird RB, Stewart WE, Lightfoot EN. *Transport Phenomena, Revised 2nd Edition* 2nd ed. John Wiley & Sons, Inc.: New York, 2002.
39. Zimmerman WBJ. *Multiphysics Modelling with Finite Elements Methods*. World Scientific Publishing Co.: Singapore, 2006.
40. *Comsol®multiphysics finite element analysis software*.

Chapter 5

Experimentation and Numerical Modeling of Cyclic Voltammetry

Paper II

Experimentation and Numerical Modeling of Cyclic Voltammetry for Electrochemical Micro-sized Sensors under the Influence of Electrolyte Flow

B. J. Adesokan[a], X. Quan[b], A. Evgrafov[a], A. Heiskanen[b], A. Boisen[b], M. P. Sørensen[a,*]

[a]*Department of Applied Mathematics and Computer Science, Technical University of Denmark, Richard Petersens Plads, Building 324, 2800 Kgs. Lyngby, Denmark*
[b]*Department of Micro and Nanotechnology, Technical University of Denmark, Building 345E, Ørsteds Plads, 2800 Kgs. Lyngby, Denmark*

Abstract

We investigate the effect of flow rate and scan rate on cyclic voltammetry in a microfluidic system for two different electrode locations. The mathematical model is based on ion transport governed by the Nernst-Planck equations coupled to the Navier-Stokes equations for hydrodynamics. The Butler-Volmer relation provides the boundary conditions which represent reaction kinetics at the electrode-electrolyte interface. The result shows that convection influences the charge transfer dynamics on the electrode surface and hence the cyclic voltammetry recorded. In terms of relative flow and scan rates, the current response is limited by the convection due to the supply of fresh ions at the electrode surface and quick removal of the products. However, at a high scan rates and a modest flow rates, peak current are recorded. The model also allows predicting the effect of varying electrolyte concentration and scan rates respectively. The numerical results with experimental findings, demonstrate qualitative and often also quantitative agreement.

Keywords: Cyclic Voltammetry, Microelectrode Location, Nernst-Planck, Navier-Stokes, Finite Element Method

*M. P. Sørensen
Email address: mapo@dtu.dk (M. P. Sørensen)

1. Introduction

The last decade has seen rapid progress in the use of microfabricated sensors in electrochemically charged environments for applications such as food safety, environmental monitoring, medical and health applications [1, 2, 3, 4, 5, 6]. These devices respond to changes in their physical, chemical and biological properties whenever they are subjected to environmental changes. In electrochemical systems, these microfabricated sensors analyse the chemical properties of a substance and translate them into electrical signals. This is done by coupling the devices with electroanalytical techniques. One of the most powerful analytical techniques employed for such task is cyclic voltammetry (CV) [7, 8, 9].

Cyclic voltammetry is widely utilized as the main mode of operation for biochemical sensing devices [1, 10, 11, 12, 13] and is also useful for probing electroactive surfaces in electrical energy storage and conversion devices [14, 15, 16]. Typically CV measurements are carried out in an electrochemical system where stationary electrodes are located in a static electrolyte solution. However, over the years rapid developments in electrochemical based sensing have inspired hydrodynamic voltammetric techniques where electrodes are placed in a fluidic cell [1, 17, 18, 19, 20, 21, 22], and electrolyte solution is pumped in and out of the system. There are several advantages one can derive from such a system. For a well defined flow, the mass transport rate can be controlled quantitatively by varying the electrolyte flow rates. Another advantage is that fewer experimental errors are introduced. In addition, the introduction of convection naturally increases the rate of mass transport and this can notably allow one to investigate both heterogeneous and homogeneous processes as well as studying faster reaction kinetics.

The fundamental understanding of the physics involved in cyclic voltammetry necessitates the development of theory that can relate system parameters such as flow rates and scan rates used in an electrochemical system [23, 24]. However, electrode kinetics is usually non-linear and CV is a transient technique implying that the theory is not always available except in some limiting

cases. Hence, numerical simulation is necessary. Furthermore, numerical solutions along with experimental methods allow for the effective study of parameters that characterize the output of a cyclic voltammetry measurement in more details.

Numerical solutions of the CV was first introduced by Feldberg [25, 26]. Since then several other authors have numerically studied CV with diffusion as the only mode of mass transfer, see for example [27, 28, 29]. Furthermore, there is an extensive list of authors that have numerically simulated CV curves in a flowing stream, in particular the Compton's group [19, 30, 31, 32, 33]. The authors among others have employed numerical methods such as the alternating direction implicit (ADI), strongly implicit procedure (SIP), the backwards implicit (BI) method, hopscotch algorithm [34, 35, 36] with regular meshes which may results in poor spatial convergence. Furthermore in order to ease the computational procedure, simplifications are made to the specified boundary conditions. For example, a constant concentration over the electrode surface can be specified. This corresponds to the limiting current which is the highest mass transfer rate. Although these boundary conditions simplify the solution of ion transport problem from which the CV is computed, the applications of the calculated solutions are consequently limited and should be ascertained by comparing them with experimental data. Motivated by the design and optimization of the electrode to ensure accurate CV measurement and for better characterisation of the response signal in an electrochemical system, we seek a solution method that can handle complex geometry which also allows for high computational flexibility and maintain the stability properties of the method deployed.

This study focuses on simulating CV using a flexible but powerful finite element method (FEM) solver, Comsol Multiphysics, under appropriate boundary conditions and electrode configurations in a microfluidic channel. In particular we investigate cantilever electrodes mounted in a microfluidic cell. We investigate the effect of flow rates, scan rates as well as electrolyte concentration and compare simulations to experimental data recorded for a CV measurement

under different electrode configurations. We demonstrate that the location of electrodes in an electrochemical system plays a significant role while recording a CV measurement. This information will be utilized to understand the behaviour of an electrochemical system needed in designing micro electrochemical sensors with improved performance.

2. Experimental setup of the electrochemical cantilever sensor

The electrochemical cantilever sensor (ECC) chip presented here was fabricated by standard microfabrication processes [17]. As shown in Figure 1, the chip has dimension 12 mm × 11.3 mm and it was fabricated on a 375 μm thick Si substrate. Four cantilevers were placed in the middle of the chip, each having the dimensions 100 μmm(width) × 550 nm (thickness) × 400 μm(length). Each cantilever was capable of functioning as an independent working electrode (WE). The reference electrode with dimensions 100 μm × 200 μm was placed on the right side of the cantilevers and the counter electrode with dimensions 2700 μm × 400 μm on the left side. All the electrodes were coated using e-beam evaporation with a 2 nm chrome adhesion layer followed by 30 nm of gold. The chips were cleaned before use. They were immersed in a piranha solution for 6 min, and then rinsed thoroughly in MilliQ-water and ethanol [37]. Finally, the chips were blown dry with nitrogen gas and mounted in a microfluidic chamber. As shown in Figure 1, the microfluidic chamber encapsulates the ECC biosensor with a volume of approximately 105μL and creates a flow path leading into the chip and through the channel past the cantilevers. The fluid enters from the side of the reference electrode and exits from the counter electrode side. There was an access to install a reference electrode in the microfluidic chamber as well. The system was connected to a syringe pump (PHD 2000 Infuse/Withdraw syringe pump, Harvard Apparatus, USA) and set the flow rates of up to 600 μL/min.

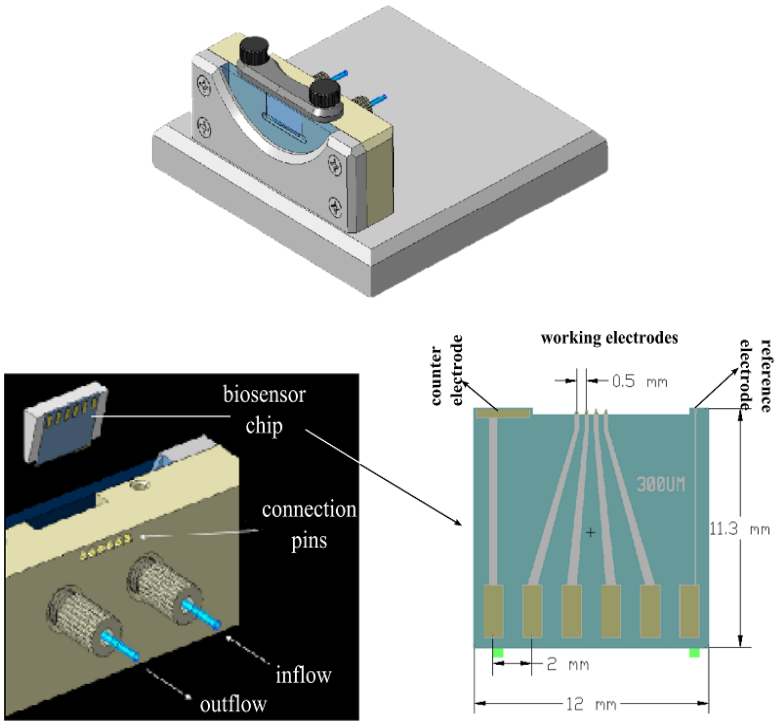

Figure 1: Fluidic cell and layout of a biosensor chip.

The electrolyte with active redox probes used in the cyclic voltammetric measurements consists of 200 mM $KNO3$ solutions with 2 mM of $K_3Fe(CN)_6$ in Milli-Q water. All the chemicals were used without further purification. A DRIREF-2SH $Ag/AgCl$ reference electrode was applied in the three-electrode electrochemical cell. Cyclic voltammetry was performed using a computer controlled CHI1030 Potentiostat.

3. Mathematical Modeling

The current response to the applied potential at the electrode surface is the rate of electron transfer across the electrolyte-electrode interface. Consider the following electrode reaction

$$Fe^{III}(CN)_6^{3-} + e^- \rightleftharpoons Fe^{II}(CN)_6^{4-} \ , \tag{1}$$

where $Fe^{III}(CN)_6^{3-}$ and $Fe^{II}(CN)_6^{4-}$ represent the oxidized and reduced species, respectively. When the potential is applied to the electrode, the electrolyte solution loses its equilibrium state due to the reaction at the electrode surface. The potential difference between the electrode and the adjacent electrolyte solution triggers the electrode-electron exchange in order for the system to relax to its original equilibrium state. Let N_j denote the ionic flux of species j in an electrolyte given by

$$N_j = -z_j u_j F C_j \nabla\phi - D_j \nabla C_j + C_j v \ , \tag{2}$$

where C_j, D_j, z_j and u_j are the ionic concentration, the diffusion constant, the charge and the mobility of the ionic species j. F, ϕ and v represent the Faraday's constant, the electrolyte potential and the convective velocity of the solution, respectively [7, 8]. The first term in the right hand side of (2) describes the electromigration driven by the gradient of the electric potential. The second term represents diffusion due to the ionic concentration gradient within the bulk electrolyte while the last term represents convection due to the fluid flow.

The current resulting from the motion of all charged species is computed as follows

$$\mathbf{i} = F \sum_j z_j N_j \ , \tag{3}$$

and the conservation of mass for species j in the bulk solution is given by

$$\frac{\partial C_j}{\partial t} = -\nabla \cdot N_j \ . \tag{4}$$

Here, we assume there is no chemical reaction within the bulk.

We shall assume that the electrolyte solution is electrically neutral except at a very thin electric double layer close to the electrode. In our analysis, we have neglected the thin layer and assumed electroneutrality throughout the solution. For an electrically neutral solution, the following holds

$$\sum_j z_j C_j = 0 \ . \tag{5}$$

From equation (4) and the electronuetrality condition (5), conservation of electric current can be derived

$$\nabla \cdot \mathbf{i} = 0 \ . \tag{6}$$

The equation for the electric potential

$$\nabla \cdot (\kappa \nabla \phi) + F \sum_j z_j \nabla \cdot D_j \nabla C_j = 0 \ , \tag{7}$$

can easily be derived from equation (6) by using the electronuetrality condition (5). Here $\kappa = F^2 \sum_j z_j^2 u_j C_j$ is the electrolyte conductivity.

Equations (4) and (7) couple the electric potential and ionic concentration of the system. Finally, in order to close the system, we need to determine the velocity field v of the electrolyte. This can be done by solving the Navier-Stokes equations for incompressible flow,

$$\nabla \cdot v = 0 \ , \tag{8}$$

$$\rho \left(\frac{\partial v}{\partial t} + v \cdot \nabla v \right) = -\nabla p + \mu \nabla^2 v + s_f \ . \tag{9}$$

The fluid density is denoted ρ, p is the pressure, μ is the dynamic viscosity and finally s_f denotes an external force per unit volume [38, 39]. Finally, equations (4), (7), (8) and (9) must be solved with appropriate boundary conditions.

3.1. Boundary conditions and computational domain

In order to facilitate the numerical simulation of the micro fluidic cell depicted in Figure 1, we will restrict our computational domain to cover a volume including the cantilever electrodes and a neighborhood of the electrodes in the electrolyte. At the left boundary of the computational domain we use inflow conditions and at the right boundary we use outflow conditions, chosen as close as possible to the experimental situation. Hereby we substantially reduce the computational task in comparison to simulating the entire microfluidic cell. Specifically, we chose the computational domain in Figure 2, which is small enough to facilitate the computational task yet sufficiently complex to provide comprehensive insight into the influence of the convective flow, scan rates and concentration of reactants on cyclic voltammetry for the cell shown in Figure 1. In what follows, we shall specify the boundary conditions for the computational domain having length L, width W and height H. The computational domain in Figure 2 encompass the working electrode of width w_e and length ℓ placed at the center of the domain but fixed to the wall of the domain anywhere between $z = 0$ and $z = H$. The counter electrode is placed far to the left of the working electrode and is not shown in the figure.

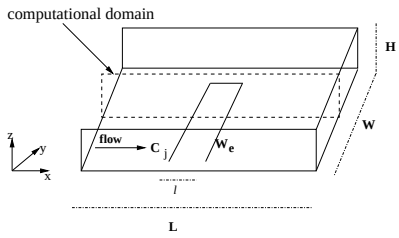

Figure 2: Schematic diagram of the fluidic channel and a micro-sized working electrode

The counter electrode allows the current flowing through the electrolyte solution via the working electrode to leave the solution. In addition, we may

insert a reference electrode in order to maintain a stable and constant potential at the working electrode. There is normally no current flow passing through the reference electrode. Furthermore, we consider a cell where $H \ll W < L$ and accordingly we assume that transport of ions and fluidic motion can be considered two dimensional. This means we restrict our model to the cross sectional xz-plane at any point on y away from the walls at $y = 0$ and $y = W$ in Figure 2.

The potential-current responses are measured at the surface of the electrode - at least within the thin layer above the electrode and hence the boundary conditions play a central role in modeling cyclic voltammetry. At the inlet we specify constant concentrations of the chemical species and a no flux boundary condition $-n \cdot N_j = 0$ on the fluidic cell walls where n is the unit normal pointing towards the electrolyte. At the outlet of the cell we specify $D\dfrac{\partial C_j}{\partial n} = 0$. At the insulating surfaces $\partial\Omega_{ins}$ there are no current flow which means that the normal current density i_n across such a boundary is zero, that is

$$i_n = 0 \qquad \text{on} \qquad \partial\Omega_{\text{ins}}. \tag{10}$$

In other words, from the conservation of the electric current (7) we can prescribe Neumann type boundary conditions

$$\kappa\frac{\partial\phi}{\partial n} = -z_j D_j \frac{\partial C_j}{\partial n} \qquad \text{on} \qquad \partial\Omega_{\text{ins}}\ . \tag{11}$$

However, at the electrode surface the ionic flux for each species j can be modeled by the normal current density determined from electrode kinetics,viz

$$\kappa\frac{\partial\phi}{\partial n} + z_j D_j \frac{\partial C_j}{\partial n} = i_n(C_j, \phi, v; \phi_{app}) \qquad \text{on} \qquad \partial\Omega\ . \tag{12}$$

Here ϕ_{app} is the applied potential on the electrode surface.

The electrode kinetics we shall model by the Butler-Volmer relation [7, 8, 40, 41],

$$i_n = i_o \left[C_R \exp\left(\frac{\alpha_a F}{RT}\eta_s\right) - C_O \exp\left(\frac{-\alpha_a F}{RT}\eta_s\right)\right] , \tag{13}$$

where

$$\eta = \phi_{app} - \phi_l - E_f , \tag{14}$$

is the overpotential, which defines the potential difference between the electrode and the adjacent electrolyte solution. E_f is the thermodynamic equilibrium potential at which no current flows and ϕ_l is the electrostatic potential within the electrode-electrolyte interface. This potential is measured at the outer edge of the concentration boundary layer. The applied potential as a function of scanning time can be modeled as follows,

$$\phi_{app}(t) = \begin{cases} \phi_{min} + \nu t & \text{if } 0 \le t \le \mathcal{T} \\ \phi_{max} - \nu t & \text{if } \mathcal{T} \le t \le 2\mathcal{T} \end{cases}$$

where ν is the scan rate and $\mathcal{T} = \dfrac{\phi_{max} - \phi_{min}}{\nu}$ is the half cycle period.

For a cyclic voltammetry curve, one computes the total current response to the applied potential on the surface of the electrode by integrating the current density expressed in (13) at the electrode surface $\partial\Omega$

$$i_{cv} = \int_{\partial\Omega} i_n dS . \tag{15}$$

Finally, the boundary conditions for the Navier-Stokes equations (8) and(9) are no-slip and no penetration conditions at the fluidic cell wall and at the surface of the electrode. For the inlet flow, we considered a pressure driven flow with a fully developed parabolic flow profile

$$v_x = v_{max}\left[1 - \frac{(z - (H/2))^2}{(H/2)^2}\right] , \tag{16}$$

$$v_z = 0 , \tag{17}$$

characterized by its maximum velocity v_{max} [42, 43]. The v_x and v_z are the components of the velocity along the x and z axis, respectively. v_{max} is the

maximum velocity at the tip of the parabola. This approximation is valid because the flow regime is characterized by low Reynolds number and the width of the fluidic cell in the y-direction is far larger than the height H. Hence, the velocity flow is uniform across the y-direction. The volumetric flow rate U is calculated from the input velocity through

$$U = \bar{v}_x HW \ , \tag{18}$$

where W is the width of the fluidic cell and

$$\bar{v}_x = \frac{1}{H}\int_0^H v_x dy = \frac{2}{3} v_{max} \tag{19}$$

is the average velocity [44]. At the outlet, we specify a constant pressure value.

4. Numerical methods and parameters

We solved numerically the test problem using the commercial software package COMSOL Multiphysics [45, 46] on a Windows work station (Core i7 CPU, 4 cores, 2.40GHz, 16.0GB RAM). The geometries are shown in Figure 3. They consist of the flow ducts with two configurations for the electrodes. We consider a case where the electrode is placed at the bottom of the cell and the case where it is placed in the center of the cell. In both cases the electrodes are fixed to the cell wall. We have simulated a 2D approximation to the full system in Figure 2.

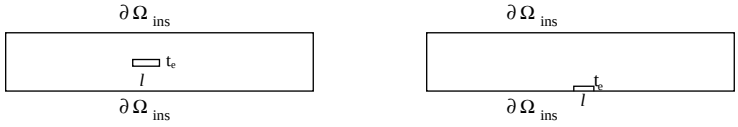

Figure 3: Computational domain with different electrode configurations. (a) center placed, (b) bottom placed.

We employed a two step approach in solving the coupled fluid and ion-transport problem. First, we find a steady state solution to the incompressible Navier-Stokes equations.

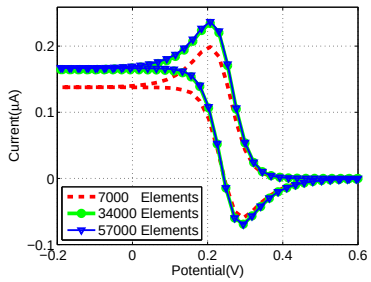

Figure 4: The computations are conducted for the fluid cell geometry in Figure 3b.

The steady state velocity is then substituted into the ion transport problem. We solved the fluid flow problem by discretizing the computational domain using the linear Lagrange finite elements for the pressure field and quadratic elements for the velocity field. In addition, we have utilized quadratic elements for the ion transport problem [39, 46, 45].

In order to assess the accuracy of the solution method, we performed several studies based on finer and finer meshes until there are only small changes in the estimated current-potential curves, Figure 4 are observed. The high density of mesh is due to local mesh refinement around the electrode where there are large solution gradients. In order to ensure a good compromise between computational time and the accuracy of the results we have used about 35000 elements in our computations. For the time integration, we have employed implicit Euler method. Table 1 shows the parameters used throughout in the simulation.

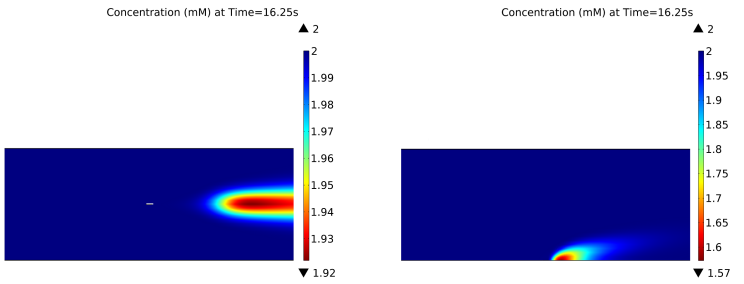

(a) (b)

Figure 5: The Concentration of $Fe^{III}(CN)_6^{3-}$ showing the effect of the flow pattern on the electrode position. The flow rate is $250\,\mu L/min$.

5. Results and Discussion

Figures 5a and 5b show a snapshot of the concentration of $Fe^{III}(CN)_6^{3-}$ taken at time $t = 16.25\,s$, that is at the final time of one scan with 50 mV/s scan rate. For the center placed electrode in Figure 5a, the concentration of $Fe^{III}(CN)_6^{3-}$ downstream of the cantilever electrode is slightly lower than the upstream concentration. As the concentration is high close to the electrode we may expect higher currents. For the bottom placed electrode in Figure 5b the electrolyte flow velocity is very small close to the bottom surface. This suggests that mass transport due to convection is limited and that mass flow is dominated by diffusion and the electric forces, which means fewer electro active species are brought towards the electrode surface for the bottom placed electrode. However, for the center placed electrode, electro active species are brought fast to the electrode surface.

Parameters	Values	Definition
l	400μm	electrode length
w_e	100μm	electrode width
t_e	550nm	electrode thickness
L	12mm	channel length
H	1mm	channel height
C_b	2mM	bulk concentration
ρ	$997kg/m^3$	fluid density
μ	0.36mPa	dynamic viscosity
P	1Pa	outlet pressure
T	298K	room temperature
ν	(50 - 250)mV/s	scan rates
D	$1 \times 10^{-10} m^2 s$	diffusion constant
F	96485C/mol	Faraday's constant
R	8.314J/(mol K)	gas constant
α_a,α_c	0.5	anodic and cathodic transfer coefficients
u_j	$2.529 \times 10^{-8} m^2/Vs$	ionic mobility
U	$(50 - 250)\mu L/min$	volumetric flow rates

Table 1: Cell dimensions and other parameters used in the simulations.

5.1. Cyclic voltammetry in a static electrolyte

In order to validate the model, we perform experiments and simulations using a static electrolyte by varying the bulk concentration from 500μM to 2mM before flow is introduced into the respective systems. In Fig. 6, we show the plots of the current (μA) against potential E(v) for forward and reverse scans performed between 0.6 V and -0.2 V. Note here that both experiments and simulation were performed at a scan rate of $50\,mV/s$.

Focusing on the experimental results presented in Fig. 6a, a first observation for all concentrations is that the peak current is reached before the end of the

forward scan. Interestingly, for all concentrations, the anodic peak current is reached at a potential $E \approx 0.25$ V. This indicates a non-dependence of the peak potential reached on the concentration. Secondly, we observe that the current recorded at end of the forward scan $E =$ -0.2 V is higher with increasing concentration, even though they were all initiated at zero current. During the reverse scan, a non-symmetric evolution of the current is seen with respect to the forward scan. The non-symmetry of the current is possibly a feature arising from the non-symmetric range of potential chosen. The minimum current is reached at a higher potential $E \approx 0.35$ V and is also independent of concentration. At the end of the reverse scan, the initial state is not recovered, indicating hysteretic and memory effects.

In Fig. 6b, we plot the corresponding numerical results of the experiment described above. For the sake of brevity, we note that qualitative features reported for experiments, namely the independence of potential at peak current and increase in current at the end of the forward scan with increasing concentration are well captured by the simulation. Slight quantitative differences in the anodic peak current reached in simulation and the current obtained at the end of the forward scans are possibly due to the dimensionality of the current simulations.

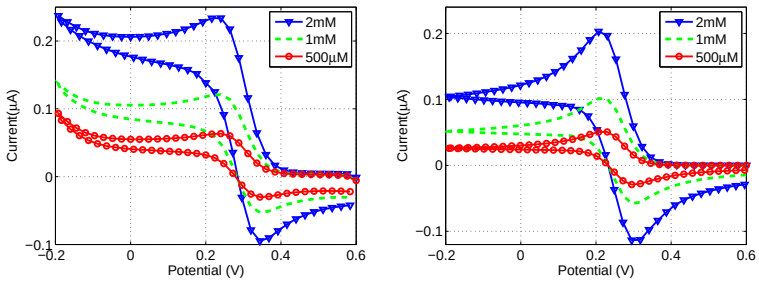

(a) (b)

Figure 6: Comparison of a) experimental and b) simulation results of steady-state cyclic voltammograms as a function of concentration recorded at a center placed microelectrode in a solution of 200mM KNO_3 with $K_3Fe(CN)_6$ of a static electrolyte. Other parameter values taken from Table 1.

5.2. The effect of flow rates on cyclic voltammetry measurements at a micro-sized electrode

In Figure 7a we show experimental voltammograms at different flow rates compared to numerical simulations depicted in Figure 7b for an electrode positioned in the center of the flow chamber with 50 mV/s scan rate. As both the experiments and the simulations suggest, flow rates clearly affect the current recorded during voltammetry measurements. At low flow rates of $(50 - 150)\mu L/min$, the results suggest that the ionic mass transport is dominated by the diffusion of the ionic species towards the working electrode. This ensures that even at a slow scan rate of $50mV/s$ we record enough peak currents shown in Figure 7b. However, as the flow rate increases, the hysteresis of the voltammograms diminishes and the appearance of peak currents becomes less pronounced. For higher flow rates of $250\mu L/min$ the mass transport due to convection dominates that due to diffusion. We believe that the higher flow rates lead to fresh supply of $Fe^{III}(CN)_6^{3-}$ at high concentration to the electrode and

hence the current increases, in particular at voltage values less than about $0.2V$ as is evident in Figure 7.

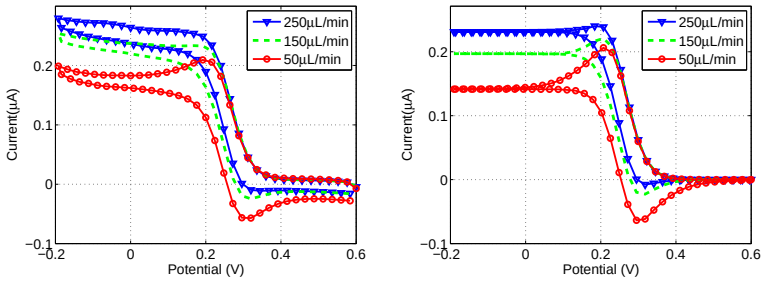

(a) (b)

Figure 7: Comparison of a) experimental and b) simulation results of cyclic voltammograms as a function of flow rates recorded at a centre placed microelectrode in a solution of 200mM KNO_3 with $K_3Fe(CN)_6$. The scan rate is $50mV/s$. Other parameter values taken from Table 1.

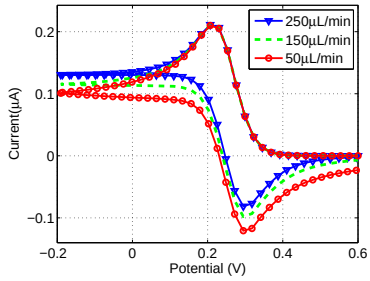

Figure 8: Effect of flow rates - Simulation with electrode at the bottom of the cell. Scan rate at $50mV/s$. Other parameter values taken from Table 1.

In Figure 8 we show simulations of cyclic voltammetry for a microfluidic

cell with the working electrode placed at the bottom. The same flow rates have been used as in Figure 7. Comparing the results in Figure 7 and Figure 8 demonstrates that the position of the electrode impacts the shape of the recorded CV. At the bottom of the cell the flow velocity decreases and the ion transport is dominated by diffusion leading to lower concentrations of $Fe^{III}(CN)_6^{3-}$ at the electrode (see Figure 5) and hence lower currents, in particular for voltages less than about 0.2 V. Our simulation results in Figure 8 fitted well with the previous calculations reported in [19].

At high flow rates the hysteresis of the voltammograms become less pronounced as opposed to the pure diffusion dominated mass-transport in which a quasi-steady state is obtained. This suggests the reduction of the diffusion layer built up by depleting electro active species. In other words, the depleted region thickness for electro active species will be limited by the average diffusion layer thickness and the current response is only mass-transport limited through convection.

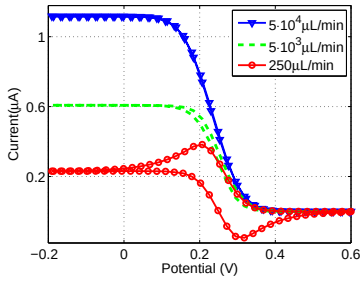

Figure 9: Simulation results for a center placed electrode showing the effect of using extreme higher flow rates at high scan rate 250 mV/s. Other parameter values taken from Table 1.

Finally, we considered the extreme cases of flow rates at high scan rate of $250mV/s$. The intention is to show the limit to which convection should be introduced into a cyclic voltammetry measurement, see Figure 9. We in-

creased the volumetric flow rate to as high as $10^4 \mu L/min$. The hysteresis of the voltammograms vanishes completely at the highest flow rate. This implies that compromise must be made as to what flow rates and scan rates are admissible depending on the object of interest in the voltammetry study.

5.3. The effect of scan rates on cyclic voltammetry measurements at a micro-sized electrode

Depending on the direction of scan, oxidation or reduction, it is expected that at high scan rates one records the highest current response in voltammetry. This is indeed observed in Figure 10a where we sweep the potential from $0.6V$ to -$0.2V$ at different scan rates and at a fixed volumetric flow rate of $250\mu L/min$. The associated simulation results are depicted in Figure 10b, which demonstrate fair agreement with the experimental measurements but deviates at more negative and more positive potentials. As expected, the current response increases with scan rate. At the scan rate of $250mV/s$, the peak currents are observed in both directions of scan while at $50mV/s$ a diminished hysteresis is recorded.

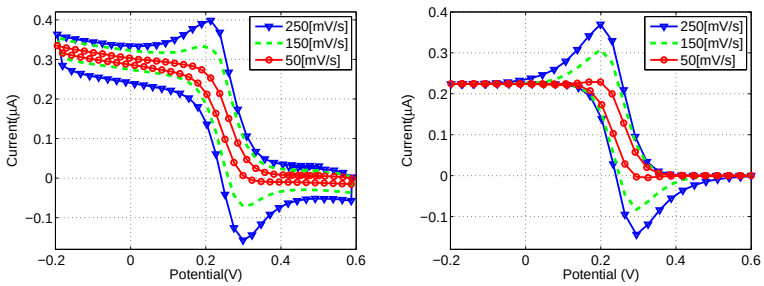

(a) (b)

Figure 10: Comparison of a) experimental and b) simulation results of cyclic voltammograms as a function of scan rates recorded at a centre placed micro-electrode in a solution of 200mM KNO3 with 2mM $K_3Fe(CN)_6$ with flow rate of 250 μL/min. Other parameter values taken from Table 1.

The peak at high scan rates recorded at the flow rate of $250\mu L/min$ can be explained since at high scan rates surface kinetics is fast enough for electron exchange to occur before fresh electro-active ions are brought onto and the products are washed away from the electrode surface. When the potential is scanned from positive to negative potentials, the reactants lose electrons fast enough leading to the increase in current response. The products then deplete away from the electrode surface. At low scan rates, e.g $50mV/s$, current is controlled mainly by diffusion and convection of the reactant to the electrode surface. However, at high flow rates, convection increases relative to diffusion and fresh reactants are brought to the electrode surface. In addition, because of the slow scan, electrode surface kinetics is not fast enough for the electron exchange to record a peak current and hence the narrow and flattened voltammograms as shown in Figure 10b. Comparison between the experimental data and the simulation results show a very good agreement. See Figure 10a.

6. Conclusions

The above results show the successful model of a two step finite element method for simulating cyclic voltammetry under flow conditions. We found that the flow rates has a strong influence on the current response recorded during cyclic voltammetry. At high flow rates, a peak current disappears and the hysteresis is reduced while at low rates steady current response with peak current is recorded. In addition, the placement of electrodes is critical when performing cyclic voltammetry under flow. The main difference between the centered placed electrode and the bottom placed electrode is the delay in the conversion of the fresh ionic species brought to the electrode surface for the bottom placed electrode. In the centered placed electrode the influence is more apparent since the variation can be seen in the current response. We were able to identify the characteristics of the hydrodynamic effect on the the dynamics of the current response to the applied voltage in cyclic voltammetry measurements. Qualitative and often also quantitative agreement are found between experimental and

theoretical predictions for cyclic voltammetry measurements. For the design and optimization of the electrodes, investigation of a full 3D problem is needed. In addition, since electroneutrality condition does not hold at the electric double layer (EDL) one can extend the present model by including the phenomenon in order to capture the complete Physics at the electrode-electrolyte interface.

7. Acknowledgement

We aknowledge financial support from the Villum Kann Rasmussen centre of Excellence: Nano Mechanical Sensors and Actuators, fundamentals and new directions (NAMEC).

References

[1] L. M. Fischer, C. Pedersen, K. Elkjær, N. N. Noeth, S. Dohn, A. Boisen, M. Tenje, Development of a microfabricated electrochemical-cantilever hybrid platform, Sens. Act. B: Chem. 157 (1) (2011) 321–327.

[2] A. Subramanian, P. I. Oden, S. J. Kennel, K. B. Jacobson, R. J. Warmack, T. Thundat, M. J. Doktycz, Glucose biosensing using an enzyme-coated microcantilever, Appl. Phys. Lett. 81 (2) (2002) 385–387.

[3] K. S. Hwang, S.-M. Lee, S. K. Kim, J. H. Lee, T. S. Kim, Micro- and nanocantilever devices and systems for biomolecule detection, Annu. Rev. Anal. Chem. 2 (2009) 77–98.

[4] M. Alvarez, A. Calle, J. Tamayo, L. M. Lechuga, A. Abad, A. Montoya, Development of nanomechanical biosensors for detection of the pesticide {DDT}, Biosens. Bioelectron. 18 (56) (2003) 649 – 653.

[5] S. P. A. Fodor, R. P. Rava, X. C. Huang, A. C. Pease, C. P. Holmes, C. L. Adams, Multiplexed biochemical assays with biological chips, Nature 364 (1993) 555 – 556.

[6] X. Quan, L. M. Fischer, A. Boisen, M. Tenje, Development of nanoporous gold electrodes for electrochemical applications, Microelectron. Eng. 88 (8) (2011) 2379–2382.

[7] A. J. Bard, L. R. Faulkner, Electrochemical Methods: Fundamentals and Applications, 2nd Edition, John Wiley & Sons, 2001.

[8] J. Newmann, K. E. Thomas-Alyea, Electrochemical Systems, 3rd Edition, Wiley-Interscience, 2004.

[9] R. G. Compton, C. E. Banks, Understanding Voltammetry, 2nd Edition, World Scientifice, 2011.

[10] S. Chevion, M. Hofmann, R. Ziegler, M. Chevion, P. P. Nawroth, The antioxidant properties of thioctic acid: characterization by cyclic voltammetry, Biochem. Mol. Biol. Int.l 41 (2) (1997) 317–327.

[11] S. Chevion, M. A. Roberts, M. Chevion, The use of cyclic voltammetry for the evaluation of antioxidant capacity, Free Radical Biol. Med. 28 (6) (2000) 860–870.

[12] D. Grieshaber, R. MacKenzie, J. Voros, E. Reimhult, Electrochemical biosensors - sensor principles and architectures, Sensors 8 (3) (2008) 1400–1458.

[13] N. Cruys-Bagger, S. F. Badino, R. Tokin, M. Gontsarik, S. Fathalinejad, K. Jensen, M. D. Toscano, T. H. Sørensen, K. Borch, H. Tatsumi, P. Väljamäe, P. Westha, A pyranose dehydrogenase-based biosensor for kinetic analysis of enzymatic hydrolysis of cellulose by cellulases, Enzyme Microb. Technol. 58 (2014) 68 – 74.

[14] M. Takahashi, S. Tobishima, K. Takei, Y. Sakurai, Reaction behavior of LiFePO4 as a cathode material for rechargeable lithium batteries, Solid State Ionics 148 (2002) 283–289.

[15] W. Sugimoto, K. Aoyama, T. Kawaguchi, Y. Murakami, Y. Takasu, Kinetics of CH3OH oxidation on PtRu/C studied by impedance and CO stripping voltammetry, J. Electroana. Chem. 576 (2) (2005) 215–221.

[16] X. Cheng, B. Yi, M. Han, J. Zhang, Y. Qiao, J. Yu, Investigation of platinum utilization and morphology in catalyst layer of polymer electrolyte fuel cells, J. Power Sources 79 (1) (1999) 75–81.

[17] X. Quan, A. Heiskanen, Y. Sun, A. Labuda, A. Wolff, J. Jorge Dulanto, P. Grutter, M. Tenje, A. Boisen, Development of electrochemical cantilever sensors for dna applications, ECS Transactions 50 (12) (2013) 77–81.

[18] J. A. Cooper, R. G. Compton, Channel electrodes - a review, Electroanalysis 10 (3) (1998) 141–155.

[19] A. C. Fisher, R. G. Compton, A general computational approach to linear sweep voltammetry at channel electrodes, J. Appl. Electrochem. 22 (1992) 38–42.

[20] N. V. Rees, R. A. W. Dryfe, J. A. Cooper, B. A. Coles, R. G. Compton, S. G. Davies, T. D. McCarthy, Voltammetry under high mass transport conditions. a high speed channel electrode for the study of ultrafast kinetics, J. Phys. Chem. 99 (18) (1995) 7096–7101.

[21] J. V. Macpherson, N. Simjee, P. R. Unwin, Hydrodynamic ultramicroelectrodes: kinetic and analytical applications, Electrochim. Acta 47 (1-2) (2001) 29–45. doi:10.1016/S0013-4686(01)00588-6.

[22] V. M. Volgin, A. D. Davydov, Mass-transfer problems in the electrochemical systems, Russ. J. Electrochem. 48 (6) (2012) 565–569. doi:10.1134/S1023193512060146.

[23] R. S. Nicholson, I. Shain, Theory of stationary electrode polarography - scan and cyclic methods applied to reversible, irreversible, and kinetic systems, Anal. Chem. 36 (4) (1964) 707–723.

[24] H. Matsuda, Y. Ayabe, On the theory of the randles-sevcik cathode-ray polarography, Z. Electrochem 59 (1955) 494.

[25] S. W. Feldberg, Digital simulation: A general method for solving electrochemical diffusion-kinetic problem, Electroanal. Chem 3 (1969) 199–296.

[26] M. Rudolph, D. P. Reddy, S. W. Feldberg, A simulator for cyclic voltammetric responses, Anal. Chem. 66 (10) (1994) 589A–600A.

[27] D. Zhao-Xiang, L. Xiang-Qin, Digital simulation of fast cyclic voltammogram by integration of the double layer charging current, J. Electroanal. Chem. 464 (1999) 215–221.

[28] M. Orlik, An improved algorithm for the numerical simulation of cyclic voltammetric curves affected by the ohmic potential drops and its application to the kinetics of bis(biphenyl)chromium(i) electroreduction, J. Electroana.l Chem. 575 (2) (2005) 281–286.

[29] G. Jidong, L. Ernö, Cyclic voltammograms at coplanar and shallow recessed microdisk electrode arrays: guidelines for design and experiment, Anal. Chem 81 (1) (2009) 130–8. doi:10.1021/ac801592j.

[30] R. G. Compton, A. C. Fisher, R. G. Wellington, P. J. Dobson, P. A. Leigh, Hydrodynamic voltammetry with microelectrodes: channel microband electrodes; theory and experiment, J. Phys. Chem. 97 (40) (1993) 10410–10415.

[31] J. A. Alden, M. A. Feldman, E. Hill, F. Prieto, M. Oyama, B. A. Coles, R. G. Compton, P. J. Dobson, P. A. Leigh, Channel microband electrode arrays for mechanistic electrochemistry. two-dimensional voltammetry: transport-limited currents, Ana. chem. 70 (9) (1998) 1707–20.

[32] C. E. Banks, A. O. Simm, R. Bowler, R. G. Dawes, Kand Compton, Hydrodynamic electrochemistry: design for a high-speed rotating disk electrode, Ana. Chem. 77 (6) (2005) 1928–30.

[33] S. M. Matthews, G. Q. Du, A. C. Fisher, Microfluidic voltammetry: simulation of the chronoamperometric response of microband electrodes sited within microreactors, J. Solid State Electrochem. 10 (10) (2006) 817–825.

[34] M. J. Bidwell, J. A. Alden, R. G. Compton, Hydrodynamic voltammetry with channel microband electrodes: the simulation of voltammetric waveshapes, Electroanal. Chem. 417 (12) (1996) 119 – 128.

[35] J. A. Alden, R. G. Compton, A comparison of finite difference algorithms for the simulation of microband electrode problems with and without convective flow, Electroanal. Chem. 402 (12) (1996) 1 – 10.

[36] D. Shoup, D. Szabo, Hopscotch: An algorithm for the numerical solution of electrochemical problems, Electroanal. Chem. Inter. Electrochem. 160 (12) (1984) 1 – 17.

[37] X. Quan, Development of an Electrochemical Cantilever Platform for Bio-Chemical Application, Ph.D. thesis, Technical University of Denmark (2013).

[38] G. Batchelor, An Introduction to fluids dynamics, Cambridge University Press, 1967.

[39] J. Fuhrmann, A. Linke, H. Langmach, A numerical method for mass conservative coupling between fluid flow and solute transport, Appl. Num. Maths. 61 (2011) 530–553.

[40] L. Uziel, Modern Aspects of Electrochemistry, Vol. 44 of Modern Aspects of Electrochemistry, Springer New York, New York, NY, 2009.

[41] J. Fuhrmann, H. Zhao, H. Langmach, Y. E. Seidel, Z. Jusys, R. J. Behm, The role of reactivereaction intermediates in two-step heterogeneous electrocatalytic reactions: A model study, Fuel Cells 11 (2011) 501–510.

[42] V. Levich, Physicochemical hydrodynamics, Prentice-Hall international series in the physical and chemical engineering sciences, Prentice-Hall, 1962.

[43] R. B. Bird, W. E. Stewart, E. N. Lightfoot, Transport Phenomena, Revised 2nd Edition, 2nd Edition, John Wiley & Sons, Inc., 2006.

[44] R. Ferrigno, P. F. Brevet, H. H. Girault, Finite element simulation of the amperometric response of recessed and protruding microband electrodes in flow channels, J. Electroanal. Chem. 430 (1-2) (1997) 235–242.

[45] Comsol®multiphysics finite element analysis software.
URL http://www.comsol.com

[46] W. B. J. Zimmerman, Multiphysics Modelling with Finite Elements Methods, World Scientific Publishing Co. Singapore, 2006.

Chapter 6

Assessing electric double layer of microelectrochemical system

---

Paper III

Transient dynamics of electric double layer (EDL) characterized by charge transfer and steric effect

B J Adesokan[a], A Evgrafov[a], M P Sørensen[a,*]

[a]*Department of Applied Mathematics and Computer Science, Technical University of Denmark, Richard Petersens Plads, Building 324, 2800 Kgs. Lyngby, Denmark*

Abstract

We provide a numerical solution for describing non-linear responses to large applied voltages at the electrode in a microelectrochemical system. In our analysis, we account for the finite size properties of ions in the equation describing the mass and the charge transport of ionic species in an electrochemical system and then analyse the responses on the charging of the electric double layer. We consider an arbitrary electrolyte solution that is sandwiched between electrodes and allow for electrochemical reactions at the electrode/electrolyte interface. The result shows a quick build up of boundary layers in the double layer which is counterbalanced by the finite size constraint on the ionic species and prevents overcrowding of the ions.

Keywords: Electric double layer, Steric effects, Modified Nernst-Planck-Equation, Boundary layers

2010 MSC: 00-01, 99-00

1. Introduction

In recent years, advancements in miniaturized electrochemical systems have brought new trends towards development of micro analytical devices that are capable of fast, quantitative and multistep detection. Such microelectrochemical systems are found in thin film batteries [1, 2, 3, 4], colloid and surface science [5, 6, 7], ion channels in biological cells [8, 9, 10, 11], electrokinetics [12, 13, 14, 15], microfluidics [16, 17], among others. These microelectrochemical systems are normally subjected to applied voltages or currents and the goal is to measure their responses to the input signals. A broad understanding of the underlying physics requires mathematical modeling and analysis.

The model for the mass and charge transport of ionic species in an electrochemical system was derived by Nernst and Planck as early as in the nineteenth century [18, 19]. Over the years, researchers have adopted various simplifications of their model. For example electroneutrality throughout the domain of the electrolyte solution is assumed in order to make the problem mathematically tractable. However, for microelectrochemical systems where the interface plays a crucial role there are limitations to which these simplified models are accurate. For example, for large electrode potentials of more than 50mV, the ionic concentration is usually

*M P Sørensen
Email address: mapo@dtu.dk (M P Sørensen)

overestimated by the theory [20, 21]. One of the reasons for this feature is the fact that ionic species are treated as point charges and finite size of ions is discarded. This assumption becomes invalid because close to the electrode surface the ion concentration can get very high due to the crowding effect. As a consequence, the ion transport model should account for the finite size of ions and the model must be coupled to appropriate boundary conditions where special attention is paid to the dynamics of the electrolyte solution in the region close to the surface of the electrode, in particular, the electric double layer (EDL).

The electric double layer is a set of nested layers, which consists of the inner compact layer referred to as the Stern layer, and the outer diffuse layer also known as the Debye layer. The typical width of an EDL is about 1-10Å depending on the electrolyte solution. Within the electric double layer there is usually no net charge separation which means that one or more ionic species can occur in excess and hence electroneutrality condition does not hold in this region. Typically, the Stern layer of the double layer is considered to be the compact layer where ions adhere to the surface of the electrodes and a capacitive effect of the ions within the compact layer is included while formulating the appropriate boundary conditions. The most important work on the Stern layer was performed both theoretically and experimentally by Stern and Grahame, respectively [22, 23]. On the other hand, the Debye layer is the layer where the diffuse-charge effect of the ionic species is normally accounted for. In addition, the dynamical charging of the layer is considered to have essential effect on the charge transfer kinetics at the electrode-electrolyte interface. The objective of this study is to incorporate the EDL model into the ion transport model for an arbitrary electrolyte. We comment that in this study, the non-linear reaction kinetics will be given by the generalized Frumkin-Butler-Volmer-Equations [24, 25] which account for the potential drop across the EDL that nullifies the electroneutrality approximation.

Numerous authors have attempted to incorporate models for the electric double layer in modeling of ion and charge transport in an electrochemical system. Bazant *et al* and Chu *et al* [10, 26] have considered steady state transport model and studied the diffuse charge effect in the electric double layer. They adopted the classical Poisson-Nernst-Planck equations for a binary and symmetric electrolyte but neglect the steric effect due to the finite size of ions. Their model is suitable for the dilute electrolyte solution. Time dependent transport models have also been studied in [27, 28, 24] for a binary and symmetric electrolyte albeit without taking the steric effect into account. Bazant *et al* [7], Kilic *et al* [29], Kilic *et al* and Olesen *et al* [30] have extended the investigation to concentrated electrolyte under large applied potential while accounting for the finite size effect of the ions. The authors investigated a modified Poisson-Nernst-Planck equations that is valid for binary and symmetric electrolytes which is characterized by large potentials. An extra term in the chemical potential and mass flux to account for the finite size of ionic species is also included in their model. Furthermore, in their model they have prescribed blocked electrode boundary conditions which means there are no electrochemical reactions at the electrodes.

In many practical applications, ionic charge of higher valency may be present in an electrolyte solution. For example, the human blood plasma contains high concentration of Na^+, Ca^{2+}, Mg^{2+}, Cl^-, HCO_3^-, HPO_3^{2-}, SO_4^{2-}. Hence, treating its mixture as an electrolyte solution with binary symmetric ions is generally not feasible. Furthermore, in most realistic electrochemical systems, reactions on electrode surfaces allows for passage of a current, which means that the conservation laws at the electrode-electrolyte interface must be augmented by the introduction of Faradaic current at the surface of the electrode and its corresponding electrolyte flux density. Due to the limitation of the available studies, there is a need to develop a model that can capture ion transport for an arbitrary electrolyte solution that will account for the EDL with proper boundary conditions, will include the finite size ionic effect, and will allow for electrochemical reaction at the electrodes.

In this study, we present diffuse charge dynamics of the electric double layer (EDL) of a concentrated electrolyte solution in a microelectrochemical system. In particular we investigate the transient response of the electrochemical system to a large applied voltage and we account for the finite size of the ions by considering the steric constraints on the maximum concentration of the ionic species. Our model deals with an arbitrary electrolyte which is one of the key features of this study. Furthermore, we allow for electrochemical reactions at the surface of the electrode.

2. Theory

In this section, we develop the theory based on work by Kilic *et al* [29]. In the present study, we extend Kilic's work which considers only the symmetric and binary ionic species to an electrolyte solution of arbitrary valence charges and of opposite signs.

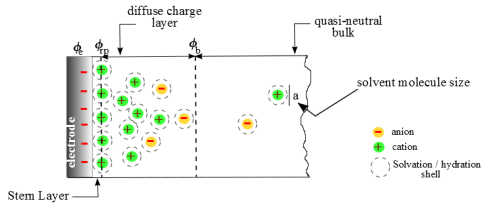

Figure 1: schematic of double layer

Throughout this study, we shall analyse a 1-dimensional electrochemical system in the region $0 \leq x \leq L$. The system consists of two electrodes which are separated by a length L and enclose a concentrated electrolyte solution. Figure 1 shows the schematic of part of the system.

Define by

$$\mu_i = z_i e\phi + k_B T[\ln C_i - \ln(1 - a^3 \sum_i C_i)] \tag{1}$$

the chemical potential of the concentrated ionic species C_i [31]. Here, ϕ is the local electrostatic potential, e is the electron charge and z_i is the valence of ionic species i. k_B and T are the Boltzmann's constant and the absolute temperature respectively. a is the spacing between the densely packed ions which is related to the entropy of the solvent molecules. It imposes the steric limit on the maximum concentration of the ions, that is $c_{max} = a^{-3}$.

The dynamics of ionic species i in an electrolyte solution is governed by the mass conservation law

$$\begin{aligned} \frac{\partial C_i}{\partial t} &= \frac{\partial}{\partial x}\left(\frac{D_i C_i}{k_B T}\frac{\partial \mu_i}{\partial x}\right), \\ &= \frac{\partial}{\partial x}\left(D_i\frac{\partial C_i}{\partial x} + sign(z_i)\frac{D_i F}{RT} z_i C_i \frac{\partial \phi}{\partial x} + \frac{a^3 D_i C_i}{1-\sum_i C_i a^3}\frac{\partial(\sum_i C_i)}{\partial x}\right). \end{aligned} \tag{2}$$

Here, F and R are the Faraday's and gas constants respectively. The first term in the right hand side of equation (2) corresponds to diffusion term due to the gradient of ionic concentration within the electrolyte solution. The second term is the electromigration driven by the gradient of the electric potential while the last term represents the nonlinear diffusion term that leads to the saturation of ion concentrations at the surface of the electrode. Similar nonlinear and singular diffusion terms play an important role in models of bio film growth [32]. It is the steric corrections to the Nernst-Planck equation that becomes significant when the ionic concentration grows large. We emphasize that in our formulation, we have neglected the effect of electrolyte convection and there is no bulk reaction to produce or consume ions in the electrolyte.

In order to close the system, together with equation (2) we solve the Poisson's equation

$$\frac{\partial}{\partial x}(-\varepsilon_b \frac{\partial \phi}{\partial x}) = F\sum_i z_i C_i, \tag{3}$$

which governs the electrostatic potential in the system where ε_b is the permittivity of the electrolyte solution. Finally, equations (2) and (3) are referred to as modified Poisson-Nernst-Planck equations (MPNP).

2.1. Boundary Conditions

Since Faradaic reactions occur at the electrodes surfaces then the ionic flux boundary conditions for the charge transfer is non-zero and is given by

$$J_i = D_i\frac{\partial C_i}{\partial x} + sign(z_i)\frac{D_i F}{RT} z_i C_i \frac{\partial \phi}{\partial x} + \frac{a^3 D_i C_i}{1-\sum_i C_i a^3}\frac{\partial(\sum_i C_i)}{\partial x}. \tag{4}$$

The current due to the motion of all charges in an electrochemical system is the Faradaic current written as the sum of all local currents, that is,

$$J_F = F\sum_i z_i J_i. \tag{5}$$

At the electrode, the Faradaic current J_F, which contributes to surface reaction and is related to local concentrations and potentials can be written as,

$$J_F = f(C_{i,S}, \triangle\phi_s, k_i), \tag{6}$$

where $C_{i,S}$ are the local ionic concentrations of the reacting ions C_i at the electrode, k_i are the rate constants, and $\triangle\phi_s = \phi\Big|_{rp} - \phi_e$ is the potential drop across the compact Stern layer. Here $\phi\Big|_{rp}$ is the electric potential of the electrolyte solution at the reaction plane and ϕ_e is the applied potential on the electrode. The function f in equation (6) depends on the type of reactions at the surface of the electrode and the physical state of the ionic species that partake in the reaction. An example of such reaction is the generalized Frumkin-Butler-Volmer kinetic relation [10, 24, 27].

Following Bazant *et al* [10] we prescribed Robin type boundary conditions for the electric potential as follows:

$$\phi\Big|_{rp} = \begin{cases} \phi_e - \lambda_S \frac{\partial \phi}{\partial \mathbf{n}} & \text{at } x = 0; \\ \phi_e + \lambda_S \frac{\partial \phi}{\partial \mathbf{n}} & \text{at } x = L. \end{cases} \tag{7}$$

where λ_S is the effective width of the compact layer of the electric double layer, and $\mathbf{n}$ is the normal pointing towards the electrolyte solution. We adopt a sign convection of positive at x=0, and negative at x=L. The boundary conditions (7) incorporate the essential capacitance of the Stern layer of the electrode-electrolyte interface. It is important to note that the layer could contain solvated ionic substance at the points immediately adjacent to the electrodes. The boundary conditions also ensure that capacitance accounts for the dielectric polarization of the solvation layer.

3. Dimensionless equations

We shall nondimensionalize the model equation and boundary conditions (2 - 7) explicitly. In order to do this, we introduce the following dimensionless parameters

$$\begin{aligned} x^* &= \frac{x}{L}, \qquad C_i^* = \frac{C_i}{C_{ref}}, \qquad \phi^* = \frac{F\phi}{RT}, \\ k_i &= \frac{D_i}{D}, \qquad t^* = \frac{tD}{L^2}, \qquad \nu = a^3 C_{ref}. \end{aligned} \tag{8}$$

Here, C_{ref}, R and D are the reference concentration, the gas constant and a constant diffusivity respectively. We insert the scaling parameters (8) into equations (2) and (3), to obtain the dimensionless model given by

$$\frac{\partial C_i^*}{\partial t^*} = k_i \frac{\partial}{\partial x^*} \left(\frac{\partial C_i^*}{\partial x^*} + sign(z_i) z_i C_i^* \frac{\partial \phi^*}{\partial x^*} + \frac{\nu C_i^*}{1 - \nu(\sum_i C_i^*)} \frac{\partial (\sum_i C_i^*)}{\partial x^*} \right). \tag{9}$$

$$-\epsilon^2 \frac{\partial^2 \phi^*}{\partial x^{*2}} = \sum_i z_i C_i, \tag{10}$$

where the parameter ϵ is another dimensionless parameter defined as $\epsilon = \frac{\lambda_D}{L}$ such that $\lambda_D = \sqrt{\frac{\varepsilon_b RT}{F^2 C_{ref}}}$ is the Debye length, that is, the width of the electrolyte region where the charge neutrality fails to be evenly approximated. Before we proceed to solve the model we prescribe the dimensionless boundary conditions.

3.1. Dimensionless B.C

By inserting the scaling parameters from equation (8) into the ionic flux boundary condition defined by equation (4), we arrive at the dimensionless fluxes

$$j_i = k_i \left(\frac{\partial C_i^*}{\partial x} + sign(z_i) z_i C_i^* \frac{\partial \phi^*}{\partial x} + \frac{\nu C_i^*}{1 - \nu \sum_i C_i^*} \frac{\partial (\sum_i C_i^*)}{\partial x} \right), \tag{11}$$

scaled by $\frac{L}{DC_{ref}}$. Furthermore, the dimensionless Faradaic current

$$j_F = \sum_i z_i j_i \tag{12}$$

is scaled by $\frac{L}{DFC_{ref}}$. At the electrode surface, the dimensionless local Faradaic current can also be obtained as

$$j_F = f^*(C_{i,S}^*, \triangle \phi_s *, k_i^*). \tag{13}$$

Finally, we define another dimensionless parameter $\delta = \frac{\lambda_S}{\lambda_D}$, the ratio of the effective width of the compact and diffuse parts of the electric double layer. It measures the strength of the surface capacitance. The non-dimensional boundary condition for the Poisson problem is thus

$$\phi^* \Big|_{rp} = \phi^*|_e \mp \delta \epsilon \frac{\partial \phi^*}{\partial x^*} \Big|_{rp}. \tag{14}$$

Before we proceed, we drop the star * accent for all non-dimensional variables in the subsequent analysis.

4. Numerical results

In what follows, we numerically analyse microelectrochemical systems where we focus on the case of an anion and a cation with possible different reactions at the electrodes. At x=0, we maintain a zero voltage and apply a voltage of 2.35V at an instant t=0 on the electrode at x=L. These correspond to voltages of 0 and 10 respectively for the dimensionless model defined on a computational domain $0 \leq x \leq 1$. We denote the concentration of the anion and cation by C_1 and C_2, respectively. Taking the valences of the anion and cation to be z_1 and z_2 respectively, equations (9) and (10) simplify to

$$\frac{\partial C_1}{\partial t} = k_1 \frac{\partial}{\partial x} \left(\frac{\partial C_1}{\partial x} - z_1 C_1 \frac{\partial \phi}{\partial x} + \frac{\nu C_1}{1 - \nu (C_1 + C_2)} \frac{\partial (C_1 + C_2)}{\partial x} \right), \tag{15}$$

$$\frac{\partial C_2}{\partial t} = k_2 \frac{\partial}{\partial x} \left(\frac{\partial C_2}{\partial x} + z_2 C_2 \frac{\partial \phi}{\partial x} + \frac{\nu C_2}{1 - \nu (C_1 + C_2)} \frac{\partial (C_1 + C_2)}{\partial x} \right), \tag{16}$$

$$-\epsilon^2 \frac{\partial^2 \phi}{\partial x^2} = z_2 C_2 - z_1 C_1, \tag{17}$$

with the following boundary conditions

$$k_1 \left(\frac{\partial C_1}{\partial x} - z_1 C_1 \frac{\partial \phi}{\partial x} + \frac{\nu C_1}{1 - \nu (C_1 + C_2)} \frac{\partial (C_1 + C_2)}{\partial x} \right) = j_F, \tag{18}$$

$$k_2\left(\frac{\partial C_2}{\partial x}+z_2C_2\frac{\partial \phi}{\partial x}+\frac{\nu C_2}{1-\nu(C_1+C_2)}\frac{\partial (C_1+C_2)}{\partial x}\right)=j_F, \tag{19}$$

$$\phi\Big|_{rp}=\phi|_e\mp\delta\epsilon\frac{\partial\phi}{\partial x}\Big|_{rp}. \tag{20}$$

For the electrode charge transfer we adopt the non-dimensional generalized Frumkin-Bulter-Volmer relation given by,

$$j_F=k_RC_{1,S}\exp(-\alpha z_1\triangle\phi_s)-k_OC_{2,S}\exp((1-\alpha)z_2\triangle\phi_s). \tag{21}$$

We implement the model using the finite element Multiphysics software package COMSOL [33, 34]. In order to test the accuracy of our numerical results, we verify the convergence by running numerous test cases for different mesh resolutions. Furthermore, we successfully verified the implementation using some of the previously published results, see for example, Figure 2 reported in [29], page 5.

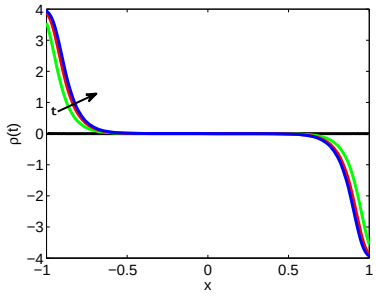

Figure 2: Dimensionless charge density $\rho(t)$.

In our computations, we locally refine the mesh (about $\triangle x_{min}\approx 10^{-6}-10^{-8}$) close to the electrode due to the large solution gradients in this region. The choice depends on the parameters being considered for the specific case. For the time integration, we have employed implicit Euler method that is stable for the numerical computations. Throughout the discussion, we present numerical solutions for time $t=0,\ 0.1,\ 0.5,\ 2.5,\ 5.$ The arrows in the figures indicate the direction of time increase.

4.1. Only Cation reaction at the electrodes, $z_1=-2,\ z_2=3$

In order to show the effects of the steric term on the model for microelectrochemical systems, we first present a comparison between the model without the steric effect, that is, $\nu=0$, and the case with the steric term. Figures (3a - 5a) and (3b - 5b) show the solutions for the case $\nu=0$ and the latter, respectively. At the earlier time, say t=0.1, in the bulk electrolyte, the transport term due to the diffusion dominates the one due to the migration. As time increases the migration transport flux overtake the diffusive fluxes. Furthermore

close to the electrode there is a sharp steep gradient of the migration fluxes, which results in the quick build up of massive ionic concentration. This in turn is due to the large applied voltage at the electrode and results in a large electric field, which pushes large ion concentration towards the electrode.

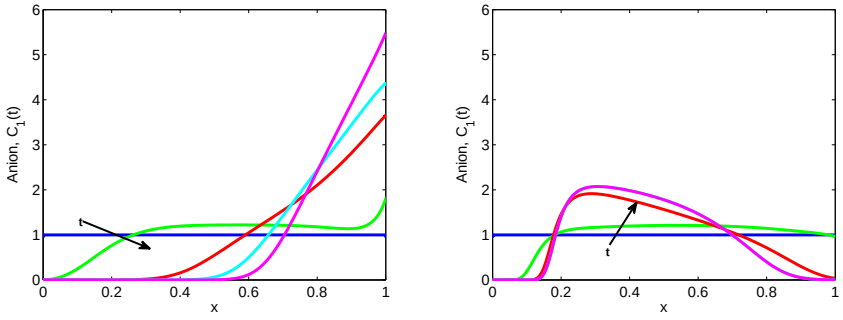

(a) Case of no steric term, $\nu = 0$

(b) Case of steric term $\nu = 0.25$

Figure 3: Numerical solutions for the model problem (15 - 21) describing the evolution of anion concentration in space and time for $\epsilon = 0.1,\ \phi_e = 10,\ k_1 = k_2 = 0.1$.

For the non-steric case, Figure 5a indicates a very steep gradient of the voltages recorded close to the left electrode. This means that the high electric field on the left counteracts the anion species which are depleted into the bulk electrolyte towards the electrode on the right. Figure 3a clearly shows shifting of the anion species towards the electrode on the right. However, we observe that in the case where finite size effect is present shown in Figure 3b, that the build up of charges on the right hand size is counterbalanced by the present steric term in the set up. Since the flux of the anion on both boundaries are zero, the total mass concentration of the anion species in the system must be conserved and remains constant throughout the simulation. It is no surprise therefore that taken the integral of the anion $C_1(t)$ under the limit $0 \leq x \leq 1$ remains constant which affirms the assertion by [27, 10].

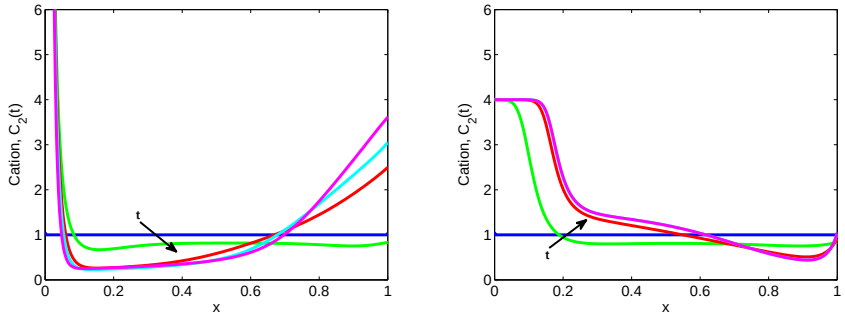

(a) Case of no steric term, $\nu = 0$ (b) Case of steric term $\nu = 0.25$

Figure 4: Numerical solutions for the model problem (15 - 21) describing the evolution of cation concentration in space and time for $\epsilon = 0.1,\ \phi_e = 10,\ k_1 = k_2 = 0.1$.

Again, we observe in Figure 4a that the evolution of the concentration of cation with time blows up to infinity even at the shortest time possible. This is because the strong electric field attracts the cations created due to faradaic reactions and there is a quick build up of the charges which results in overcrowding of the ionic species at the layer adjacent to the electrode surface. The is clearly the consequence of the absence of the finite size of ionic species. However, for the corresponding case with non-zero steric term shown in Figure 4b there is also a quick build up of the ions close to the electrode surface due to the strong electric field but the ions having finite size diffuse away and ions are depleted into the electrolyte bulk solution. The the presence of the singular steric diffusive term counter balances the crowding effect and ensures the crowding of ions does not exceed the steric limit of, $\frac{1}{\nu}$.

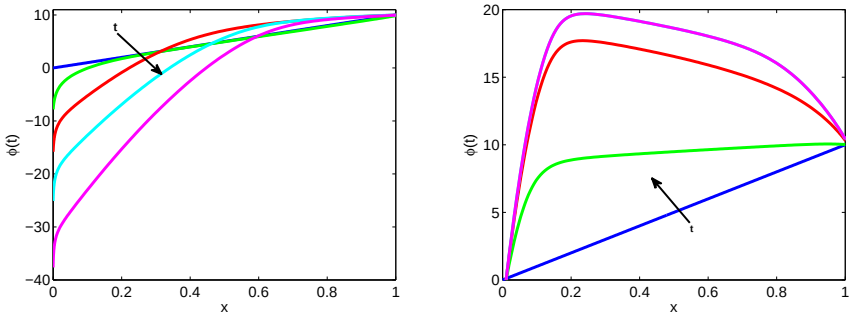

(a) Case of no steric term, $\nu = 0$ (b) Case of steric term $\nu = 0.25$

Figure 5: Numerical solutions for the model problem (15 - 21) describing the evolution of potential in space and time for $\epsilon = 0.1,\ \phi_e = 10,\ k_1 = k_2 = 0.1$.

5. Conclusion

We have simulated a dynamic mechanistic model which describe the transient response of the electric double layer in a microelectrochemical system. The model account for the finite size ion properties and incorporate charge transfer kinetics. The model also allows for simulating arbitrary electrolyte in the system. At the electrode/electrolyte interface, the reaction kinetics depends on the drop in potential within the compact layer of the electric double layer. The numerical results show dynamical changes of the the ionic concentration and the local ionic potentials. The present study could open up a promising perspective for the design of highly sensitive microchemical system. In order to achieve this, higher dimension system is necessary.

6. Acknowledgement

We acknowledge financial support from the Villum Kann Rasmussen centre of Excellence: Nano Mechanical Sensors and Actuators, fundamentals and new directions (NAMEC).

References

[1] J. Bates, N. Dudney, G. Gruzalski, R. Zuhr, A. Choudhury, C. Luck, J. Robertson, Fabrication and characterization of amorphous lithium electrolyte thin films and rechargeable thin-film batteries, Journal of Power Sources 43 (13) (1993) 103 – 110. doi:http://dx.doi.org/10.1016/0378-7753(93)80106-Y.

[2] D. Danilov, P. Notten, Mathematical modelling of ionic transport in the electrolyte of li-ion batteries, Electrochimica Acta 53 (17) (2008) 5569 – 5578. doi:http://dx.doi.org/10.1016/j.electacta.2008.02.086.

[3] R. A. Huggins, Advanced Batteries : Materials Science Aspects, Springer, New York, 2008.

[4] I. Quinzeni, S. Ferrari, E. Quartarone, D. Capsoni, M. Caputo, A. Goldoni, P. Mustarelli, M. Bini, Fabrication and electrochemical characterization of amorphous lithium iron silicate thin films as positive electrodes for lithium batteries, Journal of Power Sources 266 (0) (2014) 179 – 185. doi:http://dx.doi.org/10.1016/j.jpowsour.2014.05.012.

[5] F. Nadal, F. Argoul, P. Hanusse, B. Pouligny, A. Ajdari, Electrically induced interactions between colloidal particles in the vicinity of a conducting plane, Phys. Rev. E 65 (2002) 061409. doi:10.1103/PhysRevE.65.061409.

[6] R. J. Hunter, Foundations of colloid science, 2nd Edition, Oxford University Press, 2001.

[7] M. Z. Bazant, M. S. Kilic, B. D. Storey, A. Ajdari, Towards an understanding of induced-charge electrokinetics at large applied voltages in concentrated solutions, Advances in Colloid and Interface Science 152 (12) (2009) 48 – 88. doi:http://dx.doi.org/10.1016/j.cis.2009.10.001.

[8] V. Barcilon, D. Chen, R. Eisenberg, Ion flow through narrow membrane channels: Part ii, SIAM J. Appl. Math. 52 (5) (1992) 1405–1425. doi:10.1137/0152081.

[9] J. C. Weaver, Electroporation: A general phenomenon for manipulating cells and tissues, Journal of Cellular Biochemistry 51 (4) (1993) 426–435. doi:10.1002/jcb.2400510407.

[10] M. Bazant, K. Chu, B. Bayly, Current-voltage relations for electrochemical thin films, SIAM Journal on Applied Mathematics 65 (5) (2005) 1463–1484. doi:10.1137/040609938.

[11] H. Lu, M. A. Schmidt, K. F. Jensen, A microfluidic electroporation device for cell lysis, Lab Chip 5 (2005) 23–29. doi:10.1039/B406205A.
URL http://dx.doi.org/10.1039/B406205A

[12] T. M. Squires, M. Z. Bazant, Induced-charge electro-osmosis, Journal of Fluid Mechanics 509 (2004) 217–252. doi:10.1017/S0022112004009309.

[13] L. H. Olesen, H. Bruus, A. Ajdari, Ac electrokinetic micropumps: The effect of geometrical confinement, faradaic current injection, and nonlinear surface capacitance, Phys. Rev. E 73 (2006) 056313. doi:10.1103/PhysRevE.73.056313.

[14] A. J. Pascall, T. M. Squires, Induced charge electro-osmosis over controllably contaminated electrodes, Phys. Rev. Lett. 104 (2010) 088301. doi:10.1103/PhysRevLett.104.088301.
URL http://link.aps.org/doi/10.1103/PhysRevLett.104.088301

[15] A. Ramos, Electrokinetics and Electrohydrodynamics In Microsystems, Dordrecht: Springer, 2011.

[16] I. Sprague, P. Dutta, Depth averaged analytic solution for a laminar flow fuel cell with electric double layer effects, SIAM Journal on Applied Mathematics 72 (4) (2012) 1149–1168. doi:10.1137/110843113.

[17] I. B. Sprague, P. Dutta, Improved kinetics from ion advection through overlapping electric double layers in nano-porous electrodes, Electrochimica Acta 91 (0) (2013) 20 – 29. doi:10.1016/j.electacta.2012.12.015.

[18] N. Walther, Zur kinetik der in lösung befindlichen körper. erste abhandlung. theorie der diffusion, Z. phys.Chem. 9 (2) (1888) 613637.

[19] M. Planck, Ueber die erregung von electricität und wärme in electrolyten, Ann. Phys. Chem 275 (2) (1890) 161–186. doi:10.1002/andp.18902750202.

[20] K. G. Hans-Jrgen Butt, M. Kappl., Physics and Chemistry of Interfaces, WILEY-VCH Verlag, Weinheim, 2003.

[21] P. Geoffrey, Electrochemical Engineering Principles, Prentice Hall, New Jersey, 2003.

[22] O. Stern, Zur theorie der elektrolytischen doppelschicht, Z Electrochem. 30 (21-22) (1924) 508–516. doi:10.1002/bbpc.192400182.

[23] D. C. Grahame, The electrical double layer and the theory of electrocapillarity., Chemical Reviews 41 (3) (1947) 441–501. doi:10.1021/cr60130a002.

[24] M. Van Soestbergen, Frumkin-butler-volmer theory and mass transfer in electrochemical cells, Russian Journal of Electrochemistry 48 (6) (2012) 570–579. doi:10.1134/S1023193512060110.

[25] A. Frumkin, Hydrogen overvoltage and structure of the double layer, Z. Phys. Chem. 164 (1-2) (1933) 121–133.

[26] K. Chu, M. Bazant, Electrochemical thin films at and above the classical limiting current, SIAM J. Appl. Math. 65 (5) (2005) 1485–1505. doi:10.1137/040609926.

[27] A. Bonnefont, F. Argoul, M. Z. Bazant, Analysis of diffuse-layer effects on time-dependent interfacial kinetics, Electroana. Chem 500 (12) (2001) 52 – 61. doi:10.1016/S0022-0728(00)00470-8.

[28] M. van Soestbergen, P. M. Biesheuvel, M. Z. Bazant, Diffuse-charge effects on the transient response of electrochemical cells, Phys. Rev. E 81 (2010) 021503. doi:10.1103/PhysRevE.81.021503.

[29] M. S. Kilic, M. Z. Bazant, A. Ajdari, Steric effects in the dynamics of electrolytes at large applied voltages. II. Modified Poisson-Nernst-Planck equations, Phys. Rev. E 75 (2007) 021503. doi:10.1103/PhysRevE.75.021503.

[30] L. Højgaard Olesen, M. Z. Bazant, H. Bruus, Strongly nonlinear dynamics of electrolytes in large ac voltages, Phys. Rev. E 82 (2010) 011501. doi:10.1103/PhysRevE.82.011501.

[31] M. Z. Bazant, M. S. Kilic, B. D. Storey, A. Ajdari, Towards an understanding of induced-charge electrokinetics at large applied voltages in concentrated solutions, Advances in Colloid and Interface Science 152 (12) (2009) 48 – 88. doi:http://dx.doi.org/10.1016/j.cis.2009.10.001.

[32] M. A. Efendiev, Evolution Equations Arising in the Modelling of Life Sciences, Birkhäser, Basel, 2013.

[33] W. B. J. Zimmerman, Multiphysics Modelling with Finite Elements Methods, World Scientific Publishing Co. Singapore, 2006.

[34] Comsol®multiphysics finite element analysis software.

[35] M. S. Kilic, M. Z. Bazant, A. Ajdari, Steric effects in the dynamics of electrolytes at large applied voltages. I. Double-layer charging, Phys. Rev. E 75 (2007) 021502. doi:10.1103/PhysRevE.75.021502.

[36] M. van Soestbergen, Ionic currents exceeding the diffusion limitation in planar nano-cavities, Electrochemistry Communications 20 (0) (2012) 105 – 108. doi:10.1016/j.elecom.2012.03.034.

[37] I. Borukhov, D. Andelman, H. Orland, Steric effects in electrolytes: A modified poisson-boltzmann equation, Phys. Rev. Lett. 79 (1997) 435–438. doi:10.1103/PhysRevLett.79.435.

[38] M. Z. Bazant, K. Thornton, A. Ajdari, Diffuse-charge dynamics in electrochemical systems, Phys. Rev. E 70 (2004) 021506. doi:10.1103/PhysRevE.70.021506.

[39] P. Biesheuvel, M. van Soestbergen, M. Bazant, Imposed currents in galvanic cells, Electrochimica Acta 54 (21) (2009) 4857 – 4871. doi:http://dx.doi.org/10.1016/j.electacta.2009.03.073.

[40] A. J. Bard, L. R. Faulkner, Electrochemical Methods: Fundamentals and Applications, 2nd Edition, John Wiley & Sons, 2001.

[41] M. H. Holmes, Introduction to Perturbation Methods, Springer, New York, 2013.

[42] J. Newman, The polarized diffuse double layer, Trans. Faraday Soc. 61 (1965) 2229–2237.

Chapter 7

Conclusion and Outlook

There is a great collection of literature on the theory and numerics of electrochemical systems in general. Many complex phenomena like the charge transfer, diffusion, reaction dynamics have been researched based on these studies. This thesis focuses on the simulations of the microelectrochemical systems which deviates slightly from the standard approach.

In order to distinguish the macro and micro systems, we start by considering the Nernst-Planck equations which is a system of advection-diffusion-reaction partial differential equations solved with the Poisson equation. The assumption of electroneutrality reduces the Poisson equation to the Laplace equation and hence the right hand side of the differential equation for the potential field equals zero. Furthermore, the flux condition relates the current density to the charge transfer across the electrolyte/electrode interface through the Butler-Volmer relation. The overpotential term in the Butler-Volmer relation defines the potential drop between the electrode and the bulk electrolyte. This term is crucial when modeling microelectrochemical systems where the dynamics of the electrode/electrolyte interface cannot be ignored. In the thesis, we incorporated the electric double layer model which divides the electrode/electrolyte into the Stern and the diffuse layers. The Stern layer is modelled by a Robin type boundary condition which also affects the charge transfer and thus utilize a modified Butler-Volmer equation.

In modeling electrochemical systems, ions are normally treated as point charges, but because of huge electric fields in the double layer ionic species can become crowded in this region and the ionic concentration tends to infinity. The introduction of finite size properties of ions overcomes this effect and thus a more appropriate model for the electrochemical systems especially the miniaturized size.

The results have been reported in two parts. The first part presents the mechanism of the electrochemical systems through cyclic voltammetry in a fluidic system in which electrolyte solution was pumped in and out of the system. The results through computations show the influence of the convection and the scan rate in an electrochemical system which can affect the system dynamics. The information gathered from such computations could be very useful in the experimental design as well as very useful in providing insight when designing electrochemical systems of high sensitivity.

Another interesting contribution from the first part is that the placement of electrodes is critical when performing cyclic voltammetry experiments under flow. The main difference between the centered placed electrode and the bottom placed electrode is the delay in the conversion of the fresh ionic species brought to the electrode surface for the bottom placed electrode when the scan rate is slow. In the centered placed electrode the influence is more apparent since the variation can be seen in the current response recorded during cyclic voltammetry. We were able to identify the characteristics of the hydrodynamic effect on the the dynamics of the current response to the applied voltage in cyclic voltammetry measurements. Qualitative and often also quantitative agreement are found between experimental and the numerical predictions for cyclic voltammetry measurements.

The second part of the thesis provides simulations for the dynamic mechanistic model which described the transient response of the electric double layer in a microelectrochemical system. The model accounts for the finite size ion properties and incorporates charge transfer kinetics. The model also allows for simulating arbitrary electrolytes in the system. At the electrode/electrolyte interface, the reaction kinetics depend on the drop in potential within the compact layer of the electric double layer. The numerical results show dynamical changes of the ionic concentration and the local ionic potentials. In the example we simulated a system in which the electrolyte is non-binary and the reaction kinetics complicates the computation.

Based on the motivation from the numerical computations, we solve for the steady state solution for the mass transport equations that contains the steric properties of the ionic charges. The result suggests that the analytic solution to the problem consists of traveling wave solutions obtained from non-linear

diffusion equations. However, further investigation is needed for this result.

As a final remark, there are several challenges and extensions that could be made in the present study. Reactions like coating, functionalization of the electrodes could be modeled and simulated in cyclic voltammetry. Furthermore, for the design and optimization of the electrochemical system, the investigation of the full 3D problem may be needed. A further research area is to simulate cyclic voltammetry of the microelectrochemical system with the steric properties and proper electric double layer boundary conditions. Finally, theoretical analysis of microelectrochemical systems, for example through asymptotic expansion could also be pursued. This is still ongoing.

Appendix A

Appendix

The purpose of this section is to present the non-dimensionalization of the equations we solved in Paper III and also in chapter 3 where we present the summary of the result. We state all the equations involved for modeling the microelectrochemical system and non-dimensionalize them appropriately.

A.1 Dimensional analysis for the model equation

In a microelectrochemical system, the dynamics of ionic species satisfies the mass transport equations

$$\frac{\partial C_i}{\partial t} = \frac{\partial}{\partial x}\left(D_i \frac{\partial C_i}{\partial x} + \frac{D_i F}{RT} z_i C_i \frac{\partial \phi}{\partial x} + \frac{a^3 D_i C_i}{1 - \sum_i C_i a^3} \frac{\partial (\sum_i C_i)}{\partial x} \right). \tag{A.1}$$

The first term on the right hand side of equation (A.1) corresponds to a diffusion term due to the ionic concentration gradient within the electrolyte solution. The second term is the electromigration driven by the gradient of the electric potential while the last term represents the nonlinear diffusion term that can

lead to the saturation of ion concentrations at the surface of the electrode. Here, we do not include the term due to convection.

In order to couple the local potential term to equation (A.1), we solve the Poisson equation

$$\frac{\partial}{\partial x}(-\varepsilon_b \frac{\partial \phi}{\partial x}) = F \sum_i z_i C_i, \tag{A.2}$$

A.1.1 Boundary Conditions

In what follows, we shall consider a two electrode system that is separated by a length L and sandwiches an electrolyte solution. We consider an electrolyte solution that is arbitrary and allow the valence of ionic species to be of opposite signs. Across the electrode/electrolyte interface Faradaic reactions are involved and hence the ionic flux boundary conditions for the charge transfer is given by

$$J_i = D_i \frac{\partial C_i}{\partial x} + \frac{D_i F}{RT} z_i C_i \frac{\partial \phi}{\partial x} + \frac{a^3 D_i C_i}{1 - \sum_i C_i a^3} \frac{\partial (\sum_i C_i)}{\partial x}. \tag{A.3}$$

Here, J_i is the current density within the electrochemical system. The current due to motion of all charges in an electrochemical system is the Faradaic current written as the sum of all local currents, that is,

$$J_F = F \sum_i z_i J_i. \tag{A.4}$$

At the electrode, the Faradaic current J_F which contributes to surface reaction and is related to local concentrations and potential through the generalized Frumkin-Butler–Volmer kinetic relation [27], takes the form

$$J_F = k_R C_1 \exp(-\alpha \frac{z_1 F}{RT} \triangle \phi_s) - k_O C_2 \exp((1-\alpha) \frac{z_2 F}{RT} \triangle \phi_s), \tag{A.5}$$

where k_i are the rate constants, α is the transfer coefficient, R is the gas constant and T is the temperature. The choice C_1 and C_2 will become immediately clear in the next section. Furthermore, $\triangle \phi_s = \phi\Big|_{rp} \mp \phi_e$ is the potential drop across the compact Stern layer. The variables involved are defined below.

Following Bazant *et al* [23] we prescribed Robin type boundary conditions for the electric potential as follows

$$\phi\Big|_{rp} = \pm \phi_e \mp \lambda_S \frac{\partial \phi}{\partial \mathbf{n}}\Big|_{rp}, \tag{A.6}$$

where λ_S is the effective width of the compact layer of the electric double layer, $\phi|_{rp}$ is the electric potential at the reaction plane, $\phi|_e$ is the applied potential on the electrode and $\mathbf{n}$ is the normal pointing towards the electrolyte solution. We have adopted a sign convection that current flowing towards the cathode is negative.

A.2 Dimensionless equations

We introduce the following scaling parameters

$$x^* = \frac{x}{L}, \qquad C_i^* = \frac{C_i}{C_{ref}}, \qquad \phi^* = \frac{F\phi}{RT}, \tag{A.7}$$

$$k_i = \frac{D_i}{D}, \qquad t^* = \frac{tD}{L^2}, \qquad \nu = a^3 C_{ref}, \tag{A.8}$$

in order to nondimensionalize the equations (A.1 - A.6). Here, C_{ref}, R and D are the reference concentration, the gas constant and a constant diffusivity respectively. We insert the scaling parameters into A.1 and obtain

$$\frac{DC_{ref}}{L^2}\frac{\partial C_i^*}{\partial t^*} = \frac{\partial}{L\partial x^*}\left(\frac{k_i DC_{ref}}{L}\frac{\partial C_i^*}{\partial x^*} + \frac{sign(z_i)z_i k_i DC_{ref}C_i^*}{L}\frac{\partial \phi^*}{\partial x^*}\right. \tag{A.9}$$

$$\left. + \frac{a^3 k_i DC_{ref}C_i^*}{L(1-a^3 C_{ref}\sum_i C_i^*)}\frac{\partial(\sum_i C_{ref}C_i^*)}{\partial x^*}\right). \tag{A.10}$$

When both sides of equation (A.10) are multiplied by $\dfrac{L^2}{DC_{ref}}$ we arrive at

$$\frac{\partial C_i^*}{\partial t^*} = k_i\frac{\partial}{\partial x^*}\left(\frac{\partial C_i^*}{\partial x^*} + sign(z_i)z_i C_i^*\frac{\partial \phi^*}{\partial x^*} + \frac{\nu C_i^*}{1-\nu(\sum_i C_i^*)}\frac{\partial(\sum_i C_i^*)}{\partial x^*}\right). \tag{A.11}$$

Since we chose an electrolyte solution that is arbitrary and allow the charges of ionic species to be of opposite signs such that when the * is dropped we can write the following

$$\frac{\partial C_1}{\partial t} = k_1\frac{\partial}{\partial x}\left(\frac{\partial C_1}{\partial x} - z_1 C_1\frac{\partial \phi}{\partial x} + \frac{\nu C_1}{1-\nu(C_1+C_2)}\frac{\partial(C_1+C_2)}{\partial x}\right), \tag{A.12}$$

$$\frac{\partial C_2}{\partial t} = k_2\frac{\partial}{\partial x}\left(\frac{\partial C_2}{\partial x} + z_2 C_2\frac{\partial \phi}{\partial x} + \frac{\nu C_2}{1-\nu(C_1+C_2)}\frac{\partial(C_1+C_2)}{\partial x}\right). \tag{A.13}$$

Now recall the Poisson problem (A.2),

$$\frac{\partial}{\partial x}(-\varepsilon\frac{\partial\phi}{\partial x}) = F\sum_i z_i C_i, \tag{A.14}$$

we substitute the dimensionless parameter defined in equation (A.7) to get

$$\frac{1}{L}\frac{\partial}{\partial x^*}(-\frac{\varepsilon}{L}\frac{\partial}{\partial x^*}\left(\frac{RT\phi^*}{F}\right)) = FC_{ref}\sum_i z_i C_i^*, \tag{A.15}$$

and when we re-arrange and drop the * we obtain

$$-\left(\frac{\lambda_D}{L}\right)^2\frac{\partial^2\phi}{\partial x^2} = \sum_i z_i C_i, \tag{A.16}$$

where $\lambda_D = \sqrt{\dfrac{\varepsilon RT}{F^2 C_{ref}}}$ is the Debye length signifying the electrolyte region where charge neutrality fails to be evenly approximated. If we chose the Debye length λ_D as the natural scale for charge screening then one can define another dimensionless parameter, $\epsilon = \dfrac{\lambda_D}{L}$ such that

$$-\epsilon^2\frac{\partial^2\phi}{\partial x^2} = \sum_i z_i C_i, \text{ is satisfied.} \tag{A.17}$$

The parameter ϵ is the governing small parameter for the matched asymptotic expansion to be considered in the later section.

A.2.1 Dimensionless Ion flux B.C

Recall the ionic flux boundary conditions,

$$J_i = D_i\frac{\partial C_i}{\partial x} + \frac{D_i F}{RT}z_i C_i\frac{\partial\phi}{\partial x} + \frac{a^3 D_i C_i}{1-\sum_\pm C_i a^3}\frac{\partial(\sum_i C_i)}{\partial x}. \tag{A.18}$$

By inserting the scaling parameters from equation (A.7) one gets

$$J_i = \frac{k_i D C_{ref}}{L}\left(\frac{\partial C_i^*}{\partial x} + sign(z_i)z_i C_i^*\frac{\partial\phi^*}{\partial x} + \frac{\nu C_i^*}{1-\nu\sum_i C_i^*}\frac{\partial(\sum_i C_i^*)}{\partial x}\right), \tag{A.19}$$

which results in the dimensionless fluxes

$$j_i = k_i \left(\frac{\partial C_i^*}{\partial x} + sign(z_i) z_i C_i^* \frac{\partial \phi^*}{\partial x} + \frac{\nu C_i^*}{1 - \nu \sum_i C_i^*} \frac{\partial (\sum_i C_i^*)}{\partial x} \right), \tag{A.20}$$

defined by

$$j_i = \frac{L}{DC_{ref}} J_i. \tag{A.21}$$

Now Faradaic current is defined as the sum of individual ionic currents written as

$$J_F = F \sum_i z_i J_i. \tag{A.22}$$

When we substitute equation (A.21) into (A.22) we obtain

$$J_F = \frac{DFC_{ref}}{L} \sum_i z_i j_i, \tag{A.23}$$

which in turn gives the dimensionless Faradaic current

$$j_F = \sum_i z_i j_i \tag{A.24}$$

that scaled the dimensional Faradaic current such that $j_F = \dfrac{L}{DFC_{ref}} J_F$. Now recall the surface kinetics defined by equation (A.3),

$$J_F = k_R C_1 \exp(-\alpha \frac{z_1 F}{RT} \triangle \phi_s) - k_O C_2 \exp((1-\alpha) \frac{z_2 F}{RT} \triangle \phi_s), \tag{A.25}$$

and substitute dimensional Faradaic current equation into equation (A.25) so that

$$\frac{DFC_{ref}}{L} j_F = k_R C_1 \exp(-\alpha \frac{z_1 F}{RT} \triangle \phi_s) - k_O C_2 \exp((1-\alpha) \frac{z_2 F}{RT} \triangle \phi_s) \tag{A.26}$$

and when both sides are multiplied by $\dfrac{L}{DFC_{ref}}$ we obtain

$$j_F = \frac{Lk_R}{DF} \frac{C_1}{C_{ref}} \exp(-\alpha \frac{z_1 F}{RT} \triangle \phi_s) - \frac{Lk_O}{DFC_{ref}} \frac{C_2}{C_{ref}} \exp((1-\alpha) \frac{z_2 F}{RT} \triangle \phi_s). \tag{A.27}$$

Using the scaling parameters defined in (A.7) we formally obtain the non-dimensional surface reaction kinetics equation

$$j_F = k_R^* C_1^* \exp(-\alpha z_1 \triangle \phi_s^*) - k_O^* C_2^* \exp((1-\alpha) z_2 \triangle \phi_s^*), \tag{A.28}$$

where $k_R^* = \dfrac{L}{DF} k_R \quad ; \quad k_O^* = \dfrac{L}{DF} k_O$ are the dimensionless rate constants.

A.2.2 Dimensionless Poisson B.C

Now consider the boundary condition for the Poisson problem,

$$\phi \Big|_{rp} = \pm \phi_e \mp \lambda_S \frac{\partial \phi}{\partial x} \Big|_{rp}. \tag{A.29}$$

Again, we insert the scaling parameters in (A.7) such that

$$\left(\frac{RT}{F}\right) \phi^* \Big|_{rp} = \pm \phi_e \mp \frac{\lambda_S}{L} \left(\frac{RT}{F}\right) \frac{\partial \phi^*}{\partial x^*} \Big|_{rp}. \tag{A.30}$$

We multiply the right hand side of (A.30) by $\dfrac{\lambda_D}{\lambda_D}$ and re-arrange as follows,

$$\phi^* \Big|_{rp} = \pm \left(\frac{F}{RT}\right) \phi_e \mp \frac{\lambda_S}{\lambda_D} \frac{\lambda_D}{L} \frac{\partial \phi^*}{\partial x^*} \Big|_{rp}. \tag{A.31}$$

Finally, we define another dimensionless parameter $\delta = \dfrac{\lambda_S}{\lambda_D}$ the ratio of the effective width of the compact and diffuse parts of the electric double layer.

$$\phi^* \Big|_{rp} = \pm \phi^*|_e \mp \delta \epsilon \frac{\partial \phi^*}{\partial x^*} \Big|_{rp}. \tag{A.32}$$

A.3 The model and the boundary conditions

We want to solve the following model

$$\frac{\partial C_1}{\partial t} = k_1 \frac{\partial}{\partial x} \left(\frac{\partial C_1}{\partial x} - z_1 C_1 \frac{\partial \phi}{\partial x} + \frac{\nu C_1}{1 - \nu(C_1 + C_2)} \frac{\partial (C_1 + C_2)}{\partial x} \right), \tag{A.33}$$

$$\frac{\partial C_2}{\partial t} = k_2 \frac{\partial}{\partial x}\left(\frac{\partial C_2}{\partial x} + z_2 C_2 \frac{\partial \phi}{\partial x} + \frac{\nu C_2}{1-\nu(C_1+C_2)}\frac{\partial (C_1+C_2)}{\partial x}\right), \tag{A.34}$$

$$-\epsilon^2 \frac{\partial^2 \phi}{\partial x^2} = \sum_i z_i C_i, \tag{A.35}$$

for a microelectrochemical system satisfying the following boundary conditions

$$j_F = k_R C_1 \exp(-\alpha z_1 \triangle \phi_s) - k_O C_2 \exp((1-\alpha) z_2 \triangle \phi_s) \tag{A.36}$$

the nondimensional Faradaic current which can be accessed through equations (A.20) and (A.24), and

$$\phi\Big|_{rp} = \pm\phi|_e \mp \delta\epsilon \frac{\partial \phi}{\partial x}\Big|_{rp}, \tag{A.37}$$

with parameters δ, ϵ are defined in previous sections.

Bibliography

[1] C. A. Thomas Jr, P. A. Springer, G. E. Loeb, Y. Berwald-Netter, and L. M. Okun. A miniature microelectrode array to monitor the bioelectric activity of cultured cells. *Experimental Cell Research*, 74(1):61 – 66, 1972.

[2] A. J. Bard and L. R. Faulkner. *Electrochemical Methods: Fundamentals and Applications*. John Wiley & Sons, 2 edition, 2001.

[3] N. Walther. Zur Kinetik der in Lösung befindlichen Körper. Erste Abhandlung. Theorie der Diffusion. *Zeitschrift für Physikalische Chemie*, 9(2):613–637, 1888.

[4] M. Planck. Ueber die Erregung von Electricität und Wärme in Electrolyten. *Annual Review of Physical Chemistry*, 275(2):161–186, 1890.

[5] P. Delahay. *New Instrumental Methods in Electrochemistry*. Interscience Publishers, New York, 1954.

[6] E. Yeager, J. O'M. Bockris, B. E. Conway, and S. Sarangapani. *Comprehensive Treatise of Electrochemistry, Electrodics: Transport*, volume 6. Plenum Press, New York, 1983.

[7] I. Rubinstein. *Electro-Diffusion of Ions*. Society for Industrial and Applied Mathematics, 1990.

[8] J. Newmann and K. E. Thomas-Alyea. *Electrochemical Systems*. Wiley-Interscience, 3 edition, 2004.

[9] K. Kontturi, L. Murtomäki, and J. A. Manzanares. *Ionic Transport Processes in Electrochemistry and Membrane Science*. Oxford University Press, 2008.

[10] R. G. Compton and C. E. Banks. *Understanding Voltammetry.* World Scientifice, 2 edition, 2011.

[11] J. Leddy, V. Birss, and P. Vanỳsek. *Historical Perspectives on the Evolution of Electrochemical Tools.* The Electrochemical Society, NJ, 2004.

[12] A. J. Bard and R. W. Murray. Electrochemistry. *PNAS*, 109(12):11484–11486, 2012.

[13] V. M. Volgin and A. D. Davydov. Mass-transfer problems in the electrochemical systems. *Russian Journal of Electrochemistry*, 48(6):565–569, 2012.

[14] G. A. Prentice and C. W. Tobias. A survey of numerical methods and solutions for current distribution problems. *Journal of The Electrochemical Society*, 129(1):72–78, 1982.

[15] M. Schlesinger. *Mathematical Modeling in Electrochemistry, in Modern Aspects of Electrochemistry*, volume 43. Springer, New York, 2008.

[16] R. N. Adams. In vivo electrochemical recording — a new neurophysiological approach. *Trends in Neurosciences*, 1(2):160 – 163, 1978.

[17] H. Y. Cheng, J. Schenk, R. Huff, and R. N. Adams. In vivo electrochemistry: behavior of micro electrodes in brain tissue. *Journal of Electroanalytical Chemistry and Interfacial Electrochemistry*, 100(1–2):23 – 31, 1979.

[18] R. M. Wightman A. G. Ewing, M. A. Dayton. Pulse voltammetry with microvoltammetric electrodes. *Analytical Chemistry*, 12(53):1842–1847, 1981.

[19] H. J. Butt, K. Graf, and M. Kappl. *Physics and Chemistry of Interfaces.* WILEY-VCH Verlag, Weinheim, 2003.

[20] G. Prentice. *Electrochemical Engineering Principles.* Prentice Hall, New Jersey, 2003.

[21] O. Stern. Zur theorie der elektrolytischen doppelschicht. *Zeitschrift für Elektrochemie*, 30(21-22):508–516, 1924.

[22] D. C. Grahame. The electrical double layer and the theory of electrocapillarity. *Chemical Reviews*, 41(3):441–501, 1947.

[23] M. Bazant, K. Chu, and B. Bayly. Current-voltage relations for electrochemical thin films. *SIAM Journal on Applied Mathematics*, 65(5):1463–1484, 2005.

[24] K. Chu and M. Z Bazant. Electrochemical thin films at and above the classical limiting current. *SIAM Journal of Applied Mathematics*, 65(5):1485–1505, 2005.

[25] A. Bonnefont, F. Argoul, and M. Z. Bazant. Asymptotic analysis of diffuse-layer effects on time-dependent interfacial kinetics. *Electroanalytical Chemistry*, 500(1–2):52 – 61, 2001.

[26] M. van Soestbergen, P. M. Biesheuvel, and M. Z. Bazant. Diffuse-charge effects on the transient response of electrochemical cells. *Physical Review E*, 81:021503, Feb 2010.

[27] M. van Soestbergen. Frumkin-butler-volmer theory and mass transfer in electrochemical cells. *Russian Journal of Electrochemistry*, 48(6):570–579, 2012.

[28] M. Z. Bazant, M. S. Kilic, B. D. Storey, and A. Ajdari. Towards an understanding of induced-charge electrokinetics at large applied voltages in concentrated solutions. *Advances in Colloid and Interface Science*, 152(1–2):48 – 88, 2009.

[29] M. S. Kilic and M. Z. Bazant. Steric effects in the dynamics of electrolytes at large applied voltages. II. Modified Poisson-Nernst-Planck equations. *Physical Review E*, 75:1 – 11, 2007.

[30] O. L. Højgaard, M. Z. Bazant, and H. Bruus. Strongly nonlinear dynamics of electrolytes in large ac voltages. *Physical Review E*, 82:011501, Jul 2010.

[31] T. Erdy-Gruz and M. Volmer. *Zeitschrift für Physikalische Chemie*, 203:150–157, 1931.

[32] J. A. V. Butler. *Transactions of the Faraday Society*, 28:379, 1931.

[33] G. K. Batchelor. *An Introduction to fluids dynamics*. Cambridge University Press, 1967.

[34] J. Fuhrmann, A. Linke, and H. Langmach. A numerical method for mass conservative coupling between fluid flow and solute transport. *Applied Numerical Mathematics*, 61:530–553, 2011.

[35] M. S. Kilic, M. Z. Bazant, and A. Ajdari. Steric effects in the dynamics of electrolytes at large applied voltages. I. Double-layer charging. *Physical Review E*, 75:021502, Feb 2007.

[36] Z. Adamczyk and P. Warszyński. Role of electrostatic interactions in particle adsorption. *Advances in Colloid and Interface Science*, 63(0):41 – 149, 1996.

[37] Comsol multiphysics finite element analysis software ®. http://www.comsol.com.

[38] V. Thomee. *Galerkin Finite Element Methods for Parabolic Problems*. Springer, New York: Springer Series in Computational Mathematics, Vol. 25, 2006.

[39] S. Brenner and R. Scott. *The Mathematical Theory of Finite Element Methods*. Springer, New York: Texts in Applied Mathematics, Vol. 15, 2008.

[40] W. B. J. Zimmerman. *Multiphysics Modelling with Finite Elements Methods*. World Scientific Publishing Co. Singapore, 2006.

[41] K. Dmitri and H. Jari. *Finite Element Methods for Computational Fluid Dynamics: A Practical Guide*. SIAM, 2014.

[42] A. C. Fisher and R. G. Compton. A general computational approach to linear sweep voltammetry at channel electrodes. *Journal of Applied Electrochemistry*, 22:38–42, 1992.

[43] R. G. Compton, A. C. Fisher, R. G. Wellington, P. J. Dobson, and P. A. Leigh. Hydrodynamic voltammetry with microelectrodes: channel microband electrodes; theory and experiment. *Journal of Physical Chemistry*, 97(40):10410–10415, 1993.

[44] N. V. Rees, R. A. W. Dryfe, J. A. Cooper, B. A. Coles, R. G. Compton, S. G. Davies, and T. D. McCarthy. Voltammetry under High Mass Transport Conditions. A High Speed Channel Electrode for the Study of Ultrafast Kinetics. *Journal of Physical Chemistry*, 99(18):7096–7101, 1995.

[45] J. A. Alden, M. A. Feldman, E. Hill, F. Prieto, M. Oyama, B. A. Coles, R. G. Compton, P. J. Dobson, and P. A. Leigh. Channel microband electrode arrays for mechanistic electrochemistry. Two-dimensional voltammetry: transport-limited currents. *Analytical Chemistry*, 70(9):1707–20, 1998.

[46] N. V. Rees, O. V. Klymenko, E. Maisonhaute, B. A. Coles, and R. G. Compton. The application of fast scan cyclic voltammetry to the high speed channel electrode. *Journal of Electroanalytical Chemistry*, 542:23–32, 2003.

[47] S. M. Matthews, G. Q. Du, and A. C. Fisher. Microfluidic voltammetry: simulation of the chronoamperometric response of microband electrodes sited within microreactors. *Journal of Solid State Electrochemistry*, 10(10):817–825, 2006.

[48] F. G. E. Jones and R. A. W. Dryfe. Hydrodynamic voltammetry at the interface between immiscible electrolyte solutions: Numerical simulation of the voltarnmetric response. *Journal of electroanalytical chemistry*, 615(1):25–33, 2008.

[49] M. van Soestbergen. Ionic currents exceeding the diffusion limitation in planar nano-cavities. *Electrochemistry Communications*, 20(0):105 – 108, 2012.

[50] M. van Soestbergen, P. M. Biesheuvel, and M. Z. Bazant. Diffuse-charge effects on the transient response of electrochemical cells. *Physical Review E*, 81:021503, Feb 2010.

[51] M. A. Urtenov, E. V. Kirillova, N. M. Seidova, and V. V. Nikonenko. Decoupling of the nernst-planck and poisson equations. application to a membrane system at overlimiting currents. *The Journal of Physical Chemistry B*, 111(51):14208–14222, 2007.

[52] S. Chevion, M. Hofmann, R. Ziegler, M. Chevion, and P. P. Nawroth. The antioxidant properties of thioctic acid: characterization by cyclic voltammetry. *International Journal of Biochemistry and Molecular Biology*, 41(2):317–327, 1997.

[53] S. Chevion, M. A. Roberts, and M. Chevion. The use of cyclic voltammetry for the evaluation of antioxidant capacity. *Free Radical Biology & Medicine*, 28(6):860–870, 2000.

[54] D. Grieshaber, R. MacKenzie, J. Voros, and E. Reimhult. Electrochemical biosensors - sensor principles and architectures. *Sensors*, 8(3):1400–1458, 2008.

[55] N. Cruys-Bagger, S. F. Badino, R. Tokin, M. Gontsarik, S. Fathalinejad, K. Jensen, M. D. Toscano, T. H. Sørensen, K. Borch, H. Tatsumi, P. Väljamäe, and P. Westha. A pyranose dehydrogenase-based biosensor for kinetic analysis of enzymatic hydrolysis of cellulose by cellulases. *Enzyme and Microbial Technology*, 58:68 – 74, 2014.

[56] L. M. Fischer, C. Pedersen, K. Elkjær, N. N. Noeth, S. Dohn, A. Boisen, and M. Tenje. Development of a microfabricated electrochemical-cantilever hybrid platform. *Sensors and Actuators B: Chemical*, 157(1):321–327, 2011.

[57] R. S. Nicholson and I. Shain. Theory of stationary electrode polarography - scan and cyclic methods applied to reversible, irreversible, and kinetic systems. *Analytical Chemistry*, 36(4):707–723, 1964.

[58] G. Jidong and L. Ernő. Cyclic voltammetry at shallow recessed microdisc electrode: Theoretical and experimental study. *Journal of Electroanalytical Chemistry*, 629(1-2):180–184, 2009.

[59] C. Meng-Hsuan. A numerical method for analysis of tertiary current distribution in unsteady natural convection multi-ion electrodeposition. *Electrochimica Acta*, 45(24):3959–3972, 2000.

[60] J. V. Macpherson, N. Simjee, and P. R. Unwin. Hydrodynamic ultramicroelectrodes: kinetic and analytical applications. *Electrochimica Acta*, 47(1-2):29–45, 2001.

[61] A. J. Wain, R. G. Compton, R. Le Roux, S. Matthews, and A. C. Fisher. Microfluidic channel flow cell for simultaneous cryoelectrochemical electron spin resonance. *Analytical Chemistry*, 79(5):1865–73, 2007.

[62] C. T. J. Low, E. P. L. Roberts, and F. C. Walsh. Numerical simulation of the current, potential and concentration distributions along the cathode of a rotating cylinder hull cell. *Electrochimica Acta*, 52(11):3831–3840, 2007.

[63] L. Uziel. *Modern Aspects of Electrochemistry No. 44*, volume 44 of *Modern Aspects of Electrochemistry*. Springer New York, New York, NY, 2009.

[64] H. R. Corti, D. L. Goldfurb, M. S. Ortiz, and J. F. Magallanes. Tubular band microelectrode. I. Design and electrochemical behavior. *Electroanalysis*, 7(6):569–573, 1995.

[65] M. Takahashi, S. Tobishima, K. Takei, and Y. Sakurai. Reaction behavior of LiFePO4 as a cathode material for rechargeable lithium batteries. *Solid State Ionics*, 148:283–289, 2002.

[66] W. J. Aixill, A. C. Fisher, and Q. Fulian. Hydrodynamic microelectrodes. the microstrip electrode: Theory and experiment. *Journal of Physical Chemistry*, 3654(100):14067–14073, 1996.

[67] K. S. Hwang, S. M. Lee, S. K. Kim, J. H. Lee, and T. S. Kim. Micro- and nanocantilever devices and systems for biomolecule detection. *Annual Review Analytical Chemistry*, 2:77–98, 2009.

[68] N. V. Rees, J. A. Alden, R. A. W. Dryfe, B. A. Coles, and R. G. Compton. Voltammetry under high mass transport conditions. The high speed channel electrode and heterogeneous kinetics. *Journal of Physical Chemistry*, pages 14813–14818, 1995.

[69] X. Quan, L. M. Fischer, A. Boisen, and M. Tenje. Development of nanoporous gold electrodes for electrochemical applications. *Microelectronic Engineering*, 88(8):2379–2382, 2011.

[70] S. Yang, W. Yang, G. Sun, and H. Knickle. Secondary current density distribution analysis of an aluminum-air cell. *Journal of Power Sources*, 161(2):1412–1419, 2006.

[71] R. G. Compton, A. C. Fisher, and G. P. Tyley. Non-uniform accessibility and the use of hydrodynamic electrodes for mechanistic studies : a comparison of wall-jet and rotating disc electrodes. *Journal Applied Electrochemistry*, 21:295–300, 1991.

[72] R. Ferrigno, P. F. Brevet, and H. H Girault. Finite element simulation of the amperometric response of recessed and protruding microband electrodes in flow channels. *Journal of Electroanalytical Chemistry*, 430(1-2):235–242, 1997.

[73] J. A. Cooper and R. G. Compton. Channel electrodes - a review. *Electroanalysis*, 10(3):141–155, 1998.

[74] R. G. Compton, D. J. Page, and G. R. Sealy. The application of in situ electrochemical esr to EC and ECE processes the reduction of 2-nitropropane. *Journal of Electroanalytical Chemistry*, 161(1):129–146, 1984.

[75] M. Orlik. An improved algorithm for the numerical simulation of cyclic voltammetric curves affected by the ohmic potential drops and its application to the kinetics ofkinetics of bis(biphenyl)chromium(i) electroreduction. *Journal of Electroanalytical Chemistry*, 575(2):281–286, 2005.

[76] C. E. Banks, A. O. Simm, R. Bowler, K. Dawes, and R. G. Compton. Hydrodynamic electrochemistry: design for a high-speed rotating disk electrode. *Analytical Chemistry*, 77(6):1928–30, 2005.

[77] W. Sugimoto, K. Aoyama, T. Kawaguchi, Y. Murakami, and Y. Takasu. Kinetics of CH3OH oxidation on PtRu/C studied by impedance and CO stripping voltammetry. *Journal of Electroanalytical Chemistry*, 576(2):215–221, 2005.

[78] X. Cheng, B. Yi, M. Han, J. Zhang, Y. Qiao, and J. Yu. Investigation of platinum utilization and morphology in catalyst layer of polymer electrolyte fuel cells. *Journal of Power Sources*, 79(1):75–81, 1999.

[79] H. Matsuda and Y. Ayabe. On the theory of the randles-sevcik cathode-ray polarography. *Zeitschrift für Elektrochemie*, 59:494, 1955.

[80] S. W. Feldberg. Digital simulation: A general method for solving electrochemical diffusion-kinetic problem. *Journal of Electroanalytical Chemistry*, 3:199–296, 1969.

[81] X. Quan. Development of an electrochemical cantilever platform for bio/chemical application. *PhD thesis, Technical University of Denmark*, 2013.

[82] R. B. Bird, W. E. Stewart, and E. N. Lightfoot. *Transport Phenomena, Revised 2nd Edition*. John Wiley & Sons, Inc., 2nd edition, 2006.

[83] V. G. Levich. *Physicochemical hydrodynamics*. Prentice-Hall international series in the physical and chemical engineering sciences. Prentice-Hall, 1962.

[84] J. Fuhrmann, H. Zhao, H. Langmach, Y. E. Seidel, Z. Jusys, and R. J. Behm. The role of reactivereaction intermediates in two-step heterogeneous electrocatalytic reactions: A model study. *Fuel Cells*, 11:501–510, 2011.

[85] X. Quan, A. Heiskanen, Y. Sun, A. Labuda, A. Wolff, D. J. Jorge, P. Grutter, M. Tenje, and A. Boisen. Development of electrochemical cantilever sensors for DNA applications. *ECS Transactions*, 50(12):77–81, 2013.

[86] A. Szabo and D. Shoup. Chronoamperometric current at finite disk electrodes. *Journal of Electroanalytical Chemistry*, 140:237–245, 1982.

[87] J. Wang, R. Polsky, B. Tian, and M. P. Chatrathi. Voltammetry on microfluidic chip platforms. *Analytical chemistry*, 72(21):5285–9, 2000.

[88] J Fritz. Cantilever biosensors. *The Analyst*, 133(7):855–63, 2008.

[89] K. Gruber, T. Horlacher, R. Castelli, A. Mader, P. H. Seeberger, and B. A. Hermann. Cantilever array sensors detect specific carbohydrate-protein interactions with picomolar sensitivity. *ACS Nano*, (5):3670–3678, 2011.

[90] M. Orlik. Digital simulation of cyclic voltammetry in a two-electrode system and its application to the kinetics of bis(biphenyl)chromium(I) in N, N-dimethylformamide. *Journal of Electroanalytical Chemistry*, 434:139–152, 1997.

[91] E. A. Wachter and T. Thundat. Micromechanical sensors for chemical and physical measurements. *Review of Scientific Instruments*, 66(6):3662, 1995.

[92] P. S. Waggoner and H. G. Craighead. Micro- and nanomechanical sensors for environmental, chemical, and biological detection. *Lab on a chip*, 7(10):1238–55, 2007.

[93] Z. X. Deng and X. Q. Lin. Digital simulation of fast cyclic voltammogram by integration of the double layer charging current. *Journal of Electroanalytical Chemistry*, 464:215–221, 1999.

[94] S. W. Feldberg and A. J. Bard. *Electroanalytical Chemistry*. Marcel Dekker New York, 1969.

[95] S. W. Feldberg, J. S. Mattson, H. B. Mark, and H. C. MacDonald Jr. *Computers in Chemistry and Instrumentation*. Marcel Dekker New York, 1972.

[96] S. H. Si, K. L. Huang, C. Y. Lu, and S. Z. Yao. Electrodeless piezoelectric quartz crystal sensor for determination of total urinary reducing sugar. *Microchemical Journal*, 62(3):328 – 335, 1999.

[97] C. Jimenez-Jorquera, J. Orozco, and A Baldii. ISFET based microsensors for environmental monitoring. *Sensors*, 10:61–83, 2009.

[98] H. P. Lang, M. Hegner, and C. Gerber. *Springer Handbook of Nanotechnology*. Springer Berlin Heidelberg, 2010.

[99] D. Tsoukalas, S. Chatzandroulis, and D. Goustouridis. *Capacitive Microsensors for Biomedical Applications*. John Wiley & Sons, Inc., 2006.

[100] P Jianhong, T. Fang, and T. Thomas. Glucose biosensor based on the microcantilever. *Analytical Chemistry*, 76(2):292–297, 2004.

[101] K. M. Hansen, H. F. Ji, G. Wu, R. Datar, R Cote, A. Majumdar, and T. Thundat. Cantilever-Based Optical Deflection Assay for Discrimination of DNA Single-Nucleotide Mismatches. *Analytical Chemistry*, 73(7):1567–1571, 2001.

[102] A. M. Moulin, S. J. O'Shea, and M. E. Welland. Microcantilever-based biosensors. *Ultramicroscopy*, 82:23 – 31, 2000.

[103] N. Nugaeva, K. Y. Gfeller, N. Backmann, H. P. Lang, M. Düggelin, and M. Hegner. Micromechanical cantilever array sensors for selective fungal immobilization and fast growth detection. *Biosensors and Bioelectronics*, 21(6):849 – 856, 2005.

[104] S. Sonner, M. A. Efendiev, and H. J. Eberl. On the well-posedness of a mathematical model of quorum-sensing in patchy biofilm communities. *Mathematical Methods in the Applied Sciences*, 34:1667 – 1684, 2011.

[105] M. A. Efendiev. *Evolution Equations Arising in the Modelling of Life Sciences*. Birkhäser, Basel, 2013.

[106] M. A. Efendiev. *Attractors for Degenerate Parabolic Type Equations*, volume 192. Mathematical Surveys and Monographs, American Mathematical Society, 2013.

[107] I. B. Sprague and P. Dutta. Improved kinetics from ion advection through overlapping electric double layers in nano-porous electrodes. *Electrochimica Acta*, 91(0):20 – 29, 2013.

[108] I. Borukhov, D. Andelman, and H. Orland. Steric effects in electrolytes: A modified poisson-boltzmann equation. *Physical Review Letter*, 79:435–438, Jul 1997.

[109] I. Sprague and P. Dutta. Depth averaged analytic solution for a laminar flow fuel cell with electric double layer effects. *SIAM Journal on Applied Mathematics*, 72(4):1149–1168, 2012.

[110] M. Z. Bazant, K. Thornton, and A. Ajdari. Diffuse-charge dynamics in electrochemical systems. *Physical Review E*, 70:021506, Aug 2004.

[111] P. M. Biesheuvel, M. van Soestbergen, and M. Z. Bazant. Imposed currents in galvanic cells. *Electrochimica Acta*, 54(21):4857 – 4871, 2009.

[112] A. Frumkin. Hydrogen overvoltage and structure of the double layer. *Zeitschrift für Physikalische Chemie*, 164(1-2):121–133, 1933.

[113] A. Frumkin. Adsorptionserscheinungen und Elektrochemische Kinetik. *Zeitschrift für Elektrochemie*, 59(7-8):807–822, 1955.

[114] R. G. Compton and P. R. Unwin. Linear sweep voltammetry at channel electrodes. *Journal of electroanalytical chemistry*, 206(1-2):57–67, 1986.

[115] K. Aoki, K. Tokuda, and H. Matsuda. Hydrodynamic voltammetry at channel electrodes. VIII. Theory of reversible voltammograms for chronoamperometry and linear sweep voltammetry. *Journal of electroanalytical chemistry*, 209(2):247–258, 1986.